

[1,2,4]Triazolo[1,5-*a*]pyrimidine Phosphodiesterase 2A Inhibitors: Structure and Free-Energy Perturbation-Guided Exploration

Gary Tresadern,* Ingrid Velter, Andrés A. Trabanco, Frans Van den Keybus, Gregor J. Macdonald, Marijke V. F. Somers, Greet Vanhoof, Philip M. Leonard, Marieke B. A. C. Lamers, Yves E. M. Van Roosbroeck, and Peter J. J. A. Buijnsters*

Cite This: <https://dx.doi.org/10.1021/acs.jmedchem.0c01272>

Read Online

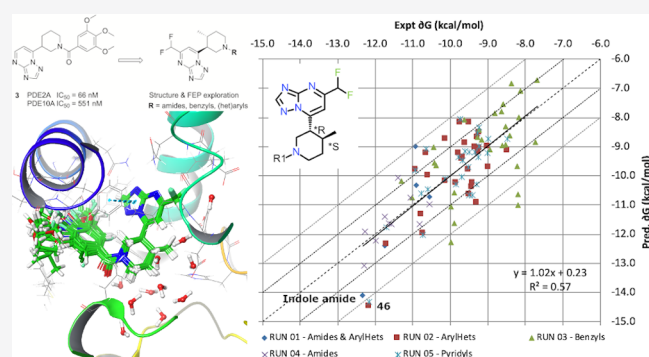
ACCESS |

Metrics & More

Article Recommendations

Supporting Information

ABSTRACT: We describe the hit-to-lead exploration of a [1,2,4]triazolo[1,5-*a*]pyrimidine phosphodiesterase 2A (PDE2A) inhibitor arising from high-throughput screening. X-ray crystallography enabled structure-guided design, leading to the identification of preferred substructural components. Further rounds of optimization used relative binding free-energy calculations to prioritize different substituents from the large accessible chemical space. The free-energy perturbation (FEP) calculations were performed for 265 putative PDE2A inhibitors, and 100 compounds were synthesized representing a relatively large prospective application providing unexpectedly active molecules with IC_{50} 's from 2340 to 0.89 nM. Lead compound **46** originating from the FEP calculations showed PDE2A inhibition IC_{50} of 1.3 ± 0.39 nM, ~ 100 -fold selectivity versus other PDE enzymes, clean cytochrome



P450 profile, *in vivo* target occupancy, and promise for further lead optimization.

INTRODUCTION

The ubiquitous nucleotides 3',5'-cyclic adenosine monophosphate (cAMP) and 3',5'-cyclic guanosine monophosphate (cGMP) are second messengers that play a critical role in many signal transduction pathways. Both cyclic nucleotides are hydrolyzed by phosphodiesterase (PDE) enzymes to the corresponding biologically inactive adenosine and guanosine monophosphates, AMP and GMP, respectively. PDE enzymes are encoded by 21 genes and are grouped into 12 families, PDE1 to PDE12.¹ Their expression is tissue- and cell-specific; moreover, the different isozymes and splice variants are expressed in specific cell compartments and targeted to particular protein complexes, resulting in a spatiotemporal integration of multiple signaling pathways.²

PDE2A is a homodimer of two monomers approximately 105 kDa each. The enzyme has two regulatory units for each monomer, a GAF-A and a GAF-B domain that have distinct roles in dimerization and activation, respectively. Binding of cGMP to the GAF-B domain allosterically activates the enzyme resulting in a 6- to 30-fold increase of cAMP hydrolysis.^{3–5} Once the enzyme is activated, it hydrolyzes both nucleotides with similar K_M values restoring the cAMP and cGMP concentrations to basal levels. PDE2A is expressed in the brain and is most prevalent in cortex, hippocampus, and striatum,^{6–8} supporting a role in cognitive processes, neuronal plasticity, and memory.⁹ Inhibition of PDE2A will result in elevation of intracellular cyclic

nucleotide levels that play a key role in processes of neuroplasticity such as long-term potentiation (LTP), which is considered as a neurophysiological correlate of memory and learning.¹⁰ The exact underlying mechanism of memory enhancement following PDE2A inhibition is not fully understood, but it is likely occurring via the nitric oxide synthase (NOS)/cGMP/protein kinase-G pathway rather than the cAMP/protein kinase A pathway.^{11,12}

Cognitive deficits are prominent in neurodegenerative disorders such as Alzheimer's disease (AD). The earliest cognitive symptoms of AD include a decline in memory function,^{13,14} manifest as problems with planning and task execution (executive function),¹⁵ described as an inability to successfully form new memory traces for integration into existing memory networks.^{16,17} While the impairment of episodic memory is frequently the earliest detectable neurocognitive sign, the earliest symptoms often cooccur with neuropsychiatric behavioral symptoms.¹⁸ Upon progression of the disease, more cognitive function is lost¹⁹ and patients

Received: July 21, 2020

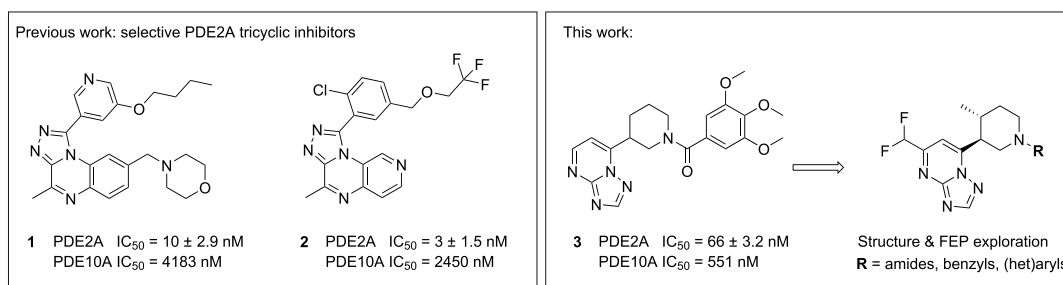


Figure 1. Previous tricyclic PDE2A inhibitor leads **1** and **2**, along with triazolopyrimidine HTS hit **3** which is the subject of this report.

develop concurrent neuropsychiatric symptoms. Disease-modifying treatments in AD are yet to be established, and currently available symptomatic treatments are only moderately effective or limited in their use because of their side effects. Therefore, improved treatments to alleviate or even reverse the symptoms of reduced cognitive function represent a significant unmet medical need. Thus, PDE2A inhibition may be procognitive and have a positive impact in the treatment of cognitive dysfunction in early stage AD,^{20,21} and PDE2 inhibition has been the subject of recent medicinal chemistry reports.^{22–26}

We previously described the structure-based optimization of tricyclic PDE2A inhibitors such as **1** and **2**.^{27,28} Although highly potent and selective, poor solubility and high plasma clearance could not be overcome, limiting their developability. Here, we report a series of [1,2,4]triazolo[1,5-*a*]pyrimidine PDE2A inhibitors arising from high throughput screening (HTS). X-ray crystallography of the initial hit **3** allowed structure-guided design, leading to improved target potency. An X-ray structure of a second example confirmed the binding mode, and we employed computational relative binding free-energy (RBFE) calculations to guide the molecular design. The accurate prediction of protein–ligand interaction energies has been, and remains, an important but very challenging goal for computational structure-based design.²⁹ We applied the free-energy perturbation (FEP) approach that calculates the binding energy difference between structurally similar ligands, making it well suited for lead optimization (LO). The method is undergoing a resurgence of interest^{30,31} and we have seen a good performance in drug discovery programs^{32–34} including PDE2A^{28,35} and for other large protein–ligand data sets.^{36–38} Here, FEP calculations on 250 triazolopyrimidines were followed by the synthesis of 100 examples, giving a valuable demonstration of FEP-guided LO. Overall, the resulting lead compounds showed excellent PDE2A inhibition potency ($IC_{50} < 1$ nM) and selectivity of up to 100- to 1000-fold versus other PDE enzymes. Brain penetration was confirmed for selected leads and the most promising examples, **42** and **46**, showed *in vivo* target engagement in a PDE2A occupancy assay.

RESULTS AND DISCUSSION

HTS hit **3** (Figure 1) had a PDE2A inhibition IC_{50} of 66 ± 3.2 nM and approximately eightfold selectivity versus PDE10A (the closest structural PDE family member to PDE2A). It was inactive ($IC_{50} > 10,000$ nM) in all cases when tested for inhibition activity in a larger panel of PDE enzymes (PDE1B, PDE3A, PDE4D, PDE5A, PDE7A, PDE9A, and PDE11A). Compound **3** originated from commercial sources and was part of our internal screening library. It was tested in over 100 internal screens and was inactive ($IC_{50} > 10,000$ nM) other than

for PDE2A and PDE10A. We began our experimental follow-up by solving the X-ray crystallographic structure of **3** with the PDE2A catalytic domain, refined to 2.35 Å resolution ($R_{work} = 21.5\%$ and $R_{free} = 29.1\%$). There were two PDE2A molecules in the asymmetric unit, but each active site overlaid well and showed minimal variation in ligand binding. Molecule **3** sits in the hydrophobic clamp between Phe830 and Phe862 (Figure 2).

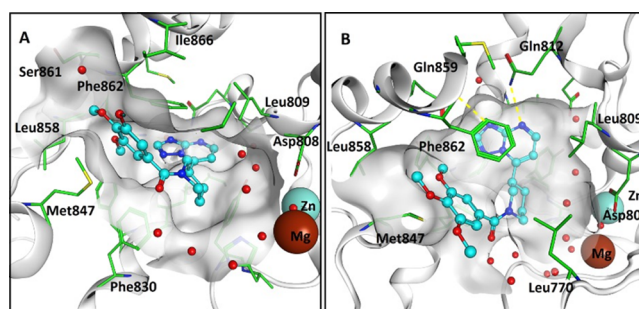
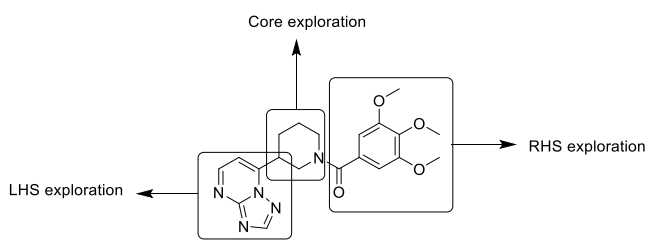


Figure 2. X-ray structure of HTS hit **3** with PDE2A viewed from the entrance to the active site (A) and top down (B), PDB accession code 6ZND. Important amino acids are highlighted in green, and catalytic Zn^{2+} and Mg^{2+} ions are shown, along with active site water molecules (red spheres); hydrogen bonds between Gln812 and Gln859 and the triazolopyrimidine scaffold are indicated with dashed yellow lines in panel B.

Most active site interactions with the ligand are formed with the triazolopyrimidine core. Gln812 donates a 2.3 Å hydrogen bond from its NH side chain to the pyrimidine sp^2 nitrogen acceptor of the bicycle. Another hydrogen bond with a distance of 2.5 Å is donated from the NH side chain of Gln859 to the triazole sp^2 nitrogen and Phe862 forms an off-center π -stack above the scaffold. The linking amido piperidinyl group has an end-on π -interaction with Phe830 and is largely solvent exposed along with the pendant trimethoxyphenyl residue that is bound on the solvent exposed surface of helix 15. The para methoxy group forms a hydrogen bond with a water molecule. The X-ray structure settled the uncertainty of whether the alkoxyphenyl in **3** may interact with the “switch” Gln859 as seen for well-known PDE inhibitors such as Papaverine and Rolipram.^{39,40} Further examination of the binding mode suggested that there was space to substitute on the free positions of the pyrimido ring along with ample opportunity for amide replacements.

The chemistry exploration of the initial hit began with the preparation of the right-hand side (RHS, Chart 1) amides **3–18** (Table 1). The compounds were tested in a full-length human PDE2A inhibition assay measuring changes in levels of cAMP by a scintillation proximity approach. Consistent with the binding mode, a variety of benzamides were tolerated as substituents on the piperidine. Initial hit **3** was racemic and a 66 nM PDE2A

Chart 1. Medicinal Chemistry Strategy for Exploration of HTS Hit 3



inhibitor. The dimethoxy analogue **4** showed similar PDE2A inhibition activity ($IC_{50} = 47 \pm 16$ nM). Homologation via a methylene spacer between the amide carbonyl and the distal aromatic resulted in a ~ 10 -fold drop in activity for **5** compared to **4** (**5**, $IC_{50} = 479 \pm 16$ nM vs **4**, $IC_{50} = 47 \pm 16$ nM). The X-ray structure of **3** (Figure 2) suggests that this was due to a loss of the optimal interactions with Met847 and Phe862. Simplification to the unsubstituted phenyl **6** ($IC_{50} = 339 \pm 31$ nM) or replacement of the distal aromatic by small aliphatic groups, **7** ($IC_{50} = 246 \pm 12$ nM) and **8** ($IC_{50} = 1580 \pm 180$ nM), were detrimental for activity, again because of the loss of preferred aromatic interactions with Met847 and Phe862.

The PDE2A activity was dependent on the position and type of substitution on the aromatic ring. For instance, meta and para substituents were preferred, exemplified with ortho methoxy **9** ($IC_{50} = 912 \pm 200$ nM) that was >12 -fold less active than meta **10** ($IC_{50} = 74 \pm 27$ nM) or para **11** ($IC_{50} = 50 \pm 22$ nM). It was expected that the ortho substituent caused the rotation of the distal aromatic ring and disrupted its interaction with Phe862. Meanwhile, it was clear that electron donating groups were beneficial for activity compared to withdrawing, for instance, the comparison of *para* methoxy **11** ($IC_{50} = 50 \pm 22$ nM) to *para* cyano **12** ($IC_{50} = 589 \pm 280$ nM) and trifluoromethyl **13** ($IC_{50} = 324 \pm 96$ nM) substituents. The electron-rich aromatic rings were preferred as they form an energetically more favorable T-shaped π -interaction with Phe862, Figure 2. Conformational restriction of the methoxy groups into the benzodioxane derivative **14** ($IC_{50} = 49 \pm 21$ nM) maintained a similar range of activity compared to **4** ($IC_{50} = 47 \pm 16$ nM), although **4** was racemic. Fully aromatic bicyclic examples such as benzofuran **15** improved the inhibition activity to 24 ± 8.5 nM. This prompted us to expand the exploration around these bicyclic heteroaromatics, resulting in analogues such as **16** and **17** that reached PDE2A potencies of 2.1 ± 0.9 and 2.6 ± 1.1 nM, respectively. The tetrahydrobenzothiophene group attached via the five-membered ring in **18** was a 10 ± 5.2 nM PDE2A inhibitor and was selected as the template to explore central core and LHS variations. Finally, the observation of the *S* stereoisomer binding in the X-ray structure was formally confirmed by chiral separation of **17**. Indeed, the *S* stereoisomer retains most of the PDE2A inhibitory activity with **20** being 60-fold more active than its enantiomer **19** (**20**, $IC_{50} = 1.5 \pm 0.1$ nM vs **19**, $IC_{50} = 87 \pm 27$ nM).

The identification of a selective inhibitor was a key aspect of our strategy to later validate the role of PDE2A inhibition for cognition. The main concern was selectivity versus PDE10A given its close structural similarity to PDE2A (34% sequence identity, 50% similarity for the catalytic domain) and its implication in other central nervous system disorders.⁴¹ Indeed, the selectivity data available for all the compounds in this article confirms only weak and sparse activity (range 3160–10,000 nM

Table 1. RHS Exploration of HTS Hit 3^{a,b}

| Compound | R _{RHS} | PDE2A IC ₅₀ ± SD (nM) | PDE3A IC ₅₀ (nM) | PDE10A IC ₅₀ (nM) |
|-------------------------|------------------|-------------------------------------|--------------------------------|---------------------------------|
| 3 (<i>RS</i>) | | 66 ± 3.2 | >10000 | 551 |
| 4 (<i>RS</i>) | | 47 ± 16 | 2399 | 589 |
| 5 (<i>S</i>) | | 479 ± 16 | 4898 | 3162 |
| 6 (<i>S</i>) | | 339 ± 31 | 4266 | 4571 |
| 7 (<i>S</i>) | | 246 ± 12 | >10000 | 1047 |
| 8 (<i>RS</i>) | | 1580 ± 183 | 617 ^c | 7762 |
| 9 (<i>S</i>) | | 912 ± 200 | 3388 ^c | 5129 |
| 10 (<i>S</i>) | | 74 ± 27 | 1513 | 1148 |
| 11 (<i>S</i>) | | 50 ± 22 | 537 | 871 |
| 12 (<i>S</i>) | | 589 ± 281 | 4786 | 6918 |
| 13 (<i>S</i>) | | 324 ± 96 | 436 | 3020 |
| 14 (<i>S</i>) | | 49 ± 21 | 398 | 1148 |
| 15 (<i>RS</i>) | | 24 ± 8.5 | 1622 ^c | 447 |
| 16 (<i>RS</i>) | | 2.1 ± 0.9 | 331 | 100 |
| 17 (<i>RS</i>) | | 2.6 ± 1.1 | 776 | 107 |
| 18 (<i>S</i>) | | 10 ± 5.2 | 89 | 288 |
| 19 (<i>R</i>) | | 87 ± 27 | >10000 | 3548 |
| 20 (<i>S</i>) | | 1.5 ± 0.1 | 282 | 54 |

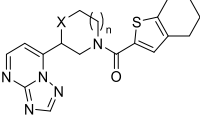
^aPrimary inhibition activity versus PDE2A, and activity versus close structural family members PDE3A/B and PDE10A. ^bPDE2A bioactivity measurements are the mean of at least two independent repeats and provided with standard deviations except **6**, **8**, and **12**, which are provided with the standard error on dose response for $n = 1$. ^cAll data were generated with PDE3A except compounds **8**, **9**, and **15** that were tested versus PDE3B.

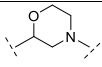
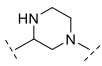
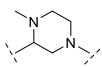
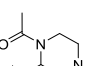
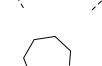
for 12 out of 140 IC_{50} measurements) versus multiple other PDE family members (PDE1B, PDE4D, PDE5A, PDE7A, PDE9A,

and PDE11A), Table S1. The HTS hit **3** showed a modest 8-fold selectivity, but this was substantially improved to approximately 30- to 50-fold with bicyclic amides such as **16–18**. This could be rationalized because of the interaction with Leu858 (Figure 2), which forms the boundary at the bottom of the benzamide pocket and interacts directly with the meta and para substituents of the distal aromatic ring, or in the case of **16–18**, the fused 5-membered ring. A glycine is found at the same position in PDE10A (Gly725), and because of the absence of the side chain, the pocket extends further, meaning that this region of the binding site, traditionally referred to as the Q2 pocket,⁴⁰ can be exploited for PDE selectivity.⁴²

Turning to the core modifications (Table 2), replacement of the piperidine in **18** by a morpholine was detrimental for activity

Table 2. Central Core Modifications^{a,b}



| Compound | Central Core | PDE2A IC ₅₀ ± SD (nM) | PDE3A IC ₅₀ (nM) | PDE10A IC ₅₀ (nM) |
|-------------------------|---|----------------------------------|-----------------------------|------------------------------|
| 21 (<i>S</i>) |  | 91 ± 29 | 178 | 2630 |
| 22 (<i>RS</i>) |  | 1412 ± 196 | > 10000 | > 10000 |
| 23 (<i>RS</i>) |  | 87 ± 41 | 5495 ^c | 2455 |
| 24 (<i>RS</i>) |  | >10000 | > 10000 | > 3020 |
| 25 (<i>RS</i>) |  | 263 ± 24 | 3631 | 1288 |

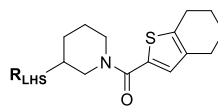
^aPrimary inhibition activity versus PDE2A, and activity versus close structural family members PDE3A/B and PDE10A. ^bPDE2A bioactivity measurements are the mean of at least two independent repeats and provided with standard deviations except **22** and **25** which are provided with the standard error on dose response for $n = 1$. ^cAll data were generated with PDE3A except compound **23** that was tested versus PDE3B.

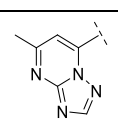
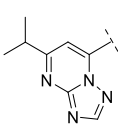
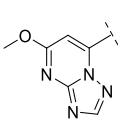
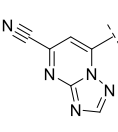
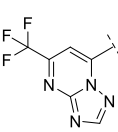
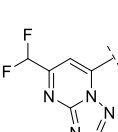
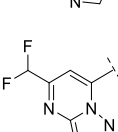
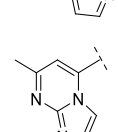
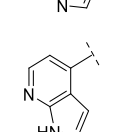
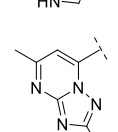
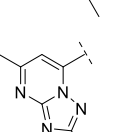
with **21** being ninefold less active than **18** (**21**, IC₅₀ 91 ± 29 vs **18**, 10 ± 5.2 nM). Although the unsubstituted piperazine was substantially less active (**22**, IC₅₀ = 1412 ± 196 nM), the *N*-methyl analogue **23** showed a double-digit nanomolar PDE2A inhibition activity (IC₅₀ = 87 ± 41 nM). Acylation of the piperazine nitrogen in **24** was inactive up to the 10 μM concentration limit. Ring enlargement was also detrimental for activity with the homopiperidine **25** being 26-fold less active than the corresponding piperidine matched pair (**25**, IC₅₀ = 263 ± 24 nM vs **18**, IC₅₀ = 10 ± 5.2 nM). Hence, the piperidine was optimal for the activity, something that could be understood from the X-ray structure because of its close lipophilic interaction with the side chains of Tyr655 and Ile826. The selectivity of the most active examples in this exploration, **21** and **23**, was similar to the parent piperidine central core, **18**. Indeed, all three examples maintained the same 28-fold selectivity versus PDE10A, demonstrating the origin of selectivity from the

constant presence of the tetrahydrobenzothiothiophene amide. In contrast, **18** and **21** displayed only 1.4- to 4-fold selectivity versus PDE3A. The sequence similarity between PDE2A and PDE3A (20% sequence identity, 33% similarity for the catalytic domain) was lower than that for PDE10A, and the loss of selectivity versus PDE3A was initially a surprise. Nevertheless, the complete lack of PDE3A inhibition activity for some benzamide replacements (**3**, **7**, and **19** Table 1) offered promise that PDE3A selectivity could be modulated in the same Q2 pocket that was targeted for PDE10A selectivity.⁴⁰ Comparison of PDE2A and PDE3B⁴³ crystal structures revealed differences, for instance, Met847 (PDE2A, Figure 1) was instead Phe976 (PDE3B) that also adopts a different conformation and changes the shape of the pocket to “for instance, Met847 in PDE2A (Figure 1) was instead Phe976 in PDE3B. The Phe976 also adopts a different conformation compared to Met847 and changes the shape of the pocket.”

To complete the initial structure–activity relationship (SAR) exploration around the triazolopyrimidine hit series, the LHS group (Chart 1) was modified while maintaining the piperidine central core and RHS residue present in **18**. The introduction of a methyl substituent on the pyrimidine ring brought immediate improvements in potency and compound **26** showed a 3.5 ± 2.3 nM PDE2A inhibitor IC₅₀ activity (Table 3). According to the crystal structure binding mode of **3**, the methyl group in **26** would occupy a small pocket deep in the binding site. The larger isopropyl group in **27** would not fit and hence the compound was much less active (**27**, IC₅₀ = 6031 ± 1943 nM). The smaller methoxy group in the same position recovered the activity (**28**, IC₅₀ = 195 ± 85 nM). Triazolopyrimidine compounds bearing electron-withdrawing cyano (**29**) and trifluoromethyl (**30**) substituents showed good PDE2A inhibition values (10 ± 5.9 and 50 ± 19 nM, respectively), although they were less potent than the methyl analogue **26**. Interestingly, the CHF₂ group in **31** delivered an equipotent PDE2A inhibitor (**31**, 3.4 ± 2.3 nM vs **26**, 3.5 ± 2.3 nM). Modification of the heterobicyclic ring (**32–34**) resulted in all cases in a substantial loss of activity. The IC₅₀ of pyrazolopyrimidine **32**, imidazolopyrimidine **33**, and azaindole **34** were 30 ± 22, 407 ± 66, and 6020 ± 1980 nM, respectively. Finally, the introduction of substituents in the triazolo ring in **26** was clearly detrimental for activity with methyl- (**35**, IC₅₀ = 562 ± 65 nM) or trifluoromethyl-substituted (**36**, IC₅₀ = 2951 ± 478 nM) analogues 160- and 842-fold less active than the PDE2A inhibitor **26**. In general, selectivity improved by the introduction of the small substituent on the pyrimidine ring, for instance **31** was nearly 200-fold and 16-fold selective versus PDE10A and PDE3A, respectively. Compound **31** was tested in a larger PDE inhibition panel including PDE1B, PDE4D, PDE5A, PDE7A, and PDE11A, where it showed >10,000 nM activity in all assays except for PDE4D, where a moderate activity (IC₅₀ = 6460 nM) was measured.

From the initial SAR studies, it was clear that although the RHS substituent tolerated a diverse set of aromatic amides, the substitution pattern and electronic nature of the substituents were important for achieving increased PDE2A inhibition. This was due to forming optimal nearby interactions, particularly with Met847 and Phe862. All modifications of the central scaffold were less active than the parent piperidine example. Meanwhile, the LHS group that hydrogen bonds with the Gln812 switch and Gln859, permitted a CH₃ and CHF₂ substituent entering deep into the binding pocket. Therefore, using the optimal LHS along with the piperidine central ring, benzylic heteroaromatic groups

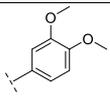
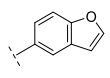
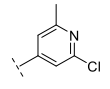
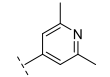
Table 3. LHS Exploration of HTS Hit 3^{a,b}


| Compound | R _{LHS} | PDE2A IC ₅₀ ± SD (nM) | PDE3A IC ₅₀ (nM) | PDE10A IC ₅₀ (nM) |
|----------|---|-------------------------------------|--------------------------------|---------------------------------|
| 26 (RS) |  | 3.5 ± 2.3 | 112 | 229 |
| 27 (RS) |  | 6031 ± 1943 | 89 | 603 |
| 28 (RS) |  | 195 ± 85 | 115 ^c | 1148 |
| 29 (RS) |  | 10 ± 5.9 | 676 ^c | 759 |
| 30 (RS) |  | 50 ± 19 | 3236 | 2692 |
| 31 (RS) |  | 3.4 ± 2.3 | 56 | 912 |
| 32 (RS) |  | 30 ± 22 | 78 ^c | 724 |
| 33 (RS) |  | 407 ± 66 | 347 ^c | 1096 |
| 34 (RS) |  | 6020 ± 1980 | 38 | >10000 |
| 35 (RS) |  | 562 ± 65 | >10000 | 100 |
| 36 (RS) |  | 2951 ± 478 | 2291 | 550 |

^aPrimary inhibition activity versus PDE2A, and activity versus close structural family members PDE3A/B and PDE10A. ^bPDE2A bioactivity measurements are the mean of at least two independent repeats and provided with standard deviations except for 33, 35, and 36, which are provided with the standard error on dose response for $n = 1$. ^cAll data were generated with PDE3A except for compounds 28, 29, 32, and 33 that were tested versus PDE3B.

were studied as RHS benzamide replacements (Table 4). The SAR obtained did not correlate well with the phenyl amide

Table 4. Second Round RHS Modifications^{a,b}

| Compound | R _{RHS} | PDE2A IC ₅₀ ± SD (nM) | PDE3B IC ₅₀ (nM) | PDE10A IC ₅₀ (nM) |
|----------|---|----------------------------------|-----------------------------|------------------------------|
| 37 (RS) |  | 741 ± 345 | 5623 | 661 |
| 38 (RS) |  | 1148 ± 207 | 3467 | 7586 |
| 39 (S) |  | 24 ± 6.3 | 6166 | 5623 |
| 40 (S) |  | 69 ± 39 | >10000 | 8318 |

^aPrimary inhibition activity versus PDE2A, and activity versus close structural family members PDE3B and PDE10A. ^bPDE2A bioactivity measurements are the mean of at least two independent repeats and provided with standard deviations.

subseries. First, both the dimethoxyphenyl- (37) and the benzofuran-containing (38) triazolopyrimidine analogues were less active than the equivalent amides 4 and 15 (37, IC₅₀ = 741 ± 345 nM vs 4, IC₅₀ = 47 ± 16 nM and 38, IC₅₀ = 1148 ± 207 nM vs 15, IC₅₀ = 24 ± 8.5 nM, respectively). Furthermore, the relative order of activity was reversed. Interestingly, the benzyl-like pyridine derivatives 39 and 40 were 24 ± 6.3 and 69 ± 39 nM PDE2A inhibitors and recovered selectivity, being >120-fold selective for both PDE3A and PDE10A. This confirmed the comparison between PDE2A and PDE3B X-ray structures that revealed that the sequence and structural differences in the Q2 pocket could lead to PDE3A selectivity. It was expected that these electron-rich heteroaromatics would make favorable interactions with Phe862 as mentioned above, but the differences in activity suggested that different ligand conformations were possible compared to equivalent amides. Therefore, intrigued to understand if this would translate into structural differences when bound to the enzyme, we attempted and solved an X-ray crystal structure of 39 with the PDE2A catalytic domain.

The structure of PDE2A in complex with lead 39 was solved at 1.9 Å resolution ($R_{\text{work}} = 19.6\%$ and $R_{\text{free}} = 24.4\%$), and the binding site is shown in Figure 3. There were four PDE2A monomers per asymmetric unit and each had a single 39 molecule bound in its active site. Structural overlay indicated little conformational difference between the four subunits; the electron density was best defined for subunit D. The triazolopyrimidine core of 39 was again anchored by two hydrogen bonds to Gln859 and Gln812 while being held in a hydrophobic clamp by Ile826, Phe830 and Phe862. The difluoro methyl group sits in a small, well-buried pocket, as expected from the X-ray structure of 3. The proton of the difluoro methyl group is electropositive and makes a favorable electrostatic interaction

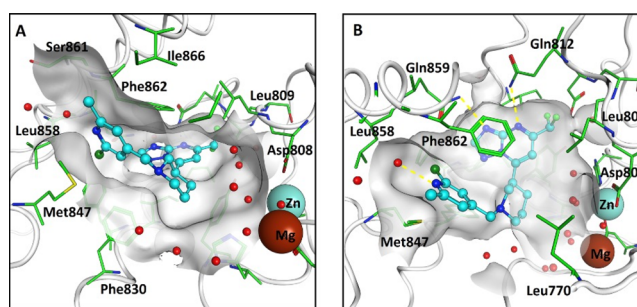


Figure 3. X-ray structure of lead 39 with PDE2A viewed from the entrance to the active site (A) and top down (B), PDB accession code 6ZQZ. Important amino acids are highlighted in green, and catalytic Zn²⁺ and Mg²⁺ ions are shown, along with active site water molecules (red spheres); hydrogen bonds are indicated with dashed yellow lines in panel B.

with the phenol oxygen of the neighboring Tyr655. The piperidine core is largely solvent exposed along with the pendant pyridine ring. Positive electron density peaks in the final difference density maps indicated a second alternative conformation of the pyridine ring related by a 180° rotation of the pyridine, positioning the chlorine substituent toward the solvent space. B-Factor refinement indicated less than 20% occupancy of this second conformation in each of the four subunits. The alternative orientation was therefore not included in the final model. Nevertheless, the second possible orientation was consistent with conformational effects contributing to lower inhibition activity of benzyl- compared to benzamide-substituents (Table 4). The pyridyl ring was again sandwiched between Met847 and Phe862, and the nitrogen formed a hydrogen bond to a crystallographic water at the bottom of the Q2 pocket.

Racemization of the Central Scaffold. Up to this point, we had several promising leads, including 15–18, 26, and 31 that showed PDE2A inhibition <10 nM and in most cases >10-fold selectivity versus PDE3A and PDE10A. Unfortunately, it was noticed that after chiral separation, in some cases, enantiopure compounds in solution turned into mixtures after several days. Racemization presented a challenge for the progression of the series. Interestingly, the problem was overcome by introducing a methyl substituent into the 4-position of the piperidine ring. Several examples were synthesized and shown not only to maintain but even improve potency (Figure 4). This was likely because of the preference for hydrophobic interactions with the side chains of Tyr655 and Ile826, as seen for the central core modifications (Table 2). Compound 41 showed high PDE2A inhibition activity (IC₅₀ = 1.1 ± 0.4 nM) and >90-fold selectivity versus PDE3A (IC₅₀ = 2240 nM) and PDE10A (IC₅₀ = 97 nM). It was also tested for inhibition against a larger panel of PDE enzymes and was inactive (IC₅₀ > 10,000 nM) in all cases (PDE1B, PDE4D, PDE7A, and PDE11A) except for PDE5A, where a weak activity was detected (IC₅₀ = 6760 nM). The chiral example 42 showed sub-nanomolar PDE2A inhibition (IC₅₀ = 0.6 ± 0.3 nM) and was 2200- and 90-fold selective versus PDE3A and PDE10A, respectively.

RBFE Calculations. Up to this point, we had mostly used amide substitution on the piperidine nitrogen to explore the hit series. However, molecules with benzylic functionality such as 39 and 40 demonstrated that a large chemically accessible space may be possible. Hence, we turned to computational

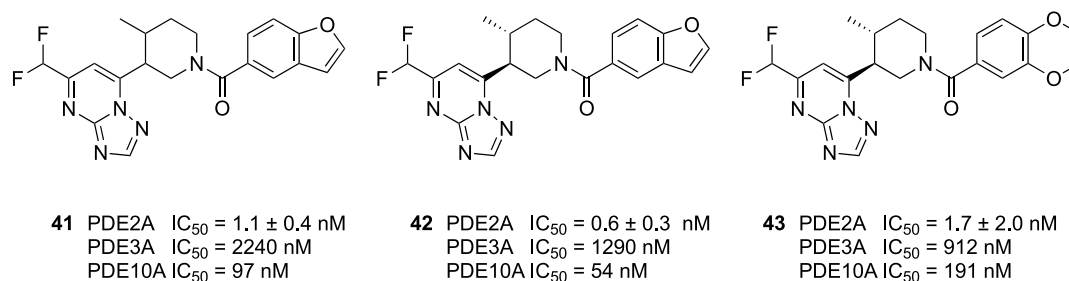


Figure 4. 4-Methyl-substituted piperidines **41**–**43**, introduction of the methyl group at the 4-position of the piperidine central scaffold to prevent racemization.

prioritization using RBEF calculations with FEP methodology. The method requires that perturbed molecules share an overlapping binding mode during the computational simulations. This was expected here as the two crystallographic binding orientations of **3** and **39** were highly similar, suggesting that different chemical decoration can be probed with FEP calculations. Others have used binding free-energy calculations for PDE10⁴⁴ and for other PDE enzymes.⁴⁵ We have described accurate RBEF predictions for ligand modifications in a different subpocket of the PDE2A binding site.³⁵ Here, the ligand changes are relatively solvent exposed and that was expected to help the performance of the calculations by avoiding issues with kinetically trapped solvent.

We began by testing the FEP performance with a small retrospective validation study using 20 existing molecules involving a mixture of structurally similar amides and benzyls covering a 4 log unit range of activity. A good correlation, R^2 0.69, and mean unsigned error (MUE) of 0.89 ± 0.35 kcal/mol was seen when comparing experimental and calculated binding affinities, Figure S1 and Table S2. This prompted us to continue and perform successive rounds of FEP to help prioritize ongoing chemistry explorations on a roughly monthly basis. The calculations were applied to different virtual libraries containing varied substituents on the piperidine nitrogen. The input for the FEP calculations was guided using docking that performed well at reproducing the expected binding modes, Figure S2. The reagents for each virtual library were selected based on their similarity to the known actives, that is, aromatic amides, and their chemical feasibility and availability. These included amides, benzylic groups, and heteroaromatic halide ((het)aryl) reagents (Table 5). This study was part of a larger in-house evaluation^{28,32,33,35} of FEP, and therefore, we chose compounds from across the range of predicted affinity to avoid issues of selection bias and deliver a fair evaluation of the FEP performance.⁴⁶

In total, 100 molecules were synthesized from the different libraries. The experimental and predicted binding free energies (δG , kcal/mol) are compared in Figure 5. The most active molecules are those in the bottom left of the plot with the largest negative favorable binding free energy. The correlation of R^2 0.57 and overall MUE of 0.79 ± 0.16 kcal/mol were consistent with the retrospective validation. A key reason for exploring quantitative RBEF predictions is the poor activity prediction for congeneric series by methods such as docking. This was also the case here because the docking, although able to reproduce the binding pose, was unable to predict binding affinity for the same set of compounds, R^2 0.01 and MUE of 2.27 ± 0.33 kcal/mol, Figure S2.

There were various expected and unexpected examples amongst the FEP results. The calculations predicted multiple

Table 5. Summary of the Rounds of FEP Calculations That Were Applied to Prospective Molecular Design

| round | R-substituents | no calculated | no synthesized | R^2 | MUE (kcal/mol) ^a |
|-------|----------------------|---------------|----------------|-------|-----------------------------|
| 1 | amides & (het) aryls | 59 | 5 | 0.77 | 1.02 ± 0.90 |
| 2 | (het)aryl | 57 | 29 | 0.51 | 0.78 ± 0.27 |
| 3 | benzyls | 58 | 29 | 0.28 | 1.01 ± 0.33 |
| 4 | amides | 39 | 10 | 0.41 | 0.47 ± 0.32 |
| 5 | pyridyls | 52 | 27 | 0.58 | 0.62 ± 0.29 |

^a $\pm 99\%$ confidence interval. (Het)aryl—heteroaromatic halide reagents delivering compounds with a heteroaromatic ring directly bonded to the piperidine nitrogen.

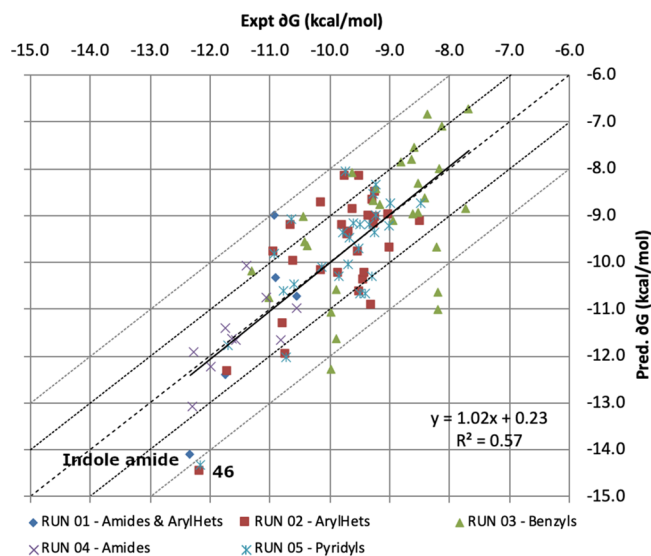


Figure 5. Correlation of experimental and calculated binding activity (δG) for the compounds synthesized in each round of the FEP-guided design. The compound data points are colored and shaped according to the rounds of FEP and synthesis, see Table 5. The diagonal lines of unity and ± 1 or 2 kcal/mol errors are shown. The trendline (black, partly obscured by the line of unity), equation, and R^2 were calculated based on all the data combined, showing almost linear slope and very little offset. Selected compounds are labeled.

amides as highly active. An analogue of **42** where the benzofuran was replaced by indole (changing only the oxygen atom for NH) was a high affinity 0.9 ± 0.4 nM PDE2A inhibitor but structurally

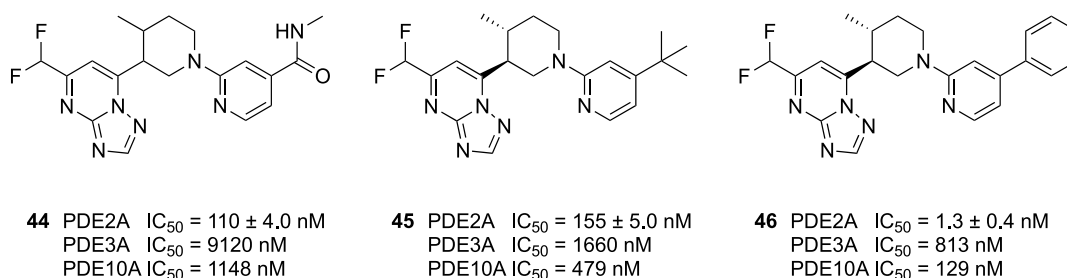


Figure 6. Comparative examples of 4-substituted pyridine RHS substituents arising from the FEP calculations.

very close to previous examples. Therefore, although this was an interesting example of successful activity prediction, that is itself a difficult achievement, it is a relatively obvious result. However, amongst a series of 4-substituted pyridyls, **44–46**, example **46** with the 4-phenyl substituted pyridine was a surprising 1.3 ± 0.4 nM PDE2A inhibitor that showed ~ 100 -fold increase in activity compared to analogues **44** and **45** (Figure 6). The phenyl ring in the 4-pyridyl position would have been disregarded based on the relatively low activity of **44** that presents an amide with an aromatic character in this position and **45** with a lipophilic *t*-butyl group. Curiously, the FEP calculation for this molecule was performed twice in two separate libraries of compounds, as seen by the almost overlapping star and square labels highlighted in Figure 5. It was part of a general library of heteroaromatic halide reagents (round 2), and again in the more focused halo-pyridyl reagent library (round 5). In both cases, it was predicted to be a potent example that was confirmed after synthesis and testing and without the calculations this example would have been overlooked.

The difference in activity between **45** and **46** was correctly predicted by the FEP calculations, predicted to be 4.0 kcal/mol in favor of **46** compared to 2.9 kcal/mol experimentally. In other words, the calculations were capturing the multiple SAR effects that include the aromatic interaction with Phe862, the CH– π interactions between the 4-phenyl substituent of the ligand and Ile866, and displacement of the crystallographic water at the bottom of the Q2 pocket from a relatively hydrophobic and exposed region of the protein surface (Figures 2 and 3 for binding site details). This is manifest in the mostly good correlation seen for the different FEP rounds. Overall, relatively substantial improvements in potency were seen for a pocket that while solvent exposed contains multiple hydrophobic side chains, Met847, Leu858, Phe862, and Ile866. This makes it an ideal pocket for improving binding affinity and also avoids difficulties for FEP calculations, such as trapped solvent in buried pockets or needing to introduce polar interactions with optimal distance and angles to compete with the solvent. Altogether these factors may explain the good performance of FEP in this case.

The error between experimental and predicted binding affinity of the successive rounds of FEP improved, for instance, rounds 4 and 5 showed MUE of 0.47 ± 0.32 and 0.62 ± 0.29 kcal/mol, respectively, compared to the first rounds with MUE ~ 1 kcal/mol. The first round included molecules with two different types of substitution on the piperidine nitrogen, all the subsequent rounds only used one type of chemical substituent. The benzyl library, round 3, performed the worst, R^2 0.28 and MUE 1.01 ± 0.33 kcal/mol.

The lower correlation could be due to alternative binding conformations, although the low populated conformation in the X-ray structure of **39** was seen in the simulations, or it could be

due to a change in the ionization state of the piperidine nitrogen, which was treated as neutral in all cases but may vary based on the benzylic substituent. The correlation of the amide library in round 4 was low, but this was due to a smaller range of the resulting experimental activity (1.3 log units), making it difficult to achieve high correlation but the MUE remained good.

Overall, the improvement with each round was attributed to the closer structural similarity between the compounds (beneficial for the convergence of the calculations) because each library became more focused on analogues of previously identified actives. We did not include additional experimental reference molecules in the subsequent rounds, although this can be used as a strategy to improve results. In our experience, this application of FEP has been particularly successful for various reasons. On the one hand, the SAR is relatively easy to capture with important hydrophobic interactions in a solvent accessible region, where water displacement can be modeled. The site of perturbation is exposed, does not require protein movement, and is far away from the active site metal ions which can cause difficulties, all in contrast to our previous FEP studies on PDE2.³⁵ Practical issues also make this system amenable, the high-resolution crystal structures were convergent on a common binding mode for different substituents, the substituents themselves are distal and often unlikely to disturb the conformation of the remaining molecule, there is no expected change in formal charge of the ligands, and all perturbations took place in only one region of the molecule. Thus, many reasons combine to make this an ideal system for studying with RBFE calculations.⁴⁷

Finally for the calculations, it is worthwhile to consider the value and impact that accurate binding energy predictions can have on drug discovery. An analysis of 50,000 medicinal chemistry transformations from 30 projects revealed only 8.5% having a potency gain of >1 log unit (~ 1.4 kcal/mol).⁴⁸ For a small set of 10 compounds, a prediction with 1 kcal/mol of error increases the chance a log unit improvement in activity to 36%, a ~ 4 -fold gain.⁴⁷ As more compounds are assessed, the impact improves. This simple model is informative but has various caveats, for instance not all transformations are intended to improve potency. More recent analysis for a prototypical drug discovery program has suggested a 2- to 4-fold increase in the number of potent molecules when assessing at least five ideas for each synthesized compound.⁴⁹ In this study, we synthesized 100 molecules from across a range of activity prediction. FEP correctly identified 90% (9 out of 10) of the 10 most active amongst its best ranked 10, compared to 20% (2 out of 10) from docking. Although this represents an unexpectedly good performance, it highlights the benefits for increased computational assistance in molecular design and the value of RBFE predictions compared to classical approaches.

Table 6. Emerging Leads from the Initial Exploration of HTS Triazolopyrimidine Hit 3^a

| compd | PDE2A IC ₅₀ (nM) | selectivity ^b | solubility (μ M pH 7.4) | CYP450 ^c | rat Cl _{int} ^d (μ L/min/mg) | hum Cl _{int} ^d (μ L/min/mg) | rat t _{1/2} ^d (min) | hum t _{1/2} ^d (min) |
|-------|--------------------------------|--------------------------|---------------------------------|-------------------------------|---|---|--|--|
| 15 | 24 \pm 8.5 | 21 | n.d. | n.d. | 14 | 19 | 98 | 72 |
| 17 | 2.6 \pm 1.1 | 30 | 105 | 0, -, 2, 9, 0, 0 | 35 | 32 | 40 | 43 |
| 18 | 10 \pm 5.2 | 4 | 102 | 69, -, 44, 16, 0, 51 | >347 | >347 | <4 | <4 |
| 31 | 3.4 \pm 2.3 | 11 | 92 | 28, -, 31, 7, 43, 41 | >347 | >347 | <4 | <4 |
| 39 | 24 \pm 6.3 | 234 | n.d. | n.d. | 74 | 49 | 19 | 28 |
| 42 | 0.6 \pm 0.3 | 89 | n.d. | n.d. | 11 | 14 | 129 | 98 |
| 43 | 1.7 \pm 2.0 | 112 | >100 | n.d. | 26 | 14 | 55 | 99 |
| 46 | 1.3 \pm 0.4 | 99 | 4 | >10, >10, 9, >10, >10, >10 | 157 | 38 | 9 | 37 |

^an.d. not determined. ^bMinimum fold-selectivity calculated with respect to either PDE3A or PDE10A. ^cCytochrome P450 inhibition, all compounds measured as % inhibition at 10 μ M compound concentration, except 46, which corresponds to IC₅₀ in μ M. All measurements follow the same order: 3A4, 2C8, 2C9, 2C19, 2D6, 1A2. ^dAll compounds incubated at 1 μ M for 60 min in human and rat liver microsomes to determine the metabolic turnover (half-life, Cl_{int}).

The initial systematic exploration of the HTS hit 3, followed by the computationally guided library exploration, led to a collection of early lead candidates with PDE2A inhibition activity in the range of 0.6–24 nM (Table 6). Selectivity was improved during the optimization with later examples such as 39, 42, 43, and 46 showing approximately 100-fold selectivity versus either PDE3A or PDE10A. This set of promising compounds was further profiled *in vitro* for its ADMET properties. In general, solubility was good and no relevant cytochrome P450 (CYP450) inhibition was seen for most compounds up to 10 μ M. The metabolic stability was an issue for the leads that contained the tetrahydrobenzothiophene amide such as 18 and 31 with both showing high turnover in human and rat liver microsomal stability assays. Meanwhile, examples such as the benzofuran-containing lead 42 suggested the high metabolic turnover could be overcome. This compared favorably with the previous tricycle 1 that was highly metabolized (compound was undetectable after 15 min of incubation in human and rat liver microsomes) in similar assays.²⁷

We investigated the ability of a representative set of compounds to cross the blood–brain barrier (BBB). Plasma and brain levels measured 1 h after dosing at 10 mg/kg are listed in Table 7. The tetrahydrobenzothiophene amides (18 and 31)

Table 7. Brain and Plasma Levels for Compounds after 1 h of a Single Dose at 10 mg/kg in Rats

| compd | plasma levels (ng/mL) ^a | brain levels (ng/mL) ^a | B/P ratio | c log P ^b | TPSA |
|-----------------|---------------------------------------|--------------------------------------|--------------|----------------------|------|
| 18 ^c | 679 \pm 28 | 240 \pm 1 | 0.4 | 1.9 | 92 |
| 31 ^c | 831 \pm 450 | 346 \pm 260 | 0.4 | 2.1 | 92 |
| 42 ^d | 1640 \pm 57 | 788 \pm 4 | 0.5 | 1.8 | 77 |
| 46 ^c | 338 \pm 68 | 596 \pm 75 | 1.8 | 3.4 | 59 |

^aData are expressed as the mean average of at least two runs and provided with standard deviations. ^bc log P calculated with Biobyte software. ^cCompound dosed s.c. at 1 mg/mL in 20% HP- β -CD solution in Sprague Dawley rat. ^dCompound dosed p.o. at 1 mg/mL in a 20% HP- β -CD solution pH 3.6–3.7 in the Long–Evans rat.

and the chiral benzofuran (42) were less brain penetrant (B/P = 0.4–0.5) than the 4-phenyl substituted pyridine (46) (B/P = 1.8). The better *in vitro* clearance seen for 42 permitted p.o. dosing with higher absolute levels in plasma and brain. Meanwhile, the better B/P ratio of 46 may be explained by its lower total polar surface area (TPSA) and higher lipophilicity, as

shown in Table 7. On the basis of these results, compound 46 showed promise with the best brain to plasma ratio, but further optimization would be needed to resolve metabolic clearance and increase absolute levels.

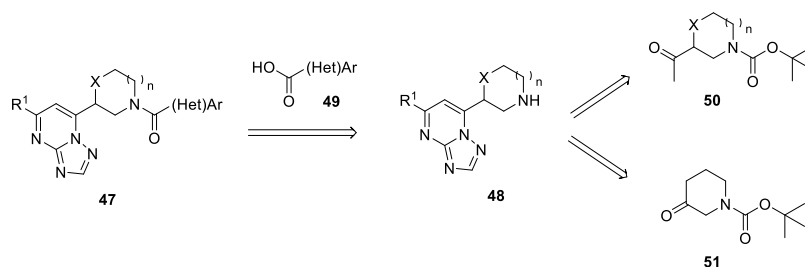
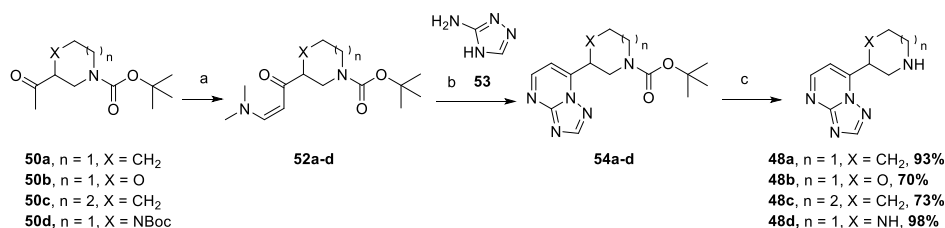
An *in vivo* target occupancy assay was used to evaluate PDE2 target engagement of compounds 42 and 46 in rat brain slices. A tritiated version of compound 1^{27,28} was used as a radioactive tracer (10 μ Ci i.v.). In this experiment, MP-10⁴² (2.5 mg/kg s.c.), a potent and selective PDE10 inhibitor, was pre-dosed because it was found to greatly increase the signal-to-noise ratio of the tracer.²⁷ This is understood to be due to PDE10 inhibition, leading to increased intracellular cGMP that is known to activate PDE2 through its GAF domain. Using this protocol, 42 showed 92% occupancy of PDE2 after p.o. administration (10 mg/kg suspension in 20% HP- β -CD solution). Compound 46 showed 90% PDE2 occupancy after s.c. administration (10 mg/kg suspension in 20% HP- β -CD solution).

Chemistry. A general retrosynthesis toward targeted amide compounds⁵⁰ is outlined in Scheme 1. The final compounds 47 were synthesized via amide coupling between the cyclic amines 48 and readily accessible or commercially available (hetero)aryl carboxylic acids 49. In turn, triazolopyrimidine-amines 48 were obtained from the acetylaminines 50 or from the piperidin-3-one 51 via known procedures.

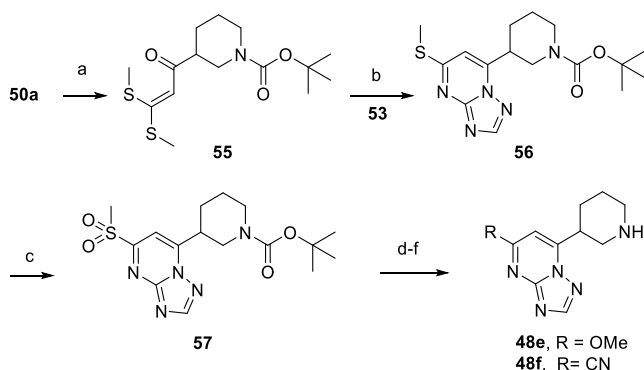
5-Unsubstituted triazolo[1,5-a]pyrimidine amines 48a–d were prepared, as shown in Scheme 2. Thus, condensation of the Boc-protected acetylaminines 50a–d with *N,N*-dimethylformamide dimethylacetal (DMF/DMA) provided the intermediate 3-dimethylaminobuten-2-ones 52a–d, which were then cyclized with 1*H*-1,2,4-triazol-3-amine (53) in acetic acid at 100 $^{\circ}$ C, to provide triazolopyrimidines 54a–d. Cleavage of the Boc-protecting group in 54a–d gave the desired intermediates 48a–d. Optionally, intermediates 48a–b were also separated in their enantiomers via supercritical fluid chromatography (SFC) purification to provide intermediates 48aa (R)–48ab (S) and 48ba (R)–48bb (S), respectively.⁵¹

The synthesis of 5-substituted triazolopyrimidine amines 48e–f commenced with the condensation of 3-acetylpiperidine 50a with carbon disulfide, followed by *S*-methylation using methyl iodide and sodium hydride, which gave the bismethylsulfanyl butenone intermediate 55 (Scheme 3). Cyclization of 55 with the aminotriazole 53 provided the 5-thiomethyl-triazolopyrimidine 56. Oxidation of the thiomethyl substituent in 56 with mCPBA gave the corresponding sulfone 57, which was then converted via aromatic nucleophilic substitution with sodium methoxide and sodium cyanide to the respective

Scheme 1. General Retrosynthetic Route

Scheme 2. Synthesis of Intermediates 48a–d^a

^aReagents and conditions: (a) DMF/DMA, 120 °C, 3 h; (b) AcOH, 100 °C, 1 h, 28–62% over 2 steps; (c) HCl, 1,4-dioxane, RT, 1 h, 70–93%.

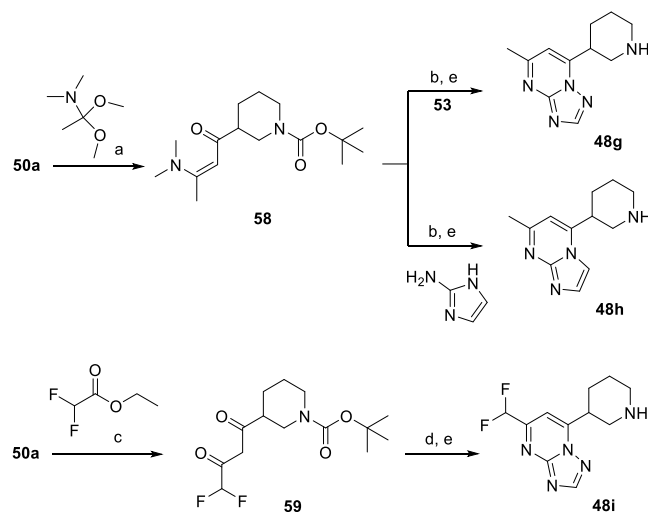
Scheme 3. Synthesis of Intermediates 48e–f^a

^aReagents and conditions: (a) NaH, CS₂, CH₃I; THF, 0 °C–RT, 16 h, 21%; (b) 150 °C, 3 h, 12%; (c) mCPBA, CHCl₃, 60 °C, 2 h, 99%; (d) R = OMe: NaOMe, MeOH, RT, 30 min; (e) R = CN: NaCN, DMSO, RT, 30 min, 43%; (f) TFA, DCM, RT, 2 h; R = OMe: 99%, R = CN: 68%.

methoxy (48e) and cyano (48f) triazolopyrimidine intermediates after Boc deprotection.

The synthetic sequence for the preparation of intermediates 48g–h is shown in Scheme 4 and was similar to Scheme 1 for the synthesis of intermediates 48a–d. Condensation of Boc-protected 3-acetylpiperidine 50a with *N,N*-dimethylacetamide dimethyl acetal afforded the enaminone 58, which was then reacted with either 1*H*-imidazol-2-amine or with 53 to provide the corresponding 5- or 7-methyl-substituted [1,2,4]triazolo[1,5-*a*]pyrimidine (48g) or imidazo[1,2-*a*]pyrimidine (48h) intermediate amines. The 5-(difluoromethyl)-7-(3-piperidyl)-[1,2,4]triazolo[1,5-*a*]pyrimidine amine derivative 48i was obtained in three steps starting from 50a. First, the condensation of 50a with ethyl difluoroacetate afforded the 1,3-dicarbonyl intermediate 59 in excellent yield. Then, reaction of 59 with 53 led to intermediate 48i after Boc cleavage.

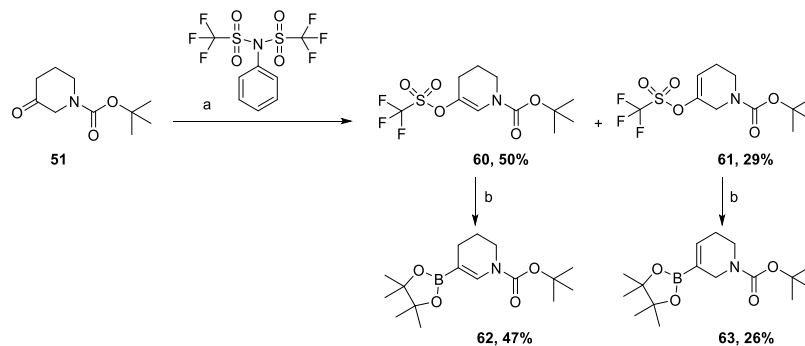
For the preparation of the piperidine intermediates 48j–o, the boronic ester intermediates 62 and 63 were prepared from Boc-protected piperidine-3-one 51, as shown in Scheme 5. First,

Scheme 4. Synthesis of Intermediates 48g–i^a

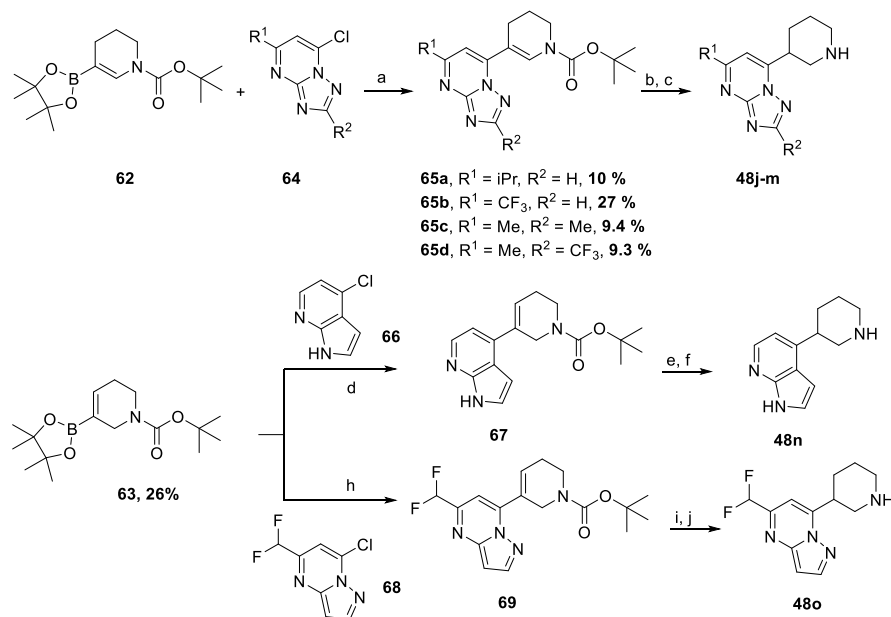
^aReagents and conditions: (a) 120 °C, 3 h, 95%; (b) AcOH, 120 °C, 30 min, for 53: 80%, for 2-aminoimidazole: 55%; (c) C₆H₆, KOtBu, 0 °C–RT, 5 h, 98%; (d) (i) 53, DMF, 60 °C, 28 h; (ii) Et₃N, di-*tert*-butyl dicarbonate, 0 °C–RT, 1 h, 86%; (e) HCl, iPrOH, MeOH, 1–24 h, RT (48g, 55%; 48h, 95%; 48i, 61%).

51 was treated with LDA in the presence of *N*-phenylbis(trifluoromethanesulfonimide), affording a mixture of triflate enol ethers 60 and 61 that could be separated by column chromatography on a silica gel. Both compounds were converted to the corresponding boronate esters 62 and 63 in moderate yields via palladium-catalyzed reaction with bis-(pinacolato)diboron.

Boronic ester 62 was used in Suzuki cross-coupling reactions with chloro-triazolopyrimidines 64 and tetrakis-(triphenylphosphine)palladium(0) to give tetrahydropyridines 65a–d in modest yields because of the instability of the chloro-heteroaromatic derivatives 64, which hydrolyzed in the reaction conditions. The double bond in derivatives 65a–d was satisfactorily reduced under catalytic hydrogenation conditions, leading to the corresponding *N*-Boc-protected piperidines using

Scheme 5. Synthesis of 3,4- and 3,6-Dihydropyridyl Pinacol Boronic Ester Intermediates^a

^aReagents and conditions: (a) LDA, THF, $-78\text{ }^{\circ}\text{C}$ –RT, 16 h; (b) AcOK, Pin₂B₂, Pd(OAc)₂, PCy₃, 2-MeTHF, $80\text{ }^{\circ}\text{C}$, 16 h.

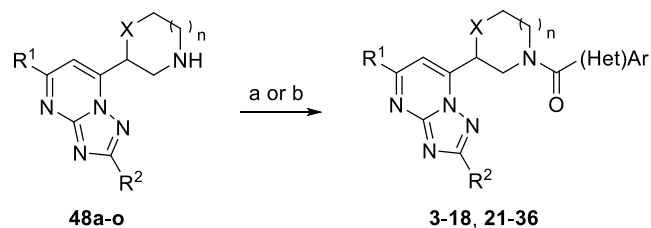
Scheme 6. Synthesis of Intermediates 48j–48o^a

^aReagents and conditions: (a) Pd(PPh₃)₄, Na₂CO₃, 1,4-dioxane, EtOH, water, (9–27%). (b) H₂, Pd/C, MeOH, (R¹ = iPr, R² = H, 99%) or Pt/C (47%–88%); (c) HCl, iPrOH. MeOH, RT, 16 h (94–100%); (d) (SiPr)Pd(allyl)Cl, Na₂CO₃, 1,4-dioxane, EtOH, water (18%); (e) H₂, Pt/C, MeOH (99%); (f) HCl, iPrOH. MeOH, RT, 16 h, 91%; (h) (SiPr)Pd(allyl)Cl, Na₂CO₃, 1,4-dioxane, EtOH, water, 63%; (i) H₂, Pd/C, MeOH, (R¹ = iPr, R² = H, 86%); (j) HCl, iPrOH. MeOH, RT, 16 h, 94%.

either Pd/C or Pt/C as catalysts. Boc removal under acidic conditions provided piperidines **48j–m** in nearly quantitative yields. In a similar fashion, the boronic ester **63** was coupled to 4-chloroazaindole (**66**) and chloro pyrazolopyrimidine (**68**) using the *N*-heterocyclic carbene complex allyl[1,3-bis(2,6-diisopropylphenyl)imidazol-2-ylidene]chloropalladium(II) to provide tetrahydropyridines **67** and **69**, respectively. Catalytic reduction of the double bond in **67** and **69**, followed by Boc cleavage afforded the piperidines **48n** and **48o**, respectively (Scheme 6).

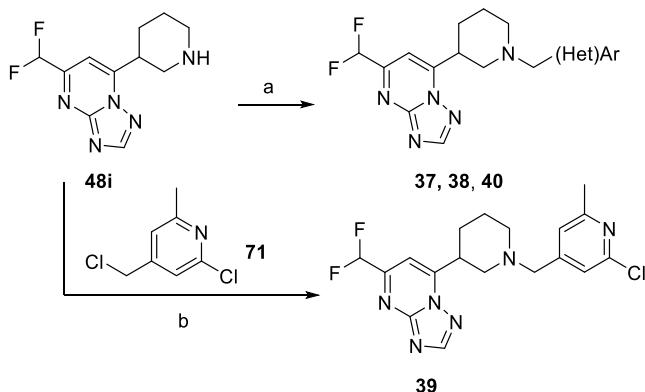
The piperidine intermediates **48a–o** were transformed into the final targets via amide coupling reaction conditions with the corresponding carboxylic acids or acid chlorides (Scheme 7).

Piperidines bearing benzyl-like substituents at the nitrogen atom **37**, **38**, and **40** were prepared by reductive amination with sodium triacetoxyborohydride of difluoromethyltriazolopyrimidine **48i** with readily available aldehydes **70** (Scheme 8). Alternatively, substitution-alkylation of **48i** (Scheme 7) with the derivative **71** provided the benzylamine **39** in 37% yield.

Scheme 7. Synthesis of Compounds **3**, **7–18**, **21–36**^a

^aReagents and conditions: for compounds **3–7**, **10–12**, **14–18**, and **21–36** (a) (Het)ArCOOH, HBTU, DIPEA, DCM, 1 h, 15–95%; for compounds **8**, **9**, and **13** (b) (Het)ArCOCl, DIPEA, DCM, RT, 1 h, 11–80%.

Finally, the target compounds containing a trisubstituted piperidine were prepared following the synthetic route outlined in Scheme 9. Thus, catalytic hydrogenation of commercially available methyl 4-methylpyridine-3-carboxylate **72** using PtO₂ in acetic acid (Scheme 9), followed by Boc-protection of the

Scheme 8. Synthesis of Compounds 37–40^a

^aReagents and conditions: (a) NaBH(OAc)₃, DIPEA, DCM, RT, 4 h (36%–86%); (b) DIPEA, DMF, 60 °C, 4 h (37%).

resulting piperidine, provided methyl 4-methylpiperidine-3-carboxylate as a *cis/trans* mixture of diastereoisomers, with *trans* isomer **73** being the major component in the mixture. The desired diastereoisomer **73** could be separated by column chromatography. Saponification of the methyl ester in **73**, followed by CDI-mediated coupling with methoxymethylamine, provided Weinreb amide **74**. Addition of methylmagnesium bromide to amide **74** led to the methylketone **75**, which was then condensed with difluoroethylacetate to afford the 1,3-dicarbonylic compound **76**. In turn, **76** was reacted with 2-aminotriazole **53** to provide the triazolopyrimidine intermediate **77**. The Boc N-protecting group was partially cleaved in the cyclization reaction conditions; therefore, the crude reaction mixture (RM) was treated with Boc₂O to reprotect the deprotected intermediate in order to enable a better separation of **77** from the reaction mixture. Deprotection of the Boc N-protecting group under acidic conditions provided piperidine **78**. SFC purification at this stage allowed isolation of the eutomer of **78**, which was then submitted to amide coupling or to nucleophilic aromatic substitution conditions to provide the target molecules **41–43** and **44–46**, respectively.⁵⁰

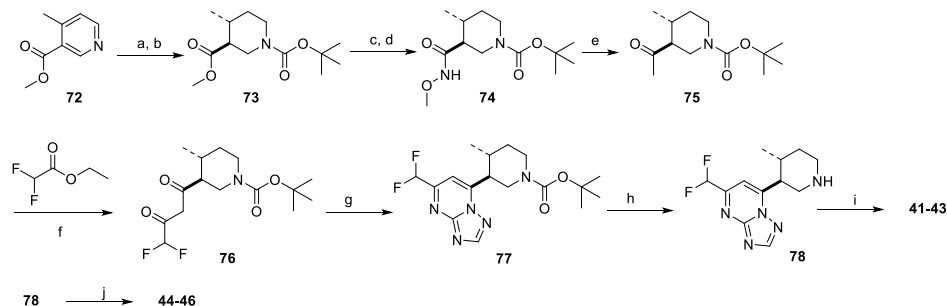
CONCLUSIONS

The initial exploration of a triazolopyrimidine PDE2A inhibitor HTS hit (**3**) has been described. Guided by the X-ray structure and later with FEP relative binding energy calculations, we were

able to rapidly identify highly potent PDE2A inhibitors with greater than 100-fold selectivity over PDE3A and PDE10A. Furthermore, several examples (**39**, **42**, and **46**) demonstrated that selectivity versus other members of the PDE enzyme family was resolved by targeting the Q2 pocket. Racemization issues were overcome by the introduction of a methyl substituent in the central core, leading to an optimal trisubstituted piperidine scaffold. Four lead compounds were evaluated to test BBB penetration with **42** and **46** showing most promise, and *in vivo* PDE2 target engagement was confirmed for these two compounds via p.o. and s.c. administration, respectively. The FEP calculations were useful for identifying unexpectedly active compounds from amongst the virtual libraries that were profiled. We consider the approach of FEP calculations on increasingly larger virtual libraries and chemical spaces to offer significant potential for future LO efforts.⁵² It provides a way to identify stand-out or unexpectedly active compounds, thereby having a larger impact on the LO process. Finally, despite the good results here, it is important to note that FEP can be problematic in real-world prospective applications as described in the recent large report of Schindler et al.⁵³ We will follow up with a detailed report on the optimization of leads from this series.

EXPERIMENTAL SECTION

X-ray Crystallography. Cocrystals of C-His tagged human 579-921 PDE2A with HTS hit **3** and lead **39** were grown in 0.2 M MgCl₂, 0.1 M Tris-HCl pH 8.0 and 20% PEG 3350 and 0.2 M MgCl₂, 0.1 M Tris-HCl pH 8.0 and 24% PEG 3350, respectively, both in the presence of 1 mM compound. Crystals were flash-frozen directly from the hanging drop without additional cryo-protectant by plunging into liquid nitrogen. The HTS hit **3** data set was collected in house on a Rigaku Saturn 944 CCD detector. The lead **39** data set was collected at the Diamond Light Source at beamline 102 on an ADSC Q315 CCD detector. Data sets were indexed, integrated, and scaled using MOSFLM and SCALA (CCP4). The PDE2A model with PDB ID 1Z1L was used for molecular replacement with the data sets using PHASER (CCP4). The resulting models were then given 10 cycles of atomic refinement with tight geometric weights using REFMAC5. In each case, the difference electron density map calculated after molecular replacement and initial refinement was examined for the presence of possible ligands. Once the ligand electron density was located, a molecular structure file and refinement library file were produced using SKETCHER (CCP4). The ligands were fitted into the electron density using COOT and refined using REFMAC5 (CCP4). Water molecules were then added using the water placement option in COOT and refined using REFMAC5 (CCP4). Metal ions were also added and

Scheme 9. Synthesis of Compounds 41–43^a

^aReagents and conditions: (a) H₂, PtO₂, AcOH, 50 °C, 5 d, 97%; (b) Boc₂O, DCM, DIPEA, DMAP, RT, 1 h, 75%; (c) NaOH, MeOH, RT, 14 h, 100%; (d) CDI, MeNHOMe, Et₃N, THF, ACN, RT–80 °C, 7 d, 100%; (e) MeMgBr, THF, –15 °C–RT, 1 h, 90%; (f) KOtBu, toluene, 0 °C–RT, 2 h, 100%; (g) (i) **53**, DMF, 80 °C, 24 h; (ii) Boc₂O, Et₃N, RT, 30 min, 30%; (h) HCl, iPrOH, MeOH, 2 h, RT (72%); (i) (Het)ArCOOH, HBTU, DIPEA, DCM, 1 h, 15–95%; (j) (Het)Cl or (Het)Br, DIPEA, *n*BuOH, 160 °C, 4 h (6–41%).

refined. The structural geometry of both the protein and ligand were finally checked using Maestro and MOE.

Protocols for Measuring Inhibition of PDE's *In Vitro*. PDEs 1B1 and 11A4 were expressed in HEK cells from full-length human recombinant clones. Human recombinant PDEs 2A, 4D3, 5A3, 7A1, 9A1, 10A2, and rat PDE10A2 were expressed in Sf9 cells using a recombinant baculovirus construct containing the full-length sequence containing a 6xHis sequence, following the start Met to allow metal affinity purification of the recombinant protein. Cells were harvested, and the PDE protein was purified by metal chelate chromatography on Ni-sepharose 6FF. PDE6A, PDE3A, and PDE8A were purchased as partially purified Sf9 cell lysates (Scottish Biomedical, UK). All enzymes were diluted in 50 mM Tris pH 7.8, 1.7 mM EGTA, and 8.3 mM MgCl₂, except for PDE9A, which was diluted in 50 mM Tris pH 7.8 and 5 mM MnCl₂, and PDE1B was diluted in 50 mM Tris pH 7.8, 8.3 mM MgCl₂, complemented with 624 U/mL calmodulin and 800 μM CaCl₂. The affinity of the compounds for PDEs was measured by a scintillation proximity assay (SPA). PDE yttrium silicate SPA beads allow the PDE activity to be measured by direct binding of the primary phosphate groups of noncyclic AMP or GMP to the beads via an iron complex chelation mechanism. The amount of bound tritiated product ([³H]-AMP or [³H]-GMP) was measured by liquid scintillation counting in a TopCount (Packard).

Compounds were dissolved and diluted in 100% dimethyl sulfoxide (DMSO) in polystyrene plates to a concentration of 100-fold the final concentration in the assay. Rat or human PDE10A or human PDE2A or human PDE3A or PDE3B enzyme solution (10 μL) was added to 20 μL of incubation buffer (50 mM Tris pH 7.8, 8.3 mM MgCl₂, 1.7 mM EGTA), 10 μL of substrate solution consisting of a mixture of nontritiated and tritiated substrate (60 nM cAMP, 0.008 μCi ³H-cAMP for human and rat PDE10A, 10 μM cGMP, 0.01 μCi ³H-cGMP for PDE2A, 0.1 μM cAMP, 0.024 μCi ³H-cAMP for PDE3A or PDE3B), and 0.4 μL of compound in 100% DMSO in a 384-well plate and incubated for 60 min at room temperature for human and rat PDE10A and PDE3A/B or for 40 min at room temperature for PDE2A. After incubation, the reaction was stopped with 20 μL of stop solution, consisting of PDE SPA beads (17.8 mg beads/mL in 18 mM zinc sulfate for human and rat PDE10A or in 200 mM zinc sulfate for PDE2A and PDE3A, and in 400 mM zinc sulfate for PDE3B). After sedimentation of the beads for 30 min, the radioactivity was measured in a PerkinElmer TopCount scintillation counter and results were expressed as counts per minute (cpm). To measure the low control, no enzyme was added to the reaction mixture. The same assay principle was applied for the measurement of the inhibition of other members of the PDE family, with appropriate modifications of enzyme concentration, incubation buffer, substrate solution, incubation time, and stop solution. Data were calculated as the percentage of inhibition of total activity measured in the absence of test compound (% control). A best-fit curve was fitted by a minimum sum of squares method to the plot of % control versus compound concentration, from which an IC₅₀ value (inhibitory concentration causing 50% inhibition of hydrolysis) was obtained. Compounds 1–40 were tested on rat PDE10A, and 41–46 were tested on human PDE10A.

CYP450 Inhibition Assay. The potential to reversibly inhibit the major human P450 isoforms (CYP450s 1A2, 2C9, 2C19, 2D6, and 3A4) was determined in the CYP450 inhibition cocktail assay. Test compounds are incubated across a concentration range (five concentrations) with human liver microsomes and probe substrates for each of the six isoforms (CYP450 1A2, 2C8, 2C9, 2C19, and 2D6 in cocktail format and 3A4 in the single probe format) to estimate the IC₅₀ for inhibition of the probe substrate by the test compound. After the defined incubation time, the reaction is quenched and samples are centrifuged and prepared for analysis by liquid chromatography/mass spectrometry (LC/MS). The percentage inhibition of the probe substrate metabolite formation is plotted against inhibitor concentration and an IC₅₀ calculated by curve fitting.

Microsomal Metabolic Stability Assay. The metabolic stability of a test compound was tested at Cyprotex by using liver microsomes (0.5 mg/mL protein) from human and preclinical species incubated up to 60 min at 37 °C with 1 μM of the test compound. The *in vitro*

metabolic half-life ($t_{1/2}$) is calculated using the slope of the log–linear regression from the percentage parent compound remaining versus time relationship. The *in vitro* intrinsic clearance (Cl_{int}) (mL/min/mg microsomal protein) is derived from the half-life taking into account the incubation volume and the weight of microsomal protein in the incubation.

***In Vivo* PDE2 Occupancy Method.** Male Wistar rats were treated by systemic administration (s.c. or p.o.) of vehicle or single dose of selective PDE2A inhibitors ($n = 3$ per dose). After 15 min, every rat received a s.c. injection of the PDE10 inhibitor MP-10 at the dose of 2.5 mg/kg, followed 55 min later by an i.v. injection of the selective PDE2A radioligand [³H]-1.^{27,28} Dosing rats with MP-10,⁴² a potent and selective PDE10 inhibitor, prior to the radioligand injection allowed to increase the signal to noise ratio of [³H]-1 because its binding is increased when intracellular cGMP concentration increased.^{27,28} Rats were sacrificed 5 min after the tracer injection, and their brains were dissected and frozen. Then, 20 μm of thick coronal sections were cut using a cryostat, collected on glass slides, and dried. Brain sections were loaded in a β-imager for 12 h. The specific binding was determined as the difference between [³H]-1 binding quantified in the striatum (a brain area showing a high density of PDE2A) and in the cerebellum (a brain area where PDE2A is virtually absent). Occupancy was calculated as the inhibition of specific [³H]-1 binding in drug-treated animals relative to vehicle-treated animals. The percentage of PDE2A occupancy was measured at one dosage.

Computational Docking Procedure. Docking used the Glide software from Schrödinger Inc. The corresponding crystal structure solved with 39 was used. The protein was prepared using the protein preparation wizard⁵⁴ in Maestro.⁵⁵ Hydrogen-bond constraints were enforced with Gln812 and Gln859 to ensure accurate placement of the triazolopyrimidine scaffold. All molecules were prepared for docking using the LigPrep tool. All default settings were used, and ionization states were manually checked. The ligands were parameterized for use with the OPLSv2.1 force field up front using the tools available in Maestro. The Glide XP scoring function was used with expanded sampling, all other docking parameters were set to the defaults. Results were visually inspected to ensure that each molecule adopted the desired binding mode consistent with the crystal structure.

Computational FEP Procedure. All FEP calculations were conducted using the Schrödinger molecular modeling suite version 2015-1, the implementation is often referred to as FEP+. Calculations were set up using the mapper technology to define the perturbations. Default protocols were used with a 5 ns simulation length for ligands both in complex and in solution. As mentioned above, the FEP calculations were performed with the molecules in the chosen docked pose. Molecules were treated in a neutral form and missing OPLS force-field parameters were calculated and fitted up front using the force-field builder tool. The results of the simulations with 5 ns simulation time and 12 Å windows were used to define the molecules recommended for synthesis in the prospective application. The experimental pIC₅₀ were converted to expected binding free energies at 298 K using the relation $RT \ln(IC_{50})$; any offset with respect to binding free energy cancels when comparing relative differences. The calculations deliver the RBFE differences between compounds, and the resulting $\delta\delta G$'s were fitted to the mean of the experimental δG to provide the calculated δG with reduced offset. MUEs are reported by comparing experimental and calculated δG (kcal/mol) and shown with the corresponding $\pm 99\%$ confidence interval. The force field available at the time was OPLSv2.1. To compare with newer versions, the predicted ΔG for the retrospective dataset was recalculated using Schrödinger suite 2019–3 and OPLSv3e. A high degree of correlation was seen with OPLSv2.1, $R = 0.9$. Input structures for FEP calculations are provided in the [Supporting Information](#).

Experimental Procedures and Compound Characterization. All reactions were carried out by employing standard chemical techniques under an inert atmosphere. Solvents used for extraction, washing, and chromatography were of high-performance liquid chromatography (HPLC) grade. Unless otherwise noted, all solvents and chemicals used were of reagent grade. Anhydrous solvents tetrahydrofuran (THF), DCM, and DMF were purchased from

Sigma-Aldrich or Acros. All final compounds were characterized by ^1H NMR and LC/MS. ^1H nuclear magnetic resonance spectra were recorded on Bruker spectrometers: DPX-360 MHz, DPX-400 MHz, Bruker Avance Neo spectrometer operating at 400 MHz, or on a Bruker Avance III-HD spectrometer operating at 600 MHz using chloroform- d (deuterated chloroform, CDCl_3) or DMSO- d_6 (deuterated DMSO, dimethyl- d_6 sulfoxide) as solvents. Chemical shifts (δ) are reported in parts per million relative to tetramethylsilane, which was used as the internal standard.

Elemental analyses were performed with a Carlo-Erba EA1110 analyzer. Thin-layer chromatography (TLC) was carried out on silica gel 60 F254 plates (Merck) using reagent grade solvents. Open column chromatography was performed on a silica gel, mesh 230–400 particle size and 60 Å pore size (Merck) under standard techniques. Automated flash column chromatography was performed using ready-to-connect cartridges from Merck, on an irregular silica gel, particle size 15–40 μm (normal phase disposable flash columns) on a SPOT or LAFLASH system from Armen Instrument. All final compounds were confirmed to be >95% pure via HPLC methods. All the LC/MS analyses were performed using an Agilent G1956A LC/MS quadrupole coupled to an Agilent 1100 series LC system consisting of a binary pump with a degasser, autosampler, thermostated column compartment, and diode array detector. The mass spectrometer was operated with an atmospheric pressure electrospray ionization source in the positive ion mode. The capillary voltage was set to 3000 V, and the fragmentor voltage was set to 70 V, and the quadrupole temperature was maintained at 100 °C. The drying gas flow and temperature values were 12.0 L/min and 350 °C, respectively. Nitrogen was used as the nebulizer gas at a pressure of 35 psig. Data acquisition was performed with Agilent ChemStation software. Analyses were carried out on a YMC pack ODS-AQ C18 column (50 mm long \times 4.6 mm I.D.; 3 μm particle size) at 35 °C, with a flow rate of 2.6 mL/min. A gradient elution was performed from 95% (water + 0.1% formic acid)/5% acetonitrile to 5% (water + 0.1% formic acid)/95% acetonitrile in 4.8 min; the resulting composition was held for 1.0 min; from 5% (water + 0.1% formic acid)/95% acetonitrile to 95% (water + 0.1% formic acid)/5% acetonitrile in 0.2 min. The standard injection volume was 2 μL . Acquisition ranges were set to 190–400 nm for the UV-PDA detector and 100–1400 m/z for the MS detector. Optical rotations measurements were carried out on a 341 PerkinElmer polarimeter in the indicated solvents. Melting points were determined with a DSC823e (Mettler Toledo) and were measured with a temperature gradient of 30 °C/min. The reported values are peak values. Purities of all new compounds were determined by analytical reverse phase (RP)-HPLC using the area percentage method on the UV trace recorded at a wavelength of 254 nm, and compounds were found to have \geq 95% purity unless otherwise specified.

The absolute stereochemical configuration for some of the compounds was determined using vibrational circular dichroism (VCD). They were measured on a Bruker Equinox 55 equipped with a PMA 37 in a KBr liquid cell using CD_2Cl_2 as the solvent (PEM: 1350 cm^{-1} , LIA: 1 mV, resolution: 4 cm^{-1}). A description on the use of VCD for the WO 2018/083101 PCT/EP2017/077918-29-5 10 15 20 25 30 determination of absolute configuration can be found in Dyatkin A.B. et al., *Chirality*, 14, 215–219 (2002). Ab initio calculations: A thorough conformational search was performed at molecular mechanics level using a MacroModel to do a mixed torsional/low-mode sampling with the OPLS-2005 force field. The located minima were optimized using Jaguar at the B3LYP/6-31G** level with a Poisson–Boltzmann continuum solvation model to mimic a dichloromethane solvent. All conformations within 10 kJ/mol interval were used to simulate VCD and IR spectra. Dipole and rotational strengths were calculated at the same B3LYP/6-31G** level using Jaguar. The calculated VCD spectra, generated after scaling the frequencies with a factor of 0.97, converting to a Lorentzian bandshape, and summing up the contribution of each conformer assuming a Boltzmann ensemble, were visually compared with the experimental spectra for assigning the correct stereo chemistry.

Intermediate 52b, *tert*-Butyl 2-[3-(Dimethylamino)prop-2-enoyl]-morpholine-4-carboxylate. A stirred mixture of *t*-butyl 2-acetylmorpholine-4-carboxylate (25 g, 0.11 mol) in *N,N*-dimethylacetamide

dimethyl acetal (58 mL) was heated at 100 °C for 16 h. The reaction mixture was concentrated *in vacuo* to give the title compound (30 g), which was used in the next step without further purification.

Intermediate 52c, *tert*-Butyl 3-[3-(Dimethylamino)prop-2-enoyl]-azepane-1-carboxylate. Prepared with the same procedure for **52b**, starting from *tert*-butyl 3-acetylazepane-1-carboxylate [1782629-29-1] (18.2 g) to give the title compound, (22 g), which was used in the next step without further purification.

Intermediate 52d, *Di-tert*-butyl 2-Acetylpiperazine-1,4-dicarboxylate, Prepared in Three Steps. Step 1, intermediate **79**, *di-tert*-butyl 2-[methoxy(methyl)carbamoyl]piperazine-1,4-dicarboxylate. To a suspension of 1,4-bis[(*t*-butoxy)carbonyl]piperazine-2-carboxylic acid [173774-48-6] (60 g, 0.18 mol) in THF (285 mL) was added *di-1H*-imidazol-1-yl-methanone (CDI, 40 g, 0.25 mol), and the mixture was stirred at RT for 2 h. In another flask, to a suspension of *N*-methoxy-methanamine hydrochloride (24.45 g, 0.25 mol) in ACN (190 mL) was added trimethylamine (36.35 mL, 0.26 mol). Both mixtures were combined and stirred at RT for 16 h. The solvents were evaporated. The residue was dissolved in DCM and washed with water, 20% AcOH solution, and finally an aqueous NaOH (1 N) solution. The organic layer was dried over MgSO_4 , filtered, and evaporated. The product was purified by column chromatography (silica gel, eluent: a gradient DCM 100 to 3% MeOH in DCM). The pure fractions were evaporated, yielding intermediate **79** (56.8 g, 83.7% yield). ^1H NMR (400 MHz, DMSO- d_6): δ ppm 1.37 (d, $J = 6.06$ Hz, 18H), 2.86–2.96 (m, 1H), 3.06–3.12 (m, 3H), 3.22–3.34 (m, 1H), 3.39–3.55 (m, 1H), 3.59–3.63 (m, 1H), 3.73 (s, 3H), 3.76–3.84 (m, 1H), 4.11–4.19 (m, 1H), 4.70 (br d, $J = 2.83$ Hz, 1H). Step 2, intermediate **80**, *di-tert*-butyl 2-acetylpiperazine-1,4-dicarboxylate. Intermediate **77** (56.8 g, 0.15 mol) in THF (200 mL) was charged in a flask under N_2 and cooled to 0 °C. Methylmagnesium bromide (265 mL, 1.4 M in toluene/THF 75/25) was added dropwise, with the temperature not exceeding 15 °C. After addition, the reaction mixture was stirred at RT for 1 h. Then, the reaction mixture was poured on ice with 100 mL of AcOH. The product was extracted with Et_2O , and the organic layer was washed with a 5% NaHCO_3 solution. The organic layer was dried over MgSO_4 , filtered, and evaporated to give intermediate **80** (36.6 g, 73%), used as such in the next step. Gas chromatography–MS m/z 328 (M). Step 3, intermediate **52d**, *di-tert*-butyl 2-acetylpiperazine-1,4-dicarboxylate. That was prepared with the same procedure as **52b**, from *di-tert*-butyl 2-acetylpiperazine-1,4-dicarboxylate (intermediate **78**) (10 g) to give the title compound (11 g, 94%). MS (ESI) m/z : 384 [M + H] $^+$.

Representative Procedure for the Preparation of Intermediates 54a–54d. **Intermediate 54a**, *tert*-Butyl 3-[[1,2,4]Triazolo[1,5-*a*]pyrimidin-7-yl]piperidine-1-carboxylate. Intermediate **52a** (33.0 g, 0.12 mol), 1*H*-1,2,4-triazol-5-amine hydrochloride (1:1) (12.3 g, 0.14 mol), and AcOH (75 mL) were stirred at 130 °C for 1 h. The reaction mixture was cooled on an ice bath and left under stirring overnight at RT. The reaction mixture was concentrated *in vacuo*, co-evaporated with toluene, diluted with Et_2O (0.7 L), and then poured onto ice (0.5 L). The layers were separated, and the aqueous layer was back extracted with Et_2O (3 \times 0.3 L). The combined organic layers were treated with brine, dried over MgSO_4 , filtered, and evaporated to give the title compound (racemic) as a brown oil (25 g, 70.5%). MS (ESI) m/z : 304 [M + H] $^+$. This material could be used as such. Alternatively, **54a** was also separated into enantiomers **54aa** and **54ab** by purification by Prep SFC (stationary phase: CHIRALPAK Daicel OJ 20 \times 250 mm; mobile phase: CO_2 , MeOH) yielding intermediate **54aa** (R_t, 10 g, 28%, R_t = 5.59 min) and intermediate **54ab** (S_t, 10 g, 28%, R_t = 7.4 min).

Intermediate 54b, *tert*-Butyl 2-[[1,2,4]Triazolo[1,5-*a*]pyrimidin-7-yl]morpholine-4-carboxylate. Prepared with the same procedure for **54a**, starting from intermediate **52b** (30 g, 0.11 mol) to give the title compound **54b** (racemic mixture, 19 g, 62%) after purification on a silica gel (eluent: DCM, 1% MeOH in DCM, 2%, 4%). MS (ESI) m/z : 305 [M + H] $^+$.

Intermediate 54c, *tert*-Butyl 3-[[1,2,4]Triazolo[1,5-*a*]pyrimidin-7-yl]azepane-1-carboxylate. Prepared with the same procedure for **54a**, starting from intermediate **52c** (5.0 g, 16.87 mmol) to give 1.69 g of the title compound **54c** (racemic mixture, 31.56%) after purification on a

silica gel (eluent: DCM, 1% MeOH in DCM, 2%). MS (ESI) m/z : 318 $[M + H]^+$.

Intermediate 54d, Di-*tert*-butyl 2-([1,2,4]Triazolo[1,5-*a*]pyrimidin-7-yl)piperazine-1,4-dicarboxylate. Prepared with the same procedure for **54a**, starting from intermediate **52d** (5 g, 13.04 mmol) to give 2.42 g of the title compound **54d** (racemic mixture, 40%) after purification on a silica gel (eluent: DCM, 1% MeOH in DCM, 2%). MS (ESI) m/z : 405 $[M + H]^+$.

Intermediate 48a, 7-(3-Piperidyl)-[1,2,4]triazolo[1,5-*a*]pyrimidine. To a solution of intermediate **54a** (53.8 g, 0.18 mol) in 1,4 dioxane (600 mL) was added HCl-1,4 dioxane (200 mL, 4 M), and the reaction mixture was stirred for 2 h at RT. The product crystallized out as a hydrochloric salt, and it was filtered and washed with ether to give very hygroscopic crystals. These were then triturated in ether, filtered, and dried to give the title compound **48a** as a HCl salt (racemic, 39.7 g, 93%). MS (ESI) 204 $[M + H]^+$. $^1\text{H NMR}$ (360 MHz, DMSO- d_6): δ ppm 1.74–2.00 (m, 3H), 2.13–2.23 (m, 1H), 2.76–3.01 (m, 1H), 3.22–3.40 (m, 2H), 3.58–3.66 (m, 1H), 3.94–4.04 (m, 1H), 7.34 (d, $J = 4.39$ Hz, 1H), 8.75 (s, 1H), 8.90 (d, $J = 4.76$ Hz, 1H), 9.27–9.51 (m, 1H), 9.65 (br d, $J = 9.15$ Hz, 1H). Anal. Calcd ($\text{C}_{25}\text{H}_{23}\text{N}_5\text{O}$): C, H, N. Alternatively, **48a** (4 g) was also separated into enantiomers by purification by Prep SFC (Stationary phase: CHIRALPAK Daicel OJ 20 \times 250 mm; mobile phase: CO_2 , EtOH with 0.5% *i*Pr NH_2) yielding intermediates: **48aa** (RI, 2g), $R_t = 6.43$ min, OR = +56.59° (589 nm, 20 °C, 0.42 w/v %; MeOH) and intermediate **48ab** (SI, 3 g), $R_t = 9.15$ min, OR = -53.9° (589 nm, 20 °C, 0.43 w/v %; MeOH).

Intermediate 48b, 2-([1,2,4]Triazolo[1,5-*a*]pyrimidin-7-yl)morpholine. To a solution of intermediate **54b** (19.0 g, 62.2 mmol) in MeOH (100 mL) was added HCl-Et $_2$ O (200 mL, 1 M), and the reaction mixture was stirred for 16 h at RT. The solvent was evaporated under reduced pressure, and the residue was placed in DCM and treated with a saturated aq sol of NaHCO_3 . The biphasic layer was separated, and then the aqueous layer was extracted 2 \times DCM. The combined OL was dried over MgSO_4 , filtered, and evaporated to provide **48b** (racemic, 9 g, 71%). MS (ESI) m/z : 206 $[M + H]^+$. $^1\text{H NMR}$ (360 MHz, DMSO- d_6): δ ppm 2.94–3.25 (m, 3H) 3.28–3.41 (m, 1H) 3.85 (br d, $J = 12.64$ Hz, 1H) 4.08–4.20 (m, 1H) 4.21–4.31 (m, 1H) 5.65 (dd, $J = 11.03, 2.45$ Hz, 1H) 7.40 (d, $J = 4.53$ Hz, 1H) 8.78 (s, 1H) 8.96 (d, $J = 4.53$ Hz, 1H) 10.03 (d, $J = 9.70$ Hz, 1H) 10.24 (br d, $J = 10.69$ Hz, 1H). This material was also separated into enantiomers by purification by Prep SFC (stationary phase: CHIRALPAK Daicel OJ 20 \times 250 mm; mobile phase: CO_2 , MeOH) yielding intermediates: **54ba** (RI, 1.52 g, 8%), $R_t = 8.19$ min and **54bb** (SI, 1.77 g), $R_t = 11.6$ min.

Intermediate 48c, 7-(Azepan-3-yl)-[1,2,4]triazolo[1,5-*a*]pyrimidine. Prepared as in the procedure for **48b**, starting from intermediate **54c** (600 mg, 1.89 mmol) to give the title compound **48c** (400 mg, 73%), and used in the next step without further purification. MS (ESI) m/z : 218 $[M + H]^+$.

Intermediate 48d, 7-Piperazin-2-yl-[1,2,4]triazolo[1,5-*a*]pyrimidine. Prepared as in the procedure for **48b**, starting from intermediate **54d** (2.42 g, 5.98 mmol) to give the title compound **48d** (1.85 g, 98%), and used in the next step without further purification.

Intermediate 55, *tert*-Butyl 3-[3,3-Bis(methylsulfonyl)prop-2-enoyl]piperidine-1-carboxylate. NaH (60% dispersion in mineral oil, 8.77 g, 0.22 mol) was added to a solution of *tert*-butyl 3-acetylpiperidine-1-carboxylate (**50a**, 45.3 g, 0.20 mol) in anhydrous THF (300 mL) at 0 °C under an atmosphere of N_2 , and the resulting mixture was stirred at this temperature for 10 min. After this time, carbon disulfide (16.7 g, 0.22 mol) and then methyl iodide (59.4 g, 0.42 mol) were added dropwise. The reaction mixture was allowed to reach RT and stirred for 4 h. Water was added, and the resulting mixture was extracted with EtOAc. The combined organic layer was washed with brine, dried over MgSO_4 , filtered, and evaporated under reduced pressure. The resulting residue was purified via flash column chromatography on a silica gel using a gradient (DCM, 0.25% MeOH in DCM, 0.5, 1%) as the eluent to give the title compound (13.88 g, 21%). MS (ESI) m/z : 332 $[M + H]^+$.

Intermediate 56, *tert*-Butyl 3-(5-Methylsulfonyl-[1,2,4]triazolo[1,5-*a*]pyrimidin-7-yl)piperidine-1-carboxylate. Intermediate **55** (8 g, 24.1 mmol) and 1*H*-1,2,4-triazol-5-amine hydrochloride (1:1) (2.03 g,

24.1 mmol) were stirred in melt at 150 °C for 3 h. The reaction mixture was cooled to RT and dissolved in DCM. The organic layer was washed with water, dried over MgSO_4 , filtered, and evaporated under reduced pressure. The resulting residue was purified by column chromatography on a silica gel using a gradient (DCM, 0.25% MeOH in DCM, 0.5, 1%) as the eluent to provide the title compound (1 g, 12%) MS (ESI) m/z : 350 $[M + H]^+$.

Intermediate 57, *tert*-Butyl 3-(5-Methylsulfonyl-[1,2,4]triazolo[1,5-*a*]pyrimidin-7-yl)piperidine-1-carboxylate. A solution of intermediate **56** (1.39 g, 3.98 mmol) and mCPBA (2.75 g, 15.9 mmol) in chloroform (CHCl_3 , 50 mL) was stirred at reflux for 2 h. After this time, the reaction mixture was cooled to RT, then washed with NaOH 1 N, dried over MgSO_4 , filtered, and evaporated *in vacuo* to yield the title compound (1.50 g, 99%), which was used as such in the next step. MS (ESI) m/z : 380 $[M - H]^+$.

Intermediate 81e, *tert*-Butyl 3-(5-Methoxy-[1,2,4]triazolo[1,5-*a*]pyrimidin-7-yl)piperidine-1-carboxylate. Sodium methoxide (NaOMe , 234 mg, 4.33 mmol) was added at RT to a solution of intermediate **57** (1.5 g, 3.93 mmol) in methanol (MeOH, 50 mL), and the resulting mixture was stirred at this temperature for 12 h. After this time, the solvent was evaporated *in vacuo* and the resulting residue was partitioned between water and DCM. The organic layer was separated, and then the aqueous layer was back extracted with DCM (2 \times). The combined organic layer was dried over MgSO_4 , filtered, and evaporated under reduced pressure. The resulting residue was purified by column chromatography on a silica gel using a gradient (DCM, 1% MeOH in DCM, 2%) as the eluent to provide the title compound (560 mg, 43%). MS (ESI) m/z : 334 $[M + H]^+$.

Intermediate 81f, *tert*-Butyl 3-(5-Cyano-[1,2,4]triazolo[1,5-*a*]pyrimidin-7-yl)piperidine-1-carboxylate. Intermediate **57** (950 mg, 2.50 mmol) and sodium cyanide (249 mg, 4.98 mmol) were stirred in DMSO (5 mL) at RT for 30 min. The reaction mixture was poured in water and extracted with EtOAc. The organic layer was washed with brine, dried on MgSO_4 , filtered, and evaporated under reduced pressure. The resulting residue was purified via flash column chromatography on a silica gel using a gradient (DCM, 1% MeOH in DCM, 2%) as the eluent to give intermediate **79f** (820 mg, 100%). MS (ESI) m/z : 329 $[M + H]^+$.

Intermediate 48e, 5-Methoxy-7-(3-piperidyl)-[1,2,4]triazolo[1,5-*a*]pyrimidine. TFA (0.626 mL, 8.18 mmol) was added at RT to a solution of intermediate **81e** (560 mg, 1.68 mmol) in DCM (50 mL), and the resulting mixture was stirred for 2 h at RT. Saturated aqueous NaHCO_3 solution was then added to the reaction mixture and stirred for 10 min. The organic layer was separated, dried on MgSO_4 , filtered, and evaporated under reduced pressure to give intermediate **48e** (390 mg, 99.5%), which was used in the next step without further purification.

Intermediate 48f, 7-(3-Piperidyl)-[1,2,4]triazolo[1,5-*a*]pyrimidine-5-carbonitrile. Prepared in a similar way to procedure **3b**, starting from intermediate **81f** (820 mg, 2.5 mmol) to give the title compound **48f** (390 mg, 68%), which was used in the next step without further purification.

Intermediate 81g, *tert*-Butyl 3-(5-Methyl-[1,2,4]triazolo[1,5-*a*]pyrimidin-7-yl)piperidine-1-carboxylate. **81g** is prepared in two steps. Step 1, intermediate **58**, *tert*-butyl 3-[(*Z*)-3-(dimethylamino)but-2-enoyl]piperidine-1-carboxylate. Intermediate **50a** (2.0 g, 8.8 mmol) was added to *N,N*-dimethylacetamide dimethyl acetal (3.52 g), and the mixture was refluxed for 3 h. The reaction mixture was evaporated to give the crude product, which was used as such in the next step (2.5 g, 95%). Step 2, intermediate **81g**, *tert*-butyl 3-(5-methyl-[1,2,4]triazolo[1,5-*a*]pyrimidin-7-yl)piperidine-1-carboxylate. A solution of intermediate **58** (2.5 g, 8.43 mmol) and 1*H*-1,2,4-triazol-5-amine hydrochloride (0.71 g, 8.43 mmol) in acetic acid (50 mL) was stirred at reflux during 30 min. Saturated aqueous Na_2CO_3 solution was added, and the product was extracted with DCM. The organic layer was dried on MgSO_4 , filtered, and evaporated. The resulting residue was purified by flash column chromatography on a silica gel using a gradient (DCM, 1% MeOH in DCM, 2%) as the eluent to give intermediate **81g** (2.14 g, 80%). MS (ESI) m/z : 318 $[M + H]^+$.

Intermediate 48g, 5-Methyl-7-(3-piperidyl)-[1,2,4]triazolo[1,5-*a*]pyrimidine and **54a**. Prepared according to procedure 3, starting from intermediate **81g** (2.14 g, 6.74 mmol), to give the title compound as a mixture with **54a** (1.07 g, 54.6%). ¹H NMR (360 MHz, DMSO-*d*₆): δ ppm 1.76–2.01 (m, 3H) 2.12–2.23 (m, 1H) 2.64 (s, 3H) 2.87–2.98 (m, 1H) 3.22–3.41 (m, 2H) 3.59 (br d, *J* = 11.71 Hz, 1H) 3.89–4.00 (m, 1H) 7.31 (s, 1H) 8.69 (s, 1H) 9.55 (br d, *J* = 10.25 Hz, 1H) 9.80 (br d, *J* = 10.25 Hz, 1H). MS (ESI) *m/z*: 218 [M + H]⁺.

Intermediate 82, tert-Butyl 3-(7-Methylimidazo[1,2-*a*]pyrimidin-5-yl)piperidine-1-carboxylate. Prepared in a similar way to intermediate **81g**, starting from intermediate **58** (2.5 g, 8.43 mmol) and 1H-imidazol-2-amine (0.71 g, 8.43 mmol) to give the title compound **82** (0.86 g, 32%). MS (ESI) *m/z*: 317 [M + H]⁺.

Intermediate 48h, 7-Methyl-5-(3-piperidyl)imidazo[1,2-*a*]pyrimidine. Prepared according to the procedure for **48a**, starting from intermediate **82** (0.86 g, 2.72 mmol), to give the title compound **48h** (0.75 g, 95%). ¹H NMR (400 MHz, DMSO-*d*₆): δ ppm 1.96–2.05 (m, 3H), 2.05–2.19 (m, 1H), 2.71 (s, 3H), 2.92–3.13 (m, 1H), 3.35–3.54 (m, 1H), 3.99–4.2 (m, 1H), 7.53 (s, 1H), 8.27 (d, *J* = 2.42 Hz, 1H), 8.69 (d, *J* = 2.83 Hz, 1H), 9.78 (br s, 1H), 9.95 (br s, 1H).

Intermediate 59, tert-Butyl 3-(4,4-Difluoro-3-oxo-butanoyl)-piperidine-1-carboxylate. Intermediate **50a** (17.4 g, 0.077 mol) was stirred in benzene (200 mL) at 0–5 °C under N₂. Potassium *tert*-butoxide (10.5 g, 93.6 mol) was added at 0–5 °C and 2,2-difluoroacetic acid ethyl ester (11.43 g, 0.92 mol) was added dropwise at 0–5 °C. The reaction mixture was stirred at RT for 5 h, then it was brought to pH = 7 with the aid of an aqueous H₂SO₄ solution (10%, 10 mL). The reaction mixture was extracted with EtOAc (2 × 50 mL), then the combined organic layer was washed with brine, dried over MgSO₄, filtered and evaporated under reduced pressure, to give intermediate **59** (23 g, 98%), which was pure enough to be used in the next step. MS (ESI) *m/z*: 304 [M – H]⁺.

Intermediate 81i, tert-Butyl 3-[5-(Difluoromethyl)-[1,2, 4]-triazolo[1,5-*a*]pyrimidin-7-yl]piperidine-1-carboxylate. Intermediate **59** (23 g, 75.3 mmol), 1H-1,2,4-triazol-5-amine hydrochloride (1:1) (18.16 g, 150.7 mmol), and DMF (270 mL) were stirred at 60 °C for 28 h, then at 50 °C for 20 h. The reaction mixture was cooled to 0 °C, then Et₃N (52 mL, 376 mmol) and *ditert*-butyl dicarbonate (16 g, 75.3 mmol) were added. The mixture was stirred for 1 h at RT, then concentrated *in vacuo*. The resulting residue was partitioned between DCM and an aqueous NH₄OH solution (20%) and stirred for 30 min. The organic layer was separated, then dried over MgSO₄, filtered and concentrated under reduced pressure. The resulting residue was purified by flash column chromatography using a gradient heptane/EtOAc, 100/0 to 60/40, as the eluent to give the title compound (23 g, 86%). MS (ESI) *m/z*: 354 [M + H]⁺.

Intermediate 48i, 5-(Difluoromethyl)-7-(3-piperidyl)-[1,2,4]-triazolo[1,5-*a*]pyrimidine. Prepared according to the procedure for **48a**, starting from intermediate **81i** (23 g, 65.09 mmol), to give the title compound as an HCl salt (13 g, 61%). ¹H NMR (360 MHz, DMSO-*d*₆): δ ppm 1.86–2.04 (m, 3H), 2.18 (br d, *J* = 7.48 Hz, 1H), 2.94 (br d, *J* = 10.79 Hz, 1H), 3.29–3.49 (m, 2H), 3.59 (br d, *J* = 12.14 Hz, 1H), 3.98–4.14 (m, 2H), 7.15 (t, *J* = 54.52 Hz, 1H), 7.62 (s, 1H), 8.89 (s, 1H), 9.46 (br d, *J* = 11.57 Hz, 1H), 9.74 (br d, *J* = 10.70 Hz, 1H). MS (ESI) *m/z*: 254 [M + H]⁺.

Intermediates 60, tert-Butyl 5-(Trifluoromethylsulfonyloxy)-3,4-dihydro-2H-pyridine-1-carboxylate, and **61**, tert-Butyl 5-(Trifluoromethylsulfonyloxy)-3,6-dihydro-2H-pyridine-1-carboxylate. A solution of commercially available 1-Boc-3-piperidinone (50 g, 250.9 mmol) in THF (125 mL) was added dropwise at –78 °C to a stirred solution of LDA in a mixture of THF/heptane/ethylbenzene (179 mL, 2 M, 358 mmol) in THF (625 mL) under a nitrogen atmosphere. After 15 min, a solution of *N,N*-bis(trifluoromethylsulfonyl)aniline (107.5 g, 300.9 mmol) in THF (250 mL) was added dropwise to the reaction mixture at –78 °C, and the resulting mixture was stirred for another 15 min. The reaction mixture was allowed to warm to RT overnight, and then it was cooled to 0 °C and quenched with a saturated aqueous NH₄Cl solution (190 mL), diluted with water, and extracted with DCM. The organic layer was dried over MgSO₄, filtered, and concentrated under reduced pressure. The resulting residue was purified by flash column chromatography on a silica gel using a gradient

as the eluent (DCM, 1% CH₃CN in DCM, 5%) to provide the intermediate **60** (42 g, 50%) and intermediate **61** (24.4 g, 29%). Intermediate **60**, ¹H NMR (400 MHz, DMSO-*d*₆): δ ppm 1.45 (s, 9H), 1.88 (quin, *J* = 6.06 Hz, 2H), 2.36–2.44 (m, 2H), 3.43–3.50 (m, 2H), 7.11 (s, 1H).

Intermediate 62, tert-Butyl 5-(4,4,5,5-Tetramethyl-1,3,2-dioxaborolan-2-yl)-3,4-dihydro-2H-pyridine-1-carboxylate. A degassed solution of intermediate **60** (24.4 g, 73.65 mmol) in 1,4-dioxane (700 mL) was added to a previously degassed mixture of PdCl₂(dppf) (1.61 g, 2.19 mmol), dppf (1.22 g, 2.2 mmol), KOAc (21.552 g, 219.6 mmol), and bis(pinacolato)diboron (20.53 g, 80.84 mmol) at RT and under a nitrogen atmosphere. The reaction mixture was stirred during 16 h at 80 °C, after which time it was filtered over Celite. The filtrate was evaporated under reduced pressure, and the resulting residue was purified via flash column chromatography on a silica gel using a gradient (DCM, 2% CH₃CN in DCM, 5%) as the eluent to give the title compound **62** as a white solid after recrystallization from heptane (10.8 g, 47%). MS (ESI) *m/z*: 209 [M-Boc + H]⁺.

Intermediate 63, tert-Butyl 5-(4,4,5,5-Tetramethyl-1,3,2-dioxaborolan-2-yl)-3,6-dihydro-2H-pyridine-1-carboxylate. Prepared in a similar way to intermediate **62**, starting from intermediate **61** (24.4 g, 73.6 mmol), to give the title compound **63** (10.8 g, 35% yield). MS (ESI) *m/z*: 209 [M-Boc + H]⁺.

General Procedure for the Suzuki Couplings of Intermediates 62 and 63 with the Corresponding Bicyclic Heteroatomic Chlorides. **Intermediate 65a**, tert-Butyl 5-(5-Isopropyl-[1,2,4]triazolo[1,5-*a*]pyrimidin-7-yl)-3,4-dihydro-2H-pyridine-1-carboxylate. A mixture of intermediate **62** (2.04 g, 6.61 mmol), commercially available 7-chloro-5-(propan-2-yl)-[1,2,4]triazolo[1,5-*a*]pyrimidine (1 g, 5.08 mmol), allylchloro[1,3-bis(2,6-di-*i*-propylphenyl)-4,5-dihydroimidazol-2-ylidene]palladium(II) (584 mg, 1.02 mmol), Na₂CO₃ (1.08 g, 10.17 mmol), 1,4-dioxane (5 mL), EtOH (5 mL), and distilled water (1 mL) was stirred under microwave irradiation at 120 °C 2 h. The volatiles were removed under reduced pressure, and the resulting residue was partitioned between water and EtOAc. The organic layer was washed with brine, dried over MgSO₄, filtered, and concentrated *in vacuo*. The resulting residue was purified by Prep HPLC using as the stationary phase a column Vydac Denali C18—10 μm, 250 g, 5 cm, and as the mobile phase a mixture of 0.25% NH₄HCO₃ solution in water and MeOH to give the title compound **65a** (180 mg, 10%). MS (ESI) *m/z*: 344 [M + H]⁺.

Intermediate 65b, tert-Butyl 5-[5-(Trifluoromethyl)-[1,2,4]-triazolo[1,5-*a*]pyrimidin-7-yl]-3,4-dihydro-2H-pyridine-1-carboxylate. Prepared in a similar way to intermediate **65a**, starting from intermediate **62** (1.00 g, 3.23 mmol) and commercially available 7-chloro-5-(trifluoromethyl)-[1,2,4]triazolo[1,5-*a*]pyrimidine (0.72 g, 3.23 mmol) and employing Pd(PPh₃)₄ (0.75 g, 0.65 mmol) as the catalyst to give the title compound **65b** (0.32 g, 26.8%). MS (ESI) *m/z*: 370 [M + H]⁺.

Intermediate 65c, tert-Butyl 5-(2,5-Dimethyl-[1,2,4]triazolo[1,5-*a*]pyrimidin-7-yl)-3,4-dihydro-2H-pyridine-1-carboxylate. Prepared in a similar way to intermediate **65a**, starting from intermediate **62** (2.2 g, 7.12 mmol) and commercially available 7-chloro-2,5-dimethyl-[1,2,4]triazolo[1,5-*a*]pyrimidine (1.0 g, 5.48 mmol) to give the title compound **65c** (0.17 g, 9.4%). MS (ESI) *m/z*: 330 [M + H]⁺.

Intermediate 65d, tert-Butyl 5-[5-Methyl-2-(trifluoromethyl)-[1,2,4]triazolo[1,5-*a*]pyrimidin-7-yl]-3,4-dihydro-2H-pyridine-1-carboxylate. Prepared in a similar way to intermediate **65a**, starting from intermediate **62** (1.31 g, 4.23 mmol) and commercially available, 7-chloro-5-methyl-2-(trifluoromethyl)-[1,2,4]triazolo[1,5-*a*]pyrimidine (1.00 g, 4.23 mmol) and employing Pd(PPh₃)₄ (0.97 g, 0.85 mmol) as the catalyst to give the title compound **65d** (0.39 g, 9.26%). MS (ESI) *m/z*: 384 [M + H]⁺.

Intermediate 83a, tert-Butyl 3-(5-Isopropyl-[1,2,4]triazolo[1,5-*a*]pyrimidin-7-yl)piperidine-1-carboxylate. Intermediate **65a** (180 mg, 0.52 mmol) and a solution of thiophenol (0.1 mL, 4%, 0.039 mmol) was added to a suspension of Pd/C (10%) (100 mg, 0.094 mmol) in methanol (40 mL) under N₂ flow. The reaction mixture was stirred at RT under H₂ atmosphere until 1 equiv hydrogen was absorbed. The catalyst was removed by filtration over Celite and the filtrate was

evaporated to give the title compound **83a** (180 mg, 99.4%), which was used in the next step without further purification.

Intermediate 83b, *tert*-Butyl 3-[5-(Trifluoromethyl)-[1,2,4]-triazolo[1,5-*a*]pyrimidin-7-yl]piperidine-1-carboxylate. Intermediate **62b** (320 mg, 0.87 mmol) and a solution of thiophenol (0.1 mL, 4%, 0.039 mmol) was added to a suspension of Pt/C (5%) (100 mg) in methanol (40 mL) under N₂ flow. The reaction mixture was stirred at 50 °C under a H₂ atmosphere until 1 equiv hydrogen was absorbed. The catalyst was removed by filtration over Celite, and the filtrate was evaporated. The resulting residue was purified via flash column chromatography on a silica gel using a gradient (DCM, 2% MeOH in DCM) as the eluent to give the title compound **83b** (150 mg, 46.6%). MS (ESI) *m/z*: 372 [M + H]⁺.

Intermediate 83c, *tert*-Butyl 3-(2,5-Dimethyl-[1,2,4]triazolo[1,5-*a*]pyrimidin-7-yl)piperidine-1-carboxylate. Intermediate **65c** (170 mg, 0.52 mmol) and a solution of thiophenol (0.1 mL, 4%, 0.039 mmol) were added to a suspension of Pt/C (5%) (100 mg) in methanol (40 mL) under N₂ flow. The reaction mixture was stirred at 50 °C under a H₂ atmosphere until 1 equiv hydrogen was absorbed. The catalyst was removed by filtration over Celite, and the filtrate was evaporated. The resulting residue was dissolved in DCM (10 mL), and then it was treated with MnO₂ (45 mg, 0.52 mmol) and stirred at RT for 1 h. The reaction mixture was filtered over Celite, and the solvent was evaporated under reduced pressure to provide the title compound **83c** (150 mg, 87.7%), which was used in the next step without further purification.

Intermediate 83d, *tert*-Butyl 3-[5-Methyl-2-(trifluoromethyl)-[1,2,4]triazolo[1,5-*a*]pyrimidin-7-yl]piperidine-1-carboxylate. Prepared in a similar way to intermediate **83c**, starting from intermediate **65d** (150 mg, 0.39 mmol) to give the title compound **83d** (100 mg, 66%). MS (ESI) *m/z*: 386 [M + H]⁺.

Intermediate 48j, 5-Isopropyl-7-(3-piperidyl)-[1,2,4]triazolo[1,5-*a*]pyrimidine. To a solution of intermediate **83a** (180 mg, 0.52 mmol) in MeOH (50 mL) was added HCl-*i*PrOH (50 mL), and the reaction mixture was stirred for 16 h at RT. The reaction mixture was evaporated to give the title compound as an HCl salt (160 mg, 96%) MS (ESI) *m/z*: 246 [M + H]⁺.

Intermediate 48k, 7-(3-Piperidyl)-5-(trifluoromethyl)-[1,2,4]triazolo[1,5-*a*]pyrimidine. Prepared in a similar way to **48j**, starting from intermediate **83b** (150 mg, 0.40 mmol) to give the title compound **48k** as an HCl salt (140 mg, quantitative) MS (ESI) *m/z*: 272 [M + H]⁺.

Intermediate 48l, 2,5-Dimethyl-7-(3-piperidyl)-[1,2,4]triazolo[1,5-*a*]pyrimidine. Prepared in a similar way to **48j**, starting from intermediate **83c** (150 mg, 0.45 mmol) to give the title compound **48l** as an HCl salt (130 mg, 94%). MS (ESI) *m/z*: 232 [M + H]⁺.

Intermediate 48m, 5-Methyl-7-(3-piperidyl)-2-(trifluoromethyl)-[1,2,4]triazolo[1,5-*a*]pyrimidine. Prepared in a similar way to **48j**, starting from intermediate **83d** (100 mg, 0.45 mmol) to give the title compound **48m** as an HCl salt (90 mg, 97%). MS (ESI) *m/z*: 286 [M + H]⁺.

Intermediate 67, *tert*-Butyl 5-(1H-Pyrrolo[2,3-*b*]pyridin-4-yl)-3,4-dihydro-2H-pyridine-1-carboxylate. Prepared in a similar way to **65a**, starting from intermediate **63** (1.32 g, 4.26 mmol) and commercially available 4-chloro-7-azaindole (0.5 g, 3.28 mmol). Purification via flash column chromatography on a silica gel using a gradient (DCM, 1% MeOH in DCM, 2%) as the eluent to give the title compound **67** (180 mg, 18%). MS (ESI) *m/z*: 300 [M + H]⁺.

Intermediate 84, *tert*-Butyl 3-(1H-Pyrrolo[2,3-*b*]pyridin-4-yl)piperidine-1-carboxylate. Prepared in a similar way to **83b**, starting from intermediate **67** (180 mg, 0.60 mmol) to give the title compound **84** (180 mg, 99%), which used as such in the next step.

Intermediate 48n, 4-(3-Piperidyl)-1H-pyrrolo[2,3-*b*]pyridine. Prepared in a similar way to **48a**, starting from intermediate **84** (180 mg, 0.59 mmol) to give the title compound **48n** as an HCl salt (150 mg, 91.6%), which was used directly in the next step.

Intermediate 69, *tert*-Butyl 5-[5-(Difluoromethyl)pyrazolo[1,5-*a*]pyrimidin-7-yl]-3,4-dihydro-2H-pyridine-1-carboxylate. Prepared in a similar way to **65a**, starting from intermediate **62** (0.59 g, 1.92 mmol) and 7-chloro-5-(difluoromethyl)pyrazolo[1,5-*a*]pyrimidine (0.30 g, 1.5 mmol). Purification via flash column chromatography on

a silica gel using a mixture heptane/EtOAc, 80/20, as the eluent gave the title compound **69** (1.3 g) MS (ESI) *m/z*: 351 [M + H]⁺.

Intermediate 85, *tert*-Butyl 3-[5-(Difluoromethyl)pyrazolo[1,5-*a*]pyrimidin-7-yl]piperidine-1-carboxylate. Prepared in a similar way to **83a**, starting from intermediate **69** (1.3 g, 3.71 mmol) to give the title compound **85** (820 mg, 63%), MS (ESI) *m/z*: 351 [M + H]⁺. ¹H NMR (400 MHz, DMSO-*d*₆): δ ppm 1.36 (br s, 9H), 1.49–1.63 (m, 1H), 1.74 (d, *J* = 11.3 Hz, 1H), 1.93–2.07 (m, 1H), 3.10 (ddd, *J* = 13.2, 9.7, 3.1 Hz, 1H), 3.40 (br s, 1H), 3.66–3.74 (m, 1H), 3.79 (d, *J* = 13.1 Hz, 1H), 4.15 (d, *J* = 13.2 Hz, 1H), 7.00 (t, *J* = 54.4 Hz, 1H), 6.94 (*J* = 2.5 Hz, 1H), 7.21 (s, 1H), 8.40 (d, *J* = 2.4 Hz, 1H).

Intermediate 48o, 5-(Difluoromethyl)-7-(3-piperidyl)pyrazolo[1,5-*a*]pyrimidine. Prepared in a similar way to **48a**, starting from intermediate **85** (820 mg, 2.33 mmol) to give the title compound **48o** as an HCl salt (520 mg, 88%), which used as such in the next step.

Final Compound 4, (3,4-Dimethoxyphenyl)-[3-([1,2,4]triazolo[1,5-*a*]pyrimidin-7-yl)-1-piperidyl]methanone. 3,4-Dimethoxybenzoic acid (760 mg, 4.17 mmol) was stirred in THF (40 mL). DIPEA (2.16 g, 0.75 g/mL, 16.7 mmol) and HBTU (1.74 g, 4.59 mmol) were added, stirring was continued for 20 min at RT. A solution of intermediate **48a** (1.38 g, 5.00 mmol) in DMF (10 mL) was added, and stirring was continued for 2 h at RT. The solvents were evaporated under reduced pressure, and the resulting residue was diluted with ice and water and then extracted with 2× DCM. The combined organic layers were washed with an aqueous solution of NaOH (1 N) and brine, separated, dried over MgSO₄, filtered, and then concentrated *in vacuo*. This material was purified by recrystallization from EtOAc, yielding compound **4** (1.04 g, 67.8% yield). MS (ESI) *m/z*: 368 [M + H]⁺. mp 159.2 °C; ¹H NMR (400 MHz, DMSO-*d*₆): δ ppm 1.62–1.74 (m, 1H) 1.84 (dt, *J* = 13.62, 3.89 Hz, 1H) 1.96–2.06 (m, 1H) 2.20–2.27 (m, 1H) 3.08–3.18 (m, 1H) 3.39 (dd, *J* = 12.92, 10.09 Hz, 1H) 3.68–3.74 (m, 1H) 3.79 (s, 6H) 3.96–4.08 (m, 1H) 4.38 (br d, *J* = 12.51 Hz, 1H) 6.93–7.00 (m, 3H) 7.26 (d, *J* = 4.84 Hz, 1H) 8.56 (s, 1H) 8.81 (d, *J* = 4.44 Hz, 1H).

Final Compound 5, 2-(3,4-Dimethoxyphenyl)-1-[3-([1,2,4]triazolo[1,5-*a*]pyrimidin-7-yl)-1-piperidyl]ethenone. 3,4-Dimethoxyphenylacetic acid (0.047 g, 0.24 mmol) was stirred in DCM (5 mL). DIPEA (0.14 mL, 0.86 mmol) and HBTU (90 mg, 0.24 mmol) were added, and stirring was continued for 30 min at RT. Intermediate **48a** (0.060 g, 0.22 mmol) was added, and stirring was continued for 2 h at RT. The RM was quenched with water (1 mL), and then it was filtered on an Extrelut column. The OL was evaporated *in vacuo*. This material was purified by Prep HPLC (stationary phase: RP Vydac Denali C18—10 μm, 250 × 5 cm, mobile phase: 0.25% NH₄HCO₃ solution in water, MeOH), to give compound **5** (57 mg, 69% yield). MS (ESI) *m/z*: 382 [M + H]⁺. ¹H NMR (600 MHz, DMSO-*d*₆, 100 °C): δ ppm 1.46–1.56 (m, 1H); 1.77 (m, 1H); 1.93 (dtd, *J* = 13.00, 11.21, 11.21, 4.05 Hz, 1H); 2.15–2.21 (m, 1H); 3.26–3.34 (m, 1H); 3.51 (br t, *J* = 9.91 Hz, 1H); 3.67 (m, 2H); 3.71 (s, 3H); 3.73 (m, 4H); 4.07–4.26 (m, 1H); 4.38–4.54 (m, 1H); 6.75 (br d, *J* = 7.60 Hz, 1H); 6.79–6.89 (m, 2H); 7.17 (d, *J* = 4.62 Hz, 1H); 8.59 (s, 1H); 8.78 (d, *J* = 4.62 Hz, 1H).

Final Compound 6, Phenyl-[3-([1,2,4]triazolo[1,5-*a*]pyrimidin-7-yl)-1-piperidyl]methanone. Benzoyl chloride (0.03 g, 0.22 mmol) was added at RT to a solution of intermediate **48a** (0.06 g, 0.22 mmol) and DIPEA (0.084 g, 0.75 g/mL, 0.65 mmol) in DCM (2 mL), and the resulting mixture was stirred at RT for 1 h. The RM was quenched with water (1 mL), and then it was filtered on an Extrelut column. The OL was evaporated *in vacuo*. This material was purified by flash column chromatography on a silica gel, eluting with 0–2% MeOH in DCM, to give compound **6** (47 mg, 70% yield). MS (ESI) *m/z*: 308 [M + H]⁺. ¹H NMR (600 MHz, DMSO-*d*₆, 100 °C): δ ppm 1.64–1.72 (m, 1H); 1.79–1.88 (m, 1H) 2.03 (dtd, *J* = 13.11, 10.95, 10.95, 3.96 Hz, 1H); 2.21–2.28 (m, 1H); 3.13–3.19 (m, 1H); 3.42 (dd, *J* = 12.96, 9.99 Hz, 1H); 3.65–3.76 (m, 1H); 3.91–4.03 (m, 1H); 4.31–4.42 (m, 1H); 7.24 (d, *J* = 4.62 Hz, 1H); 7.34–7.44 (m, 5H); 8.53 (s, 1H); 8.80 (d, *J* = 4.62 Hz, 1H).

Final Compound 7, Cyclopropyl-[3-([1,2,4]triazolo[1,5-*a*]pyrimidin-7-yl)-1-piperidyl]methanone. Prepared in a similar manner as compound **5**, starting from cyclopropanecarboxylic acid (0.02 g, 0.24 mmol) and intermediate **48a** (0.06 g, 0.22 mmol) to give compound **7**

(49 mg, 84% yield). MS (ESI) m/z : 272 $[M + H]^+$. 1H NMR (600 MHz, DMSO- d_6): δ ppm 0.62–0.69 (m, 1H) 0.69–0.75 (m, 2H) 0.76–0.81 (m, 1H) 1.56–1.67 (m, 1H) 1.84 (dt, $J = 13.67, 3.90$ Hz, 1H) 1.90–1.95 (m, 1H) 2.00 (dtd, $J = 13.07, 11.05, 11.05, 4.13$ Hz, 1H) 2.22 (dq, $J = 12.96, 4.16$ Hz, 1H) 3.10–3.15 (m, 1H) 3.38 (br t, $J = 11.31$ Hz, 2H) 3.55–3.65 (m, 1H) 4.14–4.28 (m, 1H) 4.54 (ddt, $J = 13.03, 3.61, 1.59, 1.59$ Hz, 1H) 7.24 (d, $J = 4.62$ Hz, 1H) 8.58 (s, 1H) 8.81 (d, $J = 4.62$ Hz, 1H).

Final Compound 8, Cyclohexyl-[3-([1,2,4]triazolo[1,5-*a*]pyrimidin-7-yl)-1-piperidyl]methanone. Cyclohexanecarbonyl chloride (0.116 mL, 0.87 mmol) was added at RT to a solution of intermediate **48a** (250 mg, 0.87 mmol) and DIPEA (0.574 mL, 0.75 g/mL, 3.47 mmol), and the resulting mixture was stirred at RT for 1 h. The reaction mixture was quenched with water (1 mL) and saturated aqueous solution of Na_2CO_3 (1 mL), and then the mixture was filtered through an Extrelut filter. The organic layer was evaporated under reduced pressure, and the resulting residue was purified via Prep HPLC (stationary phase: RP Vydac Denali C18—10 μ m, 250 \times 5 cm, mobile phase: 0.25% NH_4HCO_3 solution in water, MeOH) to afford compound **8** (30 mg, 11%). MS (ESI) m/z : 312 $[M - H]^+$. 1H NMR (360 MHz, DMSO- d_6): δ ppm 1.15 (br s, 1H) 1.28–1.39 (m, 2H) 1.47 (br s, 1H) 1.58–1.73 (m, 4H) 1.75–1.85 (m, 1H) 1.87–2.02 (m, 2H) 2.17 (br d, $J = 12.81$ Hz, 1H) 2.52–2.83 (m, 2H) 3.04–3.32 (m, 3H) 3.51 (br d, $J = 11.34$ Hz, 1H) 3.72–4.01 (m, 1H) 4.39 (br d, $J = 7.68$ Hz, 1H) 4.47–4.66 (m, 1H) 7.31 (dd, $J = 16.10, 4.39$ Hz, 1H) 8.72 (d, $J = 13.54$ Hz, 1H) 8.86 (dd, $J = 10.25, 4.39$ Hz, 1H).

Final Compound 9, (2-Methoxyphenyl)-[3(S)-([1,2,4]triazolo[1,5-*a*]pyrimidin-7-yl)-1-piperidyl]methanone. Prepared in a similar manner as compound **8**, starting from intermediate **48ab** (**S1**, 0.20 g, 0.72 mmol) and 2-methoxybenzoyl chloride (0.281 g, 2.17 mmol). Purification by flash chromatography on a silica gel, eluting with 0–2% MeOH in DCM, afforded compound **9** (167 mg, 68%). MS (ESI) m/z : 338 $[M + H]^+$. (DMSO- d_6): δ ppm 1.49 (br d, $J = 9.51$ Hz, 1H) 1.56–1.73 (m, 2H) 1.87–2.05 (m, 3H) 2.16 (br s, 2H) 2.96–3.21 (m, 2H) 3.25–3.33 (m, 2H) 3.36–3.46 (m, 1H) 3.50–3.75 (m, 5H) 3.81 (s, 1H) 3.85 (s, 3H) 4.37–4.49 (m, 1H) 4.54 (br d, $J = 13.17$ Hz, 1H) 4.74 (br d, $J = 11.34$ Hz, 1H) 6.77–6.83 (m, 1H) 6.87–7.18 (m, 5H) 7.24–7.33 (m, 3H) 7.33–7.44 (m, 2H) 8.49 (s, 1H) 8.74 (d, $J = 1.83$ Hz, 1H) 8.80 (d, $J = 4.76$ Hz, 1H) 8.90 (d, $J = 4.39$ Hz, 1H).

Final Compound 10. Prepared in a similar manner as compound **8**, starting from intermediate **48ab** (**S1**, 1 equiv) and 3-methoxybenzoyl chloride (1 equiv). MS (ESI) m/z : 338 $[M + H]^+$; 1H NMR (600 MHz, DMSO- d_6 , 100 $^\circ$ C): δ ppm 1.64–1.73 (m, 1H) 1.79–1.87 (m, 1H) 1.96–2.08 (m, 1H) 2.18–2.28 (m, 1H) 3.11–3.21 (m, 1H) 3.41 (dd, $J = 12.96, 9.99$ Hz, 1H) 3.71 (tt, $J = 10.28, 3.92$ Hz, 1H) 3.79 (s, 3H) 3.93–4.04 (m, 1H) 4.30–4.42 (m, 1H) 6.90–6.93 (m, 2H) 6.95–6.98 (m, 1H) 7.24 (d, $J = 4.46$ Hz, 1H) 7.27–7.33 (m, 1H) 8.52 (s, 1H) 8.80 (br s, 1H); 8.85 (br s, 1H).

Final Compound 11, (4-Methoxyphenyl)-[3(S)-([1,2,4]triazolo[1,5-*a*]pyrimidin-7-yl)-1-piperidyl]methanone. Prepared in a similar manner to compound **4**, starting from 4-methoxybenzoic acid (0.100 g, 0.66 mmol) and intermediate **48ab** (**S1**, 0.218 g, 0.79 mmol) and using DCM as the solvent. Purification via Prep HPLC (stationary phase: RP Vydac Denali C18—10 μ m, 250 \times 5 cm, mobile phase: 0.25% NH_4HCO_3 solution in water, MeOH) provided compound **11** (180 mg, 81%). MS (ESI) m/z : 338 $[M + H]^+$. 1H NMR (600 MHz, DMSO- d_6): δ ppm 1.56–1.90 (m, 2H); 1.99 (m, 1H); 2.18–2.25 (m, 1H); 2.93–3.27 (m, 2H); 3.64–3.74 (m, 1H); 3.79 (s, 3H); 4.03–4.83 (m, 2H); 6.97 (br s, 2H); 7.32 (br s, 1H); 7.39 (br d, $J = 7.93$ Hz, 2H); 8.68 (br s, 1H); 8.85 (br s, 1H).

Final Compound 12, 4-[3(S)-([1,2,4]triazolo[1,5-*a*]pyrimidin-7-yl)piperidine-1-carbonyl]benzonitrile. Prepared in a similar manner to compound **11**, starting from 4-cyanobenzoic acid (0.100 g, 0.68 mmol) and intermediate **48ab** (**S1**, 0.225 g, 0.82 mmol). Purification via Prep HPLC (stationary phase: RP Vydac Denali C18—10 μ m, 250 \times 5 cm, mobile phase: 0.25% NH_4HCO_3 solution in water, MeOH) provided compound **12** (35 mg, 15%). MS (ESI) m/z : 333 $[M + H]^+$. 1H NMR (600 MHz, DMSO- d_6 , 100 $^\circ$ C): δ ppm 1.65–1.75 (m, 1H); 1.81–1.90 (m, 1H); 2.04 (dtd, $J = 13.11, 11.03, 11.03, 3.96$ Hz, 1H); 2.21–2.27 (m, 1H); 3.13–3.20 (m, 1H); 3.41 (dd, $J = 13.05, 10.07$ Hz, 1H);

3.67–3.76 (m, 1H); 3.86–4.06 (m, 1H); 4.18–4.42 (m, 1H); 7.23 (d, $J = 4.46$ Hz, 1H); 7.56–7.58 (m, 2H); 7.83 (d, $J = 8.26$ Hz, 2H); 8.54 (s, 1H); 8.80 (d, $J = 4.62$ Hz, 1H).

Final Compound 13, [(3S)-([1,2,4]triazolo[1,5-*a*]pyrimidin-7-yl)-1-piperidyl]-[4-(trifluoromethyl)phenyl]methanone. Prepared in a similar manner as compound **8**, starting from intermediate **48ab** (**S1**, 0.06 g, 0.22 mmol) and 4-(trifluoromethyl)benzoyl chloride (0.045 g, 0.22 mmol). Purification by flash chromatography on a silica gel, eluting with 0–2% MeOH in DCM, afforded compound **9** (65 mg, 80%). MS (ESI) m/z : 376 $[M + H]^+$. SFC [CHIRALCEL Daicel OD 4.6 \times 500 mm; mobile phase: CO_2 , MeOH with 0.2% 2-propylamine] $R_t = 12.68$ min. 1H NMR (600 MHz, DMSO- d_6 , 100 $^\circ$ C): δ ppm 1.62–1.78 (m, 2H) 1.81–1.91 (m, 1H) 2.04 (dtd, $J = 13.13, 10.98, 10.98, 4.05$ Hz, 2H) 2.20–2.29 (m, 1H) 3.13–3.23 (m, 1H) 3.42 (dd, $J = 12.96, 9.99$ Hz, 1H) 3.66–3.76 (m, 1H) 3.85–4.08 (m, 1H) 4.23–4.47 (m, 1H) 7.24 (d, $J = 4.46$ Hz, 1H) 7.60 (d, $J = 7.93$ Hz, 2H) 7.74 (d, $J = 7.93$ Hz, 2H) 8.50 (s, 1H) 8.80 (d, $J = 4.62$ Hz, 1H).

Final compound 14, 2,3-Dihydro-1,4-benzodioxin-6-yl-[(3S)-([1,2,4]triazolo[1,5-*a*]pyrimidin-7-yl)-1-piperidyl]methanone. Prepared in a similar manner to compound **11**, starting from 2,3-dihydro-1,4-benzodioxine-6-carboxylic acid (0.100 g, 0.56 mmol) and intermediate **48ab** (**S1**, 0.184 g, 0.67 mmol). Purification via Prep HPLC (stationary phase: RP Vydac Denali C18—10 μ m, 250 \times 5 cm, mobile phase: 0.25% NH_4HCO_3 solution in water, MeOH) provided compound **14** (114 mg, 56%). MS (ESI) m/z : 366 $[M + H]^+$. SFC [CHIRALCEL Daicel OJ 4.6 \times 500 mm; mobile phase: CO_2 , MeOH with 0.2% 2-propylamine] $R_t = 13.5$ min. 1H NMR (360 MHz, DMSO- d_6): δ ppm 1.67 (br s, 1H) 1.82 (br s, 1H) 1.99 (q, $J = 10.49$ Hz, 1H) 2.21 (br dd, $J = 12.99, 3.48$ Hz, 1H) 3.12 (br s, 1H) 3.26–3.32 (m, 1H) 3.62–3.74 (m, 1H) 4.27 (s, 5H) 4.36–4.98 (m, 1H) 6.91 (br d, $J = 9.51$ Hz, 3H) 7.32 (br s, 1H) 8.68 (br s, 1H) 8.86 (br d, $J = 4.39$ Hz, 1H).

Final Compound 15, Benzofuran-5-yl-[3-([1,2,4]triazolo[1,5-*a*]pyrimidin-7-yl)-1-piperidyl]methanone. Prepared in a similar manner to compound **11**, starting from 1-benzofuran-5-carboxylic acid (0.150 g, 0.93 mmol) and intermediate **48a** (0.207 g, 1.02 mmol). Purification by flash chromatography on a silica gel, eluting with 0–2% MeOH in DCM, followed by crystallization from diethyl ether, afforded compound **15** (241 mg, 75%). MS (ESI) m/z : 348 $[M + H]^+$. mp 216.2 $^\circ$ C. 1H NMR (360 MHz, DMSO- d_6): δ ppm 1.71 (br s, 1H) 2.01 (br d, $J = 11.34$ Hz, 2H) 2.16–2.28 (m, 1H) 3.17–3.34 (m, 2H) 3.60–3.82 (m, 1H) 3.87–4.27 (m, 1H) 4.29–5.00 (m, 1H) 7.04 (dd, $J = 2.20, 0.73$ Hz, 1H) 7.38 (br d, $J = 8.42$ Hz, 2H) 7.64 (br s, 1H) 7.77 (s, 1H) 8.08 (s, 1H) 8.48–8.77 (m, 1H) 8.85 (br s, 1H).

Final Compound 16. Step 1, intermediate **16a**, 1H-indol-5-yl-[(3S)-([1,2,4]triazolo[1,5-*a*]pyrimidin-7-yl)-1-piperidyl]methanone. Intermediate **16a** was prepared in a similar manner to compound **11**, starting from indole-5-carboxylic acid (0.4 g, 2.48 mmol) and intermediate **48ab** (**S1**, 0.823 g, 2.98 mmol). Purification by flash chromatography on a silica gel, eluting with 0–2% MeOH in DCM, afforded intermediate **16a** (800 mg, 93%). MS (ESI) m/z : 347 $[M + H]^+$. SFC [CHIRALCEL Daicel OJ 4.6 \times 500 mm; mobile phase: CO_2 , MeOH with 0.2% 2-propylamine] $R_t = 17.37$ min. 1H NMR (360 MHz, DMSO- d_6): δ ppm 1.68 (br d, $J = 12.44$ Hz, 1H) 1.82 (br s, 1H) 1.88–2.07 (m, 1H) 2.23 (br d, $J = 9.51$ Hz, 1H) 3.13 (br s, 1H) 3.25–3.36 (m, 2H) 3.63–3.79 (m, 1H) 4.02 (br s, 1H) 4.28–4.75 (m, 1H) 6.52 (br s, 1H) 7.16 (br d, $J = 8.05$ Hz, 1H) 7.28–7.37 (m, 1H) 7.37–7.47 (m, 2H) 7.69 (s, 1H) 8.67 (br s, 1H) 8.85 (br d, $J = 4.02$ Hz, 1H) 11.29 (br s, 1H).

Final Compound 16, 1-[5-[(3S)-([1,2,4]triazolo[1,5-*a*]pyrimidin-7-yl)piperidine-1-carbonyl]indol-1-yl]ethanone. NaH (0.012 mg, 0.29 mmol, 60% dispersion in mineral oil) was added at RT to a solution of intermediate **16a** (100 mg, 0.29 mmol) in DMF (5 mL), and the reaction mixture was stirred at RT for 30 min. After this time, acetyl chloride (0.023 mg, 0.29 mmol) was added to the reaction mixture, which was stirred at RT for another 30 min before being quenched with water. The mixture was extracted with DCM, and then the organic layer was dried over $MgSO_4$, filtered, and evaporated under reduced pressure. The resulting residue was purified via Prep HPLC (stationary phase: RP Vydac Denali C18—10 μ m, 250 \times 5 cm, mobile phase: 0.25% NH_4HCO_3 solution in water, MeOH), which provided compound **16**

(82 mg, 73%). MS (ESI) m/z : 389 [M + H]⁺. SFC [CHIRALCEL Daicel OJ 4.6 × 500 mm; mobile phase: CO₂, EtOH with 0.2% 2-propylamine] R_t = 18.02 min and R_t = 18.4 min. ¹H NMR (360 MHz, DMSO-*d*₆): δ ppm 1.73 (m, 1H) 1.94–2.07 (m, 1H) 2.23 (br d, J = 9.15 Hz, 1H) 2.67 (s, 3H) 3.19 (br s, 1H) 3.24–3.33 (m, 1H) 3.56–3.82 (m, 2H) 3.91–4.22 (m, 1H) 4.36–4.95 (m, 1H) 6.82 (d, J = 3.66 Hz, 1H) 7.37 (br s, 2H) 7.71–7.75 (m, 1H) 7.94 (br d, J = 3.29 Hz, 1H) 8.35 (br s, 1H) 8.72 (br s, 1H) 8.85 (br s, 1H).

Final Compound 17, (1-Methylsulfonylindol-5-yl)-[3-([1,2,4]-triazolo[1,5-*a*]pyrimidin-7-yl)-1-piperidyl]methanone. Prepared in a similar manner to compound 11, starting from 1-methanesulfonyl-2,3-dihydro-1*H*-indole-5-carboxylic acid (0.500 g, 2.07 mmol) and intermediate 48a (0.687 g, 2.49 mmol). Purification by flash chromatography on a silica gel, eluting with 0–2% MeOH in DCM, followed by crystallization from diethyl ether, afforded compound 17 (511 mg, 58%). MS (ESI) m/z : 427 [M + H]⁺. mp 238.2 °C. SFC [CHIRALCEL Daicel OJ 4.6 × 500 mm; mobile phase: CO₂, MeOH with 0.2% 2-propylamine] R_t = 17.87 min and R_t = 20.28 min. ¹H NMR (360 MHz, DMSO-*d*₆): δ ppm 1.68 (br s, 1H) 1.76–1.92 (m, 1H) 2.02 (br d, J = 9.51 Hz, 1H) 2.22 (br dd, J = 12.99, 3.48 Hz, 1H) 3.05 (s, 3H) 3.14 (br t, J = 8.05 Hz, 3H) 3.37–3.52 (m, 1H) 3.62–3.75 (m, 1H) 3.98 (br t, J = 8.60 Hz, 2H) 4.18 (br s, 1H) 4.67 (br s, 1H) 7.04–7.31 (m, 3H) 7.33 (br s, 1H) 8.64 (br d, J = 11.34 Hz, 1H) 8.86 (br d, J = 4.03 Hz, 1H).

Final Compound 18, 4,5,6,7-Tetrahydrobenzothiophen-2-yl-[(3*S*)-([1,2,4]triazolo[1,5-*a*]pyrimidin-7-yl)-1-piperidyl]methanone. Prepared in a similar manner to compound 11, starting from 4,5,6,7-tetrahydrobenzo[*b*]thiophene-2-carboxylic acid (0.100 g, 0.55 mmol) and intermediate 48ab (0.687 g, 2.49 mmol). Purification by flash chromatography on a silica gel, eluting with 0–2% MeOH in DCM, followed by crystallization from diethyl ether, afforded compound 17 (511 mg, 58%). MS (ESI) m/z : 427 [M + H]⁺. mp 238.2 °C. SFC [CHIRALCEL Daicel OJ 4.6 × 500 mm; mobile phase: CO₂, EtOH with 0.2% 2-propylamine] R_t = 17.87 min and R_t = 20.28 min. ¹H NMR (360 MHz, DMSO-*d*₆): δ ppm 1.68 (br s, 1H) 1.76–1.92 (m, 1H) 2.02 (br d, J = 9.51 Hz, 1H) 2.22 (br dd, J = 12.99, 3.48 Hz, 1H) 3.05 (s, 3H) 3.14 (br t, J = 8.05 Hz, 3H) 3.37–3.52 (m, 1H) 3.62–3.75 (m, 1H) 3.98 (br t, J = 8.60 Hz, 2H) 4.18 (br s, 1H) 4.67 (br s, 1H) 7.04–7.31 (m, 3H) 7.33 (br s, 1H) 8.64 (br d, J = 11.34 Hz, 1H) 8.86 (br d, J = 4.03 Hz, 1H).

Final Compound 19, (1-Methylsulfonylindol-5-yl)-[(3*R*)-3-([1,2,4]-triazolo[1,5-*a*]pyrimidin-7-yl)-1-piperidyl]methanone. Prepared in a similar manner to compound 18, starting from 1-methanesulfonyl-2,3-dihydro-1*H*-indole-5-carboxylic acid (0.145 g, 0.60 mmol) and intermediate 48aa (R1, 0.2 g, 0.72 mmol). Purification by flash chromatography on a silica gel, eluting with 0–4% MeOH in DCM afforded compound 19 (120 mg, 46.6%). MS (ESI). SFC [CHIRALCEL Daicel OJ 4.6 × 500 mm; mobile phase: CO₂, MeOH with 0.2% 2-propylamine] R_t = 20.21 min. OR = –10.5° (589 nm, 20 °C, 0.438 w/v %; MeOH). ¹H NMR (360 MHz, DMSO-*d*₆): δ ppm 1.68 (br s, 1H) 1.76–1.92 (m, 1H) 2.02 (br d, J = 9.51 Hz, 1H) 2.22 (br dd, J = 12.99, 3.48 Hz, 1H) 3.05 (s, 3H) 3.14 (br t, J = 8.05 Hz, 3H) 3.37–3.52 (m, 1H) 3.62–3.75 (m, 1H) 3.98 (br t, J = 8.60 Hz, 2H) 4.18 (br s, 1H) 4.67 (br s, 1H) 7.04–7.31 (m, 3H) 7.33 (br s, 1H) 8.64 (br d, J = 11.34 Hz, 1H) 8.86 (br d, J = 4.03 Hz, 1H).

Final Compound 20, (1-Methylsulfonylindol-5-yl)-[(3*S*)-3-([1,2,4]-triazolo[1,5-*a*]pyrimidin-7-yl)-1-piperidyl]methanone. Prepared in a similar manner to compound 18, starting from 1-methanesulfonyl-2,3-dihydro-1*H*-indole-5-carboxylic acid (0.145 g, 0.60 mmol) and intermediate 48ab (S1, 0.2 g, 0.72 mmol). Purification by flash chromatography on a silica gel, eluting with 0–4% MeOH in DCM, afforded compound 20 (128 mg, 46.6%). MS (ESI). SFC [CHIRALCEL Daicel OJ 4.6 × 500 mm; mobile phase: CO₂, MeOH with 0.2% 2-propylamine] R_t = 17.88 min. OR = +9.36° (589 nm, 20 °C, 0.417 w/v %; MeOH). ¹H NMR (360 MHz, DMSO-*d*₆): δ ppm 1.68 (br s, 1H) 1.76–1.92 (m, 1H) 2.02 (br d, J = 9.51 Hz, 1H) 2.22 (br dd, J = 12.99, 3.48 Hz, 1H) 3.05 (s, 3H) 3.14 (br t, J = 8.05 Hz, 3H) 3.37–3.52 (m, 1H) 3.62–3.75 (m, 1H) 3.98 (br t, J = 8.60 Hz, 2H) 4.18 (br s, 1H) 4.67 (br s, 1H) 7.04–7.31 (m, 3H) 7.33 (br s, 1H) 8.64 (br d, J = 11.34 Hz, 1H) 8.86 (br d, J = 4.03 Hz, 1H).

Final Compound 21, 4,5,6,7-Tetrahydrobenzothiophen-2-yl-[(2*S*)-([1,2,4]triazolo[1,5-*a*]pyrimidin-7-yl)morpholin-4-yl]methanone. Prepared in a similar manner to compound 11, starting from 4,5,6,7-tetrahydrobenzo[*b*]thiophene-2-carboxylic acid (0.175 g, 0.96 mmol) and intermediate 48bb (S1, 0.32 g, 1.15 mmol). Purification by flash chromatography on a silica gel, eluting with 0–2% MeOH in DCM, followed by SFC purification [CHIRALCEL Daicel OJ 20 × 250 mm; mobile phase: CO₂, MeOH with 0.2% 2-propylamine] provided compound 21 (205 mg, 58%). R_t = 8.06 min. (ESI) m/z : 370 [M + H]⁺. ¹H NMR (360 MHz, DMSO-*d*₆): δ ppm 1.78 (br s, 4H) 2.63 (br s, 2H) 2.74 (br s, 2H) 3.08 (br s, 1H) 3.13–3.21 (m, 1H) 3.88 (br t, J = 11.16 Hz, 1H) 4.05–4.22 (m, 1H) 4.27 (br d, J = 13.17 Hz, 1H) 4.99 (br d, J = 12.44 Hz, 1H) 5.35 (br d, J = 9.51 Hz, 1H) 7.40 (br d, J = 4.03 Hz, 2H) 8.78 (s, 1H) 8.94 (br d, J = 4.02 Hz, 1H).

Final Compound 22, 4,5,6,7-Tetrahydrobenzothiophen-2-yl-[(1,2,4]triazolo[1,5-*a*]pyrimidin-7-yl)piperazin-1-yl]methanone. Prepared in a similar manner to compound 11, starting from 4,5,6,7-tetrahydrobenzo[*b*]thiophene-2-carboxylic acid (0.484 g, 2.66 mmol) and intermediate 48d (1.00 g, 3.19 mmol). Purification by flash chromatography on a silica gel, eluting with 0–6% MeOH in DCM, followed by crystallization from EtOAc, provided compound 22 (707 mg, 72%). (ESI) m/z : 369 [M + H]⁺. mp 193.45 °C. ¹H NMR (400 MHz, DMSO-*d*₆): δ ppm 1.72–1.83 (m, 4H) 2.57 (br t, J = 6.06 Hz, 2H) 2.71 (br t, J = 5.65 Hz, 3H) 2.89–2.98 (m, 1H) 3.13 (dt, J = 12.41, 3.68 Hz, 1H) 3.32 (ddd, J = 13.02, 9.79, 3.43 Hz, 1H) 3.39 (dd, J = 12.92, 8.48 Hz, 1H) 4.02–4.10 (m, 1H) 4.57 (ddd, J = 12.92, 3.63, 1.21 Hz, 1H) 4.67 (dd, J = 8.48, 3.63 Hz, 1H) 7.06 (s, 1H) 7.38 (d, J = 4.44 Hz, 1H) 8.52 (s, 1H) 8.82 (d, J = 4.44 Hz, 1H).

Final Compound 23, [4-Methyl-3-([1,2,4]triazolo[1,5-*a*]pyrimidin-7-yl)piperazin-1-yl]-(4,5,6,7-tetrahydrobenzothiophen-2-yl)methanone. A solution of compound 22 (0.2 g, 0.54 mmol), paraformaldehyde (0.020 g, 0.66 mmol), and NaBH(OAc)₃ (0.69 g, 3.25 mmol) in DCM (20 mL) was stirred at RT for 32 h. The mixture was then filtered through Celite, and the filtrate was washed with water. The organic layer was filtered over Extrelut, and the filtrate was evaporated under reduced pressure. The resulting residue was purified by recrystallization from DIPE to provide compound 23 (192 mg, 92%). (ESI) m/z : 383 [M + H]⁺. mp 174.6 °C. ¹H NMR (360 MHz, DMSO-*d*₆): δ ppm 1.68–1.81 (m, 4H) 2.19 (s, 3H) 2.35–2.46 (m, 1H) 2.56–2.62 (m, 2H) 2.71 (br s, 2H) 3.10 (br d, J = 11.71 Hz, 2H) 3.21–3.32 (m, 1H) 4.19 (dd, J = 9.88, 2.93 Hz, 1H) 4.28 (br d, J = 12.81 Hz, 1H) 4.51 (br d, J = 13.17 Hz, 1H) 7.28 (s, 1H) 7.41 (d, J = 4.39 Hz, 1H) 8.76 (s, 1H) 8.91 (d, J = 4.39 Hz, 1H).

Final Compound 24, 1-[4-(4,5,6,7-Tetrahydrobenzothiophen-2-carbonyl)-2-([1,2,4]triazolo[1,5-*a*]pyrimidin-7-yl)piperazin-1-yl]ethenone. Acetyl chloride (0.07 g, 0.89 mmol) was added at 0 °C to a solution of compound 22 (0.30 g, 0.81 mmol) and DIPEA (0.127 g, 0.98 mmol, 0.75 g/mL) in DCM (50 mL). The reaction mixture was allowed to reach RT and stirred until the starting material was consumed, as indicated by LC/MS and TLC. The reaction mixture was quenched with a saturated aqueous NaHCO₃ solution, and then the organic layer was separated, dried over MgSO₄, filtered, and concentrated under reduced pressure. The resulting residue was purified by flash chromatography on a silica gel, eluting with 0–2% MeOH in DCM, and the resulting material triturated in diethyl ether to provide compound 24 (293 mg, 87.6%). (ESI) m/z : 411 [M + H]⁺. mp 186 °C. ¹H NMR (360 MHz, DMSO-*d*₆): δ ppm 1.61–1.78 (m, 5H) 1.98 (s, 1H) 2.20 (s, 3H) 2.37–2.47 (m, 2H) 2.52–2.66 (m, 2H) 3.37–3.47 (m, 1H) 3.85–3.99 (m, 1H) 3.99–4.09 (m, 2H) 4.12–4.22 (m, 1H) 4.80 (br s, 1H) 5.01 (br s, 1H) 5.66–5.75 (m, 1H) 5.81 (br s, 1H) 6.21–6.98 (m, 1H) 7.25 (br d, J = 4.03 Hz, 1H) 7.35 (d, J = 4.39 Hz, 1H) 8.71 (br s, 1H) 8.81–8.88 (m, 1H) (80/20 mixture of rotamers).

Final Compound 25, 4,5,6,7-Tetrahydrobenzothiophen-2-yl-[(1,2,4]triazolo[1,5-*a*]pyrimidin-7-yl)azepan-1-yl]methanone. Prepared in a similar manner to compound 5, starting from 4,5,6,7-tetrahydrobenzo[*b*]thiophene-2-carboxylic acid [40133-07-1] (1.1 equiv) and intermediate 48c (1 equiv). (ESI) m/z : 382 [M + H]⁺. ¹H NMR (600 MHz, DMSO-*d*₆, 100 °C, mixture of rotamers): δ ppm 1.69–1.87 (m, 6H) 1.90–2.00 (m, 3H) 2.06–2.14 (m, 1H) 2.66–2.78 (m, 4H) 3.68–3.74 (m, 1H) 3.80–3.86 (m, 1H) 3.89–3.99 (m, 2H)

4.17–4.23 (m, 1H) 7.06 (s, 1H) 7.22–7.26 (m, 1H) 8.56–8.58 (m, 1H) 8.76–8.85 (m, 1H).

Final Compound 26, [3-(5-Methyl-[1,2,4]triazolo[1,5-*a*]pyrimidin-7-yl)-1-piperidyl]-(4,5,6,7-tetrahydrobenzothiophen-2-yl)methanone. Prepared in a similar manner to compound 11, starting from 4,5,6,7-tetrahydrobenzo[*b*]thiophene-2-carboxylic acid (0.100 g, 0.55 mmol) and intermediate 48g (0.687 g, 2.49 mmol). Purification by flash chromatography on a silica gel, eluting with 0–2% MeOH in DCM, followed by crystallization from diethyl ether, afforded compound 26 (511 mg, 58%). (ESI) *m/z*: 382 [M + H]⁺. mp 201.2 °C. ¹H NMR (360 MHz, DMSO-*d*₆): δ ppm 1.60–1.81 (m, 6H) 1.88 (br d, *J* = 13.54 Hz, 1H) 1.99 (br d, *J* = 12.08 Hz, 1H) 2.20 (br d, *J* = 13.17 Hz, 1H) 2.58 (br t, *J* = 5.67 Hz, 2H) 2.62 (s, 3H) 2.70 (br d, *J* = 5.12 Hz, 2H) 3.11 (br s, 1H) 3.58–3.67 (m, 1H) 4.29 (br d, *J* = 12.08 Hz, 1H) 4.60 (br d, *J* = 12.81 Hz, 1H) 7.26 (s, 2H) 8.60 (s, 1H).

Final Compound 27, [3-(5-Isopropyl-[1,2,4]triazolo[1,5-*a*]pyrimidin-7-yl)-1-piperidyl]-(4,5,6,7-tetrahydrobenzothiophen-2-yl)methanone. Prepared in a similar manner to compound 11, starting from 4,5,6,7-tetrahydrobenzo[*b*]thiophene-2-carboxylic acid (0.076 g, 0.42 mmol) and intermediate 48j (0.160 g, 0.5 mmol). Purification by flash chromatography on a silica gel, eluting with 0.5–1% MeOH in DCM, followed by crystallization from diisopropyl ether, afforded compound 27 (54 mg, 31%). (ESI) *m/z*: 410 [M + H]⁺. mp 158 °C. ¹H NMR (360 MHz, DMSO-*d*₆): δ ppm 1.30 (d, *J* = 6.95 Hz, 6H) 1.74 (br s, 5H) 1.96–2.31 (m, 3H) 2.54–2.59 (m, 2H) 2.70 (br d, *J* = 4.76 Hz, 2H) 3.11–3.24 (m, 2H) 4.11–4.36 (m, 1H) 4.45–4.63 (m, 1H) 7.24 (s, 1H) 7.28 (s, 1H) 8.62 (s, 1H).

Final Compound 28, [3-(5-Methoxy-[1,2,4]triazolo[1,5-*a*]pyrimidin-7-yl)-1-piperidyl]-(4,5,6,7-tetrahydrobenzothiophen-2-yl)methanone. Prepared in a similar manner to compound 11, starting from 4,5,6,7-tetrahydrobenzo[*b*]thiophene-2-carboxylic acid (0.101 g, 0.56 mmol) and intermediate 48e (0.130 g, 0.56 mmol). Purification by flash chromatography on a silica gel, eluting with 0.5–1% MeOH in DCM, followed by crystallization from diethyl ether, afforded compound 28 (86 mg, 39%). (ESI) *m/z*: 398 [M + H]⁺. mp 165.5 °C. ¹H NMR (360 MHz, DMSO-*d*₆): δ ppm 1.58–1.88 (m, 7H) 1.91–2.06 (m, 1H) 2.16 (br d, *J* = 12.81 Hz, 1H) 2.53–2.61 (m, 2H) 2.65–2.76 (m, 2H) 3.10 (br s, 1H) 3.20–3.30 (m, 1H) 3.51–3.60 (m, 1H) 3.99 (s, 3H) 4.26 (br d, *J* = 12.08 Hz, 1H) 4.55 (br d, *J* = 13.17 Hz, 1H) 6.80 (s, 1H) 7.25 (br s, 1H) 8.46 (s, 1H).

Final Compound 29, 7-[1-(4,5,6,7-Tetrahydrobenzothiophene-2-carbonyl)-3-piperidyl]-[1,2,4]triazolo[1,5-*a*]pyrimidine-5-carbonitrile. Prepared in a similar manner to compound 11, starting from 4,5,6,7-tetrahydrobenzo[*b*]thiophene-2-carboxylic acid (0.157 g, 0.86 mmol) and intermediate 48f (0.135 g, 1.04 mmol). Purification by flash chromatography on a silica gel, eluting with 0–1.5% MeOH in DCM, followed by crystallization from diethyl ether, afforded compound 29 (73 mg, 21%). (ESI) *m/z*: 393 [M + H]⁺. ¹H NMR (360 MHz, DMSO-*d*₆): δ ppm 1.58–1.82 (m, 5H) 1.89 (br d, *J* = 13.17 Hz, 1H) 1.97–2.14 (m, 1H) 2.20 (br d, *J* = 13.17 Hz, 1H) 2.52–2.61 (m, 2H) 2.70 (br d, *J* = 5.85 Hz, 2H) 3.11 (br s, 1H) 3.25–3.32 (m, 1H) 3.69–3.79 (m, 1H) 4.31 (br d, *J* = 12.44 Hz, 1H) 4.61 (br d, *J* = 12.81 Hz, 1H) 7.23 (s, 1H) 8.00 (s, 1H) 8.99 (s, 1H).

Final Compound 30, 4,5,6,7-Tetrahydrobenzothiophen-2-yl-[3-(5-(trifluoromethyl)-[1,2,4]triazolo[1,5-*a*]pyrimidin-7-yl)-1-piperidyl]methanone. Prepared in a similar manner to compound 11, starting from 4,5,6,7-tetrahydrobenzo[*b*]thiophene-2-carboxylic acid (0.062 g, 0.34 mmol) and intermediate 48k (0.140 g, 0.41 mmol). Purification by flash chromatography on a silica gel, eluting with 0–0.5% MeOH in DCM, afforded compound 30 (110 mg, 74%). (ESI) *m/z*: 436 [M + H]⁺. ¹H NMR (360 MHz, DMSO-*d*₆): δ ppm 1.04 (d, *J* = 6.22 Hz, 1H) 1.61–1.80 (m, 5H) 1.87 (br d, *J* = 12.81 Hz, 1H) 2.10–2.25 (m, 2H) 2.52–2.61 (m, 3H) 2.65–2.76 (m, 2H) 3.02–3.24 (m, 1H) 3.36–3.53 (m, 1H) 3.75–3.84 (m, 1H) 4.30 (br d, *J* = 13.90 Hz, 1H) 4.59 (br d, *J* = 10.25 Hz, 1H) 7.24 (s, 1H) 7.80 (s, 1H) 8.96 (s, 1H).

Final Compound 31, [3-(5-(Difluoromethyl)-[1,2,4]triazolo[1,5-*a*]pyrimidin-7-yl)-1-piperidyl]-(4,5,6,7-tetrahydrobenzothiophen-2-yl)methanone. Prepared in a similar manner to compound 11, starting from 4,5,6,7-tetrahydrobenzo[*b*]thiophene-2-carboxylic acid (0.060 g, 0.33 mmol) and intermediate 48i (0.100 g, 0.39 mmol). Purification by

prep HPLC on a RP Vydac Denali column (C18—10 μm, 250 g, 5 cm) and using as the mobile phase a mixture of a 0.25% NH₄HCO₃ solution in water and MeOH afforded compound 31 (130 mg, 95%). (ESI) *m/z*: 418 [M + H]⁺. ¹H NMR (400 MHz, DMSO-*d*₆): δ ppm 1.68–1.82 (m, 5H) 1.88 (dt, *J* = 13.52, 3.73 Hz, 1H) 2.06–2.17 (m, 1H) 2.21–2.28 (m, 1H) 2.56 (t, *J* = 5.85 Hz, 2H) 2.71 (t, *J* = 5.85 Hz, 2H) 3.19–3.28 (m, 1H) 3.54 (dd, *J* = 13.12, 9.89 Hz, 1H) 3.75–3.82 (m, 1H) 4.23 (br d, *J* = 13.32 Hz, 1H) 4.56 (dd, *J* = 13.32, 3.63 Hz, 1H) 7.03 (t, *J* = 54.50 Hz, 1H) 7.13 (s, 1H) 7.51 (s, 1H) 8.75 (s, 1H).

Final Compound 32, 3-[5-(Difluoromethyl)pyrazolo[1,5-*a*]pyrimidin-7-yl]-1-piperidyl]-(4,5,6,7-tetrahydrobenzothiophen-2-yl)methanone. Prepared in a similar manner to compound 11, starting from 4,5,6,7-tetrahydrobenzo[*b*]thiophene-2-carboxylic acid (0.108 g, 0.59 mmol) and intermediate 48o (0.150 g, 0.59 mmol). Purification by flash chromatography on a silica gel, eluting with 0–30% EtOAc in heptane, followed by crystallization from diisopropyl ether, afforded compound 32 (190 mg, 77%). (ESI) *m/z*: 417 [M + H]⁺. mp 192.8 °C. ¹H NMR (600 MHz, DMSO-*d*₆): δ ppm 1.64–1.81 (m, 5H) 1.84–1.91 (m, 1H) 2.05–2.12 (m, 1H) 2.21–2.26 (m, 1H) 2.54–2.61 (m, 2H) 2.67–2.75 (m, 2H) 3.17–3.23 (m, 1H) 3.46 (dd, *J* = 12.76, 10.12 Hz, 1H) 3.83–3.88 (m, 1H) 4.26 (br d, *J* = 13.21 Hz, 1H) 4.57 (dd, *J* = 12.76, 3.67 Hz, 1H) 6.90 (t, *J* = 54.87 Hz, 1H) 6.87–6.90 (m, 1H) 7.19 (d, *J* = 8.80 Hz, 2H) 8.34 (dd, *J* = 2.35, 0.88 Hz, 1H).

Final Compound 33, [3-(7-Methylimidazo[1,2-*a*]pyrimidin-5-yl)-1-piperidyl]-(4,5,6,7-tetrahydrobenzothiophen-2-yl)methanone. Prepared in a similar manner to compound 11, starting from 4,5,6,7-tetrahydrobenzo[*b*]thiophene-2-carboxylic acid (0.131 g, 0.72 mmol) and intermediate 48h (0.250 g, 0.86 mmol). Purification by flash chromatography on a silica gel, eluting with 0–3% MeOH in DCM, followed by crystallization from diethyl ether, afforded compound 33 (168 mg, 61%). (ESI) *m/z*: 381 [M + H]⁺. mp 192.7 °C. ¹H NMR (360 MHz, DMSO-*d*₆): δ ppm 1.63–1.91 (m, 8H); 2.17 (br d, *J* = 12.44 Hz, 1H); 2.52 (s, 3H); 2.53–2.59 (m, 2H); 2.64–2.81 (m, 2H); 3.22 (br d, *J* = 16.10 Hz, 2H); 3.27–3.31 (m, 1H); 4.32 (br d, *J* = 12.81 Hz, 1H); 4.51 (br d, *J* = 11.34 Hz, 1H); 6.90 (s, 1H); 7.14 (s, 1H); 7.67 (s, 1H); 8.01 (br s, 1H).

Final Compound 34, [3-(1H-Pyrrolo[2,3-*b*]pyridin-4-yl)-1-piperidyl]-(4,5,6,7-tetrahydrobenzothiophen-2-yl)methanone. Prepared in a similar manner to compound 11, starting from 4,5,6,7-tetrahydrobenzo[*b*]thiophene-2-carboxylic acid (0.083 g, 0.46 mmol) and intermediate 48n (0.150 g, 0.55 mmol). Purification by crystallization from methanol afforded compound 34 (114 mg, 68%). (ESI) *m/z*: 366 [M + H]⁺. mp 275.7 °C. ¹H NMR (360 MHz, DMSO-*d*₆): δ ppm 1.59–1.87 (m, 6H); 1.89–2.07 (m, 2H); 2.52–2.58 (m, 2H); 2.67–2.75 (m, 2H); 3.02–3.32 (m, 3H); 4.37 (br d, *J* = 11.71 Hz, 2H); 6.57 (br s, 1H); 6.97 (d, *J* = 5.12 Hz, 1H); 7.10 (s, 1H); 7.44 (t, *J* = 3.11 Hz, 1H); 8.15 (d, *J* = 4.76 Hz, 1H); 11.65 (br s, 1H).

Final Compound 35, [3-(2,5-Dimethyl-[1,2,4]triazolo[1,5-*a*]pyrimidin-7-yl)-1-piperidyl]-(4,5,6,7-tetrahydrobenzothiophen-2-yl)methanone. Prepared in a similar manner to compound 11, starting from 4,5,6,7-tetrahydrobenzo[*b*]thiophene-2-carboxylic acid (0.065 g, 0.36 mmol) and intermediate 48l (0.130 g, 0.43 mmol). Purification by flash chromatography on a silica gel, eluting with 0.5–1% MeOH in DCM, followed by crystallization from diisopropyl ether, afforded compound 35 (12 mg, 39%). (ESI) *m/z*: 396 [M + H]⁺. ¹H NMR (600 MHz, DMSO-*d*₆): δ ppm 1.62–1.70 (m, 1H) 1.81 (br s, 6H) 1.86–1.91 (m, 1H) 1.96–2.04 (m, 1H) 2.17–2.24 (m, 1H) 2.46 (s, 3H) 2.54–2.56 (m, 2H) 2.57 (s, 3H) 2.71 (br t, *J* = 6.19 Hz, 2H) 3.19 (ddd, *J* = 13.33, 11.11, 3.30 Hz, 1H) 3.43 (dd, *J* = 13.05, 10.07 Hz, 1H) 3.59 (tt, *J* = 10.30, 3.90 Hz, 1H) 4.21 (dt, *J* = 13.29, 4.00 Hz, 1H) 4.53 (ddt, *J* = 12.98, 3.65, 1.59, 1.59 Hz, 1H) 7.04 (s, 1H) 7.05 (s, 1H).

Final Compound 36, [3-(5-Methyl-2-(trifluoromethyl)-[1,2,4]triazolo[1,5-*a*]pyrimidin-7-yl)-1-piperidyl]-(4,5,6,7-tetrahydrobenzothiophen-2-yl)methanone. Prepared in a similar manner to compound 11, starting from 4,5,6,7-tetrahydrobenzo[*b*]thiophene-2-carboxylic acid (0.038 g, 0.21 mmol) and intermediate 48m (0.09 g, 0.25 mmol). Purification by flash chromatography on a silica gel, eluting with 0.5–1% MeOH in DCM, afforded compound 36 (75 mg, 78%). (ESI) *m/z*: 450 [M + H]⁺. ¹H NMR (400 MHz, DMSO-*d*₆): δ ppm 1.63–1.81 (m, 5H); 1.85–2.06 (m, 2H); 2.19–2.26 (m, 1H); 2.50–2.55 (m, 2H); 2.64–2.72 (m, 5H); 3.16–3.26 (m, 1H); 3.44 (dd, *J* = 12.9, 10.1

H_z, 1H); 3.57–3.67 (m, 1H); 4.18–4.25 (m, 1H); 4.52–4.57 (m, 1H); 7.02 (s, 1H); 7.38 (s, 1H).

Final Compound 37, 5-(Difluoromethyl)-7-[1-[(3,4-dimethoxyphenyl)methyl]-3-piperidyl]-[1,2,4]triazolo[1,5-*a*]pyrimidine. DIPEA (0.52 mL, 3.02 mmol) and 3,4-dimethoxybenzaldehyde [120-14-9] (0.076 g, 0.46 mmol) were added to a solution of intermediate 48i (0.15 g, 0.46 mmol) in DCM (30 mL). The reaction mixture was stirred at RT for 1 h, and then sodiumtriacetoxymethylborohydride [56553-60-7] (0.15 g, 1.84) was added. The reaction mixture was stirred at RT for 2 h, and then it was washed with sat. aq NaHCO₃ solution, dried over MgSO₄, filtered, and concentrated by evaporation. The resulting residue was purified by flash column chromatography on a silica gel using a mixture of EtOAc and heptane, 80/20, as the eluent to provide compound 37 (160 mg, 86%). ESI *m/z*: 404 [M + H]⁺. ¹H NMR (400 MHz, DMSO-*d*₆, 80 °C): δ ppm 1.60–1.71 (m, 2H); 1.79–1.89 (m, 1H); 2.00–2.08 (m, 1H); 2.35–2.43 (m, 1H); 2.59–2.68 (m, 2H); 2.96–3.01 (m, 1H); 3.50 (s, 2H); 3.73 (s, 3H); 3.76 (s, 3H); 3.78–3.88 (m, 1H); 6.83 (dd, *J* = 8.1, 1.61 Hz, 1H); 6.85–6.89 (d, *J* = 8.5 Hz, 1H); 7.09 (t, *J* = 54.5 Hz, 1H); 6.93 (d, *J* = 1.84 Hz, 1H); 7.66 (s, 1H) 8.72 (s, 1H).

Final Compound 38, 7-[1-(Benzofuran-5-ylmethyl)-3-piperidyl]-5-(difluoromethyl)-[1,2,4]triazolo[1,5-*a*]pyrimidine. Prepared in a similar manner to compound 37, starting from benzo[*b*]furan-5-carboxaldehyde (0.10 g, 0.69 mmol) and intermediate 48i (0.15 g, 0.46 mmol). Purification by Prep HPLC on a RP Vydac Denali column (C18—10 μm, 250 g, 5 cm) and using as mobile phase a mixture of a 0.25% NH₄HCO₃ solution in water and ACN afforded the title compound as a free base, which was then dissolved in DIPE and treated with HCl to afford compound 38 as a HCl salt (180 mg, 86%). ESI *m/z*: 384 [M + H]⁺. ¹H NMR (360 MHz, DMSO-*d*₆): δ ppm 1.80–2.17 (m, 4H); 3.03 (br d, *J* = 11.71 Hz, 1H); 3.43–3.55 (m, 3H); 4.24 (br t, *J* = 12.08 Hz, 1H); 4.38–4.52 (m, 2H); 7.14 (t, *J* = 54.52 Hz, 1H); 7.01–7.05 (m, 1H); 7.55 (s, 1H); 7.57 (d, *J* = 9.88 Hz, 1H); 7.69 (d, *J* = 8.42 Hz, 1H); 7.91 (s, 1H); 8.08 (d, *J* = 2.20 Hz, 1H); 8.85 (s, 1H); 11.06 (br s, 1H). Anal. Calcd (C₂₀H₁₉F₂N₅O): C, H, N.

Final Compound 39, 7-[1-(2-Chloro-6-methyl-4-pyridyl)methyl]-3-piperidyl]-5-(difluoromethyl)-[1,2,4]triazolo[1,5-*a*]pyrimidine. A solution of 2-chloro-4-chloromethyl-6-methylpyridine [162046-59-5] (0.81 g, 4.6 mmol), intermediate 48i (1.00 g, 3.07 mmol) and DIPEA (2.13 mL, 12.4 mmol) in DMF (100 mL) was stirred and heated at 40 °C for 4 h. The reaction mixture was cooled to RT, and then it was evaporated under reduced pressure. The resulting residue was dissolved in DCM, washed with a satd aq NaHCO₃ soln (1×), dried over MgSO₄, filtered, and evaporated *in vacuo*. The resulting residue was purified by prep HPLC on a RP Vydac Denali column (C18—10 μm, 250 g, 5 cm) and using as a mobile phase a mixture of a 0.25% NH₄HCO₃ solution in water and ACN afforded the title compound as a racemic mixture (1.15 g, 95%). ESI *m/z*: 393 [M + H]⁺. Separation in enantiomers by preparative SFC [CHIRALPAK Daicel AD 20 × 250 mm; mobile phase: CO₂, EtOH with 0.2% 2-propylamine] afforded compounds 39 (R*) (430 mg, 37%) *R*_t = 3.75 min, OR = +39.71° (589 nm, 20 °C, 0.345 w/v %; DMF), mp 164.56 °C, ¹H NMR (360 MHz, DMSO-*d*₆): δ ppm 1.62–1.73 (m, 2H); 1.74–1.88 (m, 1H); 2.04 (br dd, *J* = 12.62, 4.21 Hz, 1H); 2.37 (br s, 1H); 2.44 (s, 3H); 2.53–2.71 (m, 2H); 2.99 (br d, *J* = 10.98 Hz, 1H); 3.54–3.62 (m, 2H); 3.82 (dt, *J* = 8.51, 4.35 Hz, 1H); 7.04 (t, *J* = 55.30 Hz, 1H); 7.26 (d, *J* = 6.59 Hz, 2H); 7.70 (s, 1H); 8.82 (s, 1H) and 41 (S*) (407 mg, 35%). *R*_t = 4.67 min, OR = –42.56° (589 nm, 20 °C, 0.43 w/v %; DMF), mp 165.83 °C.

Final Compound 40, 5-(Difluoromethyl)-7-[1-[(2,6-dimethyl-4-pyridyl)methyl]-3-piperidyl]-[1,2,4]triazolo[1,5-*a*]pyrimidine. Prepared in a similar manner to compound 37, starting from 2,6-dimethylisonicotinaldehyde [182006-06-9] (0.99 g, 7.36 mmol) and intermediate 48i (1.20 g, 3.68 mmol). Purification by prep HPLC on a Uptisphere column (C18—10 μm, 200 g, 5 cm) and using as the mobile phase a mixture of a 0.25% NH₄HCO₃ solution in water and MeOH afforded the title compound as a racemic mixture (1.04 g, 76%). ESI *m/z*: 373 [M + H]⁺. Separation in enantiomers by preparative SFC [CHIRALPAK Daicel AD 30 × 250 mm; mobile phase: CO₂, EtOH with 0.2% 2-propylamine] afforded compounds 40 (R*) (373 mg, 36%) *R*_t = 3.53 min, OR = +48.93° (589 nm, 20 °C, 0.515 w/v %;

DMF), mp 153.3 °C, ¹H NMR (360 MHz, DMSO-*d*₆): δ ppm 1.62–1.73 (m, 2H); 1.74–1.88 (m, 1H); 2.04 (br dd, *J* = 12.62, 4.21 Hz, 1H); 2.37 (br s, 1H); 2.44 (s, 3H); 2.53–2.71 (m, 2H); 2.99 (br d, *J* = 10.98 Hz, 1H); 3.54–3.62 (m, 2H); 3.82 (dt, *J* = 8.51, 4.35 Hz, 1H); 7.04 (t, *J* = 55.30 Hz, 1H); 7.26 (d, *J* = 6.59 Hz, 2H); 7.70 (s, 1H); 8.82 (s, 1H) and 42 (S*) (348 mg, 33%). *R*_t = 4.66 min, OR = –48.46° (589 nm, 20 °C, 0.43 w/v %; DMF), mp 154.4 °C.

Final Compound 41, Benzofuran-5-yl-[3-[5-(difluoromethyl)-[1,2,4]triazolo[1,5-*a*]pyrimidin-7-yl]-4-methyl-1-piperidyl]-methanone. Prepared in a similar manner to compound 42, starting from intermediate 78 (rac, 220 mg, 0.82 mmol). Purification by flash chromatography on a silica gel, eluting with 0–1% MeOH in DCM, afforded compound 41 %. ESI *m/z*: 412 [M + H]⁺. ¹H NMR (400 MHz, DMSO-*d*₆): δ ppm 0.82 (d, *J* = 6.46 Hz, 3H) 1.37–1.50 (m, 1H) 1.84–1.92 (m, 1H) 2.41–2.46 (m, 1H) 2.50–2.53 (m, 1H) 3.15 (td, *J* = 12.92, 2.83 Hz, 1H) 3.34–3.40 (m, 1H) 3.56–3.64 (m, 1H) 4.17 (br d, *J* = 12.92 Hz, 1H) 4.32 (br d, *J* = 12.51 Hz, 1H) 6.84–7.14 (m, 1H) 6.96 (dd, *J* = 2.42, 0.81 Hz, 1H) 7.38 (dd, *J* = 8.48, 1.61 Hz, 1H) 7.55–7.56 (m, 1H) 7.58 (d, *J* = 8.48 Hz, 1H) 7.75 (d, *J* = 1.61 Hz, 1H) 7.94 (d, *J* = 2.02 Hz, 1H) 8.70 (s, 1H).

Final Compound 42, Benzofuran-5-yl-[(3*S*,4*R*)-3-[5-(difluoromethyl)-[1,2,4]triazolo[1,5-*a*]pyrimidin-7-yl]-4-methyl-1-piperidyl]-methanone. 1-Benzofuran-5-carboxylic acid (214 mg, 1.32 mmol) was stirred in DCM (10 mL). DIPEA (851 mg, 0.75 g/mL, 6.58 mmol) and HBTU (499 mg, 1.32 mmol) were added, and stirring was continued for 20 min at RT. Intermediate 78 (RS!, 400 mg, 1.32 mmol; WO 2018/083098) was added, and stirring was continued for 1 h at RT. The RM was quenched with 1 N aqueous NaOH (1 mL) solution and stirred for 5 min, then the OL was separated and dried over MgSO₄, filtered, and concentrated *in vacuo*. This material was purified by silica gel flash chromatography eluting with 0–3% MeOH in DCM to afford compound 42 (120 mg, yield 52.931%). ESI *m/z*: 412 [M + H]⁺. ¹H NMR (400 MHz, DMSO-*d*₆): δ ppm 0.82 (d, *J* = 6.46 Hz, 3H) 1.37–1.50 (m, 1H) 1.84–1.92 (m, 1H) 2.41–2.46 (m, 1H) 2.50–2.53 (m, 1H) 3.15 (td, *J* = 12.92, 2.83 Hz, 1H) 3.34–3.40 (m, 1H) 3.56–3.64 (m, 1H) 4.17 (br d, *J* = 12.92 Hz, 1H) 4.32 (br d, *J* = 12.51 Hz, 1H) 6.84–7.14 (m, 1H) 6.96 (dd, *J* = 2.42, 0.81 Hz, 1H) 7.38 (dd, *J* = 8.48, 1.61 Hz, 1H) 7.55–7.56 (m, 1H) 7.58 (d, *J* = 8.48 Hz, 1H) 7.75 (d, *J* = 1.61 Hz, 1H) 7.94 (d, *J* = 2.02 Hz, 1H) 8.70 (s, 1H).

Final Compound 43, (3,4-Dimethoxyphenyl)-[(3*S*,4*R*)-3-[5-(difluoromethyl)-[1,2,4]triazolo[1,5-*a*]pyrimidin-7-yl]-4-methyl-1-piperidyl]-methanone. Prepared in a similar manner to compound 42, starting from 3,4-dimethoxybenzoic acid (120 mg, 0.66 mmol) and intermediate 78 (SR!, 200 mg, 0.66 mmol). Purification by flash chromatography on a silica gel, eluting with 0–2% MeOH in DCM, afforded compound 41 %. ESI *m/z*: 432 [M + H]⁺. mp 227 °C. ¹H NMR (360 MHz, DMSO-*d*₆): δ ppm 0.00 (s, 1H) 0.77 (d, *J* = 6.59 Hz, 3H); 1.35–1.47 (m, 1H); 1.79–1.95 (m, 1H); 2.40–2.47 (m, 1H); 3.55–3.63 (m, 1H); 3.77 (br s, 3H); 3.79 (s, 4H); 3.93–4.65 (m, 1H); 6.95 (br s, 1H); 7.01 (br s, 3H); 7.10 (s, 1H); 7.68 (br s, 1H); 8.83 (s, 1H).

Final Compound 44, [3-[2-(5-Bromo-2-methyl-pyrazol-3-yl)-ethyl]-6-fluoro-1-naphthyl]oxy-*tert*-butyl-diphenyl-silane; 2-[3-[5-(Difluoromethyl)-[1,2,4]triazolo[1,5-*a*]pyrimidin-7-yl]-4-methyl-1-piperidyl]-*N*-methyl-pyridine-4-carboxamide; Methane. DIPEA [7087-68-5] (372 mg, 2.88 mmol) was added at RT to a solution of intermediate 78 (RS!, 175 mg, 0.58 mmol) and 2-bromo-*n*-methyl-4-pyridinecarboxamide [337536-01-3] (372 mg, 1.73 mmol) in *n*BuOH [71-36-3] (3 mL). The resulting mixture was then stirred for 4 h at 180 °C under microwave irradiation, then it was cooled to RT, and the solvent was evaporated under reduced pressure. The resulting residue was dissolved in DCM (5 mL) and washed with a saturated aqueous NaHCO₃ solution (1 mL). The biphasic mixture was passed through an Extrelut filter, which was afterward washed with DCM (×2). The combined OL was evaporated under reduced pressure. The resulting residue was purified by Prep HPLC using as the stationary phase a Uptisphere C18 ODB—10 μm, 200 g, 5 cm column and as the mobile phase a mixture of 0.25% NH₄HCO₃ solution in water and CH₃CN, to provide the title compound. This was recrystallized from ether, to give compound 44 (95 mg, 41%). ESI *m/z*: 402 [M + H]⁺. mp 180.87 °C. ¹H NMR (400 MHz, DMSO-*d*₆): δ ppm 0.78 (d, *J* = 6.53 Hz, 3H) 1.42

(br dd, $J = 12.42, 3.89$ Hz, 1H) 1.91 (br dd, $J = 13.55, 3.51$ Hz, 1H) 2.44 (br s, 2H) 2.78 (d, $J = 4.52$ Hz, 3H) 3.11 (td, $J = 12.80, 3.01$ Hz, 1H) 3.36 (dd, $J = 12.80, 11.04$ Hz, 1H) 3.51–3.58 (m, 1H) 4.45 (br d, $J = 13.30$ Hz, 1H) 4.53–4.59 (m, 1H) 6.95 (dd, $J = 5.14, 1.13$ Hz, 1H) 7.16–7.19 (m, 1H) 7.61 (s, 1H) 8.16 (d, $J = 5.02$ Hz, 2H) 8.74 (s, 1H).

Final Compound 45, 7-[1-(4-*tert*-Butyl-2-pyridyl)-4-methyl-3-piperidyl]-5-(difluoromethyl)-[1,2,4]triazolo[1,5-*a*]pyrimidine. Prepared in a similar manner to compound 44, starting from 4-*tert*-butyl-2-chloropyridine (112 mg, 0.66 mmol) and intermediate 78 (SR!, 100 mg, 0.33 mmol) and using NMP (3 mL) as the solvent. Purification by flash chromatography on a silica gel, eluting with 0–2% MeOH in DCM, followed by crystallization from diisopropyl ether, afforded compound 45 (37.6 mg, 29%). ESI m/z : 401 $[M + H]^+$. 1H NMR (360 MHz, chloroform-*d*): δ ppm 0.80–0.98 (m, 5H); 1.21–1.35 (m, 11H); 1.41–1.56 (m, 1H); 1.61–1.79 (m, 1H); 1.91–1.99 (m, 1H); 2.36 (br s, 1H); 3.03–3.23 (m, 2H); 3.66 (br s, 1H); 4.55 (br dd, $J = 12.26, 2.74$ Hz, 2H); 6.53–6.85 (m, 2H); 6.86 (s, 1H); 7.33 (s, 1H); 8.10 (d, $J = 5.12$ Hz, 1H); 8.60 (s, 1H).

Final Compound 46, 5-(Difluoromethyl)-7-[4-methyl-1-(4-phenyl-2-pyridyl)-3-piperidyl]-[1,2,4]triazolo[1,5-*a*]pyrimidine. Prepared in a similar manner to compound 44, starting from 2-chloro-4-phenylpyridine [42260-39-9] (139 mg, 0.74 mmol) and intermediate 78 (SR!, 112 mg, 0.37 mmol) and using NMP (3.5 mL) as the solvent. Purification by flash chromatography on a silica gel, eluting with 0–2% MeOH in DCM, followed by crystallization from diisopropyl ether, afforded compound 46 (8.6 mg, 6%). ESI m/z : 421 $[M + H]^+$. mp 127.58 °C. 1H NMR (360 MHz, chloroform-*d*): δ ppm 0.76–0.96 (m, 4H) 1.40–1.61 (m, 1H) 1.93–2.01 (m, 1H) 2.41 (br s, 1H) 3.09–3.30 (m, 2H) 3.61–3.77 (m, 1H) 4.58–4.67 (m, 2H) 6.52–6.87 (m, 1H) 6.91 (dd, $J = 5.31, 1.28$ Hz, 1H) 7.12 (s, 1H) 7.34 (s, 1H) 7.41–7.53 (m, 3H) 7.64–7.72 (m, 2H) 8.25 (d, $J = 5.49$ Hz, 1H) 8.62 (s, 1H).

■ ASSOCIATED CONTENT

Supporting Information

The Supporting Information is available free of charge at <https://pubs.acs.org/doi/10.1021/acs.jmedchem.0c01272>.

Selectivity data for all compounds; data for retrospective validation of FEP approach; comparison of binding affinity predictions from docking with experiment; and additional chemistry details (PDF)

Molecular formula strings for 3–46 (CSV)

Input structures for FEP calculations (ZIP)

Accession Codes

Atomic coordinates and structure factors for compounds 3 and 39 have been deposited in the RCSB Protein Data Bank under the accession code 6ZND and 6ZQZ respectively. Authors will release the atomic coordinates and experimental data upon article publication.

■ AUTHOR INFORMATION

Corresponding Authors

Gary Tresadern – Computational Chemistry, Janssen Pharmaceutica N. V., B-2340 Beerse, Belgium; orcid.org/0000-0002-4801-1644; Phone: +32 1464 1569; Email: gtresade@its.jnj.com

Peter J. J. A. Buijnsters – Medicinal Chemistry, Janssen Pharmaceutica N. V., B-2340 Beerse, Belgium; Phone: +32 1460 7439; Email: pbuijnst@its.jnj.com

Authors

Ingrid Velter – Medicinal Chemistry, Janssen Pharmaceutica N. V., B-2340 Beerse, Belgium

Andrés A. Trabanco – Medicinal Chemistry, Janssen Research & Development, Janssen-Cilag S. A., 45007 Toledo, Spain; orcid.org/0000-0002-4225-758X

Frans Van den Keybus – Medicinal Chemistry, Janssen Pharmaceutica N. V., B-2340 Beerse, Belgium

Gregor J. Macdonald – Medicinal Chemistry, Janssen Pharmaceutica N. V., B-2340 Beerse, Belgium

Marijke V. F. Somers – Discovery Sciences, Janssen Research & Development, Janssen Pharmaceutica N. V., B-2340 Beerse, Belgium

Greet Vanhoof – Discovery Sciences, Janssen Research & Development, Janssen Pharmaceutica N. V., B-2340 Beerse, Belgium

Philip M. Leonard – Structural Biology, Charles River Discovery (Previously BioFocus), Chesterford Research Park, CB10 1XL Essex, U.K.

Marieke B. A. C. Lamers – Structural Biology, Charles River Discovery (Previously BioFocus), Chesterford Research Park, CB10 1XL Essex, U.K.

Yves E. M. Van Roosbroeck – Medicinal Chemistry, Janssen Pharmaceutica N. V., B-2340 Beerse, Belgium

Complete contact information is available at:

<https://pubs.acs.org/doi/10.1021/acs.jmedchem.0c01272>

Author Contributions

The manuscript was written through contributions of all authors. All authors have given approval to the final version of the manuscript.

Notes

The authors declare no competing financial interest.

■ ACKNOWLEDGMENTS

We thank Thomas Steinbrecher and Amr Ragab at Schrodinger for assistance with the free-energy perturbation calculations. We also thank Ilse Lenaerts for performing the occupancy experiments. We thank the members of analysis and purification department, in particular Michel Carpentier and Alex de Groot for help with data analysis.

■ ABBREVIATIONS

AD, Alzheimer's disease; cAMP, 3',5'-cyclic adenosine monophosphate; cGMP, 3',5'-cyclic guanosine monophosphate; CYP450, cytochrome P450; HTS, high-throughput screening; FEP, free-energy perturbation; HP- β -CD, (2-hydroxypropyl)-beta-cyclodextrin; LHS, left-hand side; LO, lead optimization; LTP, long-term potentiation; MUE, mean unsigned error; NOS, nitric oxide synthase; PDB, protein data bank; PDE, phosphodiesterase; RBEF, relative binding free energy; RHS, right-hand side; SAR, structure–activity relationship; SD, standard deviation; SFC, supercritical fluid chromatography

■ REFERENCES

- (1) Maurice, D. H.; Ke, H.; Ahmad, F.; Wang, Y.; Chung, J.; Manganiello, V. C. Advances in targeting cyclic nucleotide phosphodiesterases. *Nat. Rev. Drug Discovery* **2014**, *13*, 290–314.
- (2) Francis, S. H.; Blount, M. A.; Corbin, J. D. Mammalian cyclic nucleotide phosphodiesterases: molecular mechanisms and physiological functions. *Physiol. Rev.* **2011**, *91*, 651–690.
- (3) Pandit, J.; Forman, M. D.; Fennell, K. F.; Dillman, K. S.; Menniti, F. S. Mechanism for the allosteric regulation of phosphodiesterase 2A deduced from the X-ray structure of a near full-length construct. *Proc. Natl. Acad. Sci. U.S.A.* **2009**, *106*, 18225–18230.
- (4) Wu, A. Y.; Tang, X.-B.; Martinez, S. E.; Ikeda, K.; Beavo, J. A. Molecular determinants for cyclic nucleotide binding to the regulatory domains of phosphodiesterase 2A. *J. Biol. Chem.* **2004**, *279*, 37928–37938.

- (5) Erneux, C.; Couchie, D.; Dumont, J. E.; Baraniak, J.; Stec, W. J.; Abbad, E. G.; Petridis, G.; Jastorff, B. Specificity of cyclic GMP activation of a multi-substrate cyclic nucleotide phosphodiesterase from rat liver. *Eur. J. Biochem.* **1981**, *115*, 503–510.
- (6) Lakics, V.; Karran, E. H.; Boess, F. G. Quantitative comparison of phosphodiesterase mRNA distribution in human brain and peripheral tissues. *Neuropharmacology* **2010**, *59*, 367–374.
- (7) Stephenson, D. T.; Coskran, T. M.; Wilhelms, M. B.; Adamowicz, W. O.; O'Donnell, M. M.; Muravnick, K. B.; Menniti, F. S.; Kleiman, R. J.; Morton, D. Immunohistochemical localization of phosphodiesterase 2A in multiple mammalian species. *J. Histochem. Cytochem.* **2009**, *57*, 933–949.
- (8) Stephenson, D. T.; Coskran, T. M.; Kelly, M. P.; Kleiman, R. J.; Morton, D.; O'Neill, S. M.; Schmidt, C. J.; Weinberg, R. J.; Menniti, F. S. The distribution of phosphodiesterase 2A in the rat brain. *Neuroscience* **2012**, *226*, 145–155.
- (9) Blokland, A.; Menniti, F. S.; Prickaerts, J. PDE Inhibition and cognition enhancement. *Expert Opin. Ther. Pat.* **2012**, *22*, 349–354.
- (10) Bliss, T. V. P.; Collingridge, G. L. A synaptic model of memory: long-term potentiation in the hippocampus. *Nature* **1993**, *361*, 31–39.
- (11) Bollen, E.; Puzzo, D.; Rutten, K.; Privitera, L.; De Vry, J.; Vanmierlo, T.; Kenis, G.; Palmeri, A.; D'Hooge, R.; Balschun, D.; Steinbusch, H. M.; Blokland, A.; Prickaerts, J. Improved long-term memory via enhancing cGMP-PKG signaling requires cAMP-PKA signaling. *Neuropsychopharmacology* **2014**, *39*, 2497–2505.
- (12) Lueptow, L. M.; Zhan, C.-G.; O'Donnell, J. M. Cyclic cGMP-mediated memory enhancement in the object recognition test by inhibitors of phosphodiesterase-2 in mice. *Psychopharmacology* **2016**, *233*, 447–456.
- (13) Elias, M. F.; Beiser, A.; Wolf, P. A.; Au, R.; White, R. F.; D'Agostino, R. B. The preclinical phase of Alzheimer disease: A 22-year prospective study of the Framingham Cohort. *Arch. Neurol.* **2000**, *57*, 808–813.
- (14) Newman, S. K.; Warrington, E. K.; Kennedy, A. M.; Rossor, M. N. The earliest cognitive change in a person with familial Alzheimer's disease: presymptomatic neuropsychological features in a pedigree with familial Alzheimer's disease confirmed at necropsy. *J. Neurol., Neurosurg. Psychiatry* **1994**, *57*, 967–972.
- (15) Mayeux, R. Early Alzheimer's Disease. *N. Engl. J. Med.* **2010**, *362*, 2194–2201.
- (16) Gabrieli, J. D. E. Memory systems analyses of mnemonic disorders in aging and age-related diseases. *Proc. Natl. Acad. Sci. U.S.A.* **1996**, *93*, 13534–13540.
- (17) Belleville, S.; Sylvain-Roy, S.; de Boysson, C.; Ménard, M.-C. Chapter 23 Characterizing the memory changes in persons with mild cognitive impairment. *Prog. Brain Res.* **2008**, *169*, 365–375.
- (18) Lyketsos, C. G.; Lopez, O.; Jones, B.; Fitzpatrick, A. L.; Breitner, J.; DeKosky, S. Prevalence of neuropsychiatric symptoms in dementia and mild cognitive impairment: results from the cardiovascular health study. *JAMA* **2002**, *288*, 1475–1483.
- (19) Blennow, K.; de Leon, M. J.; Zetterberg, H. Alzheimer's disease. *Lancet* **2006**, *368*, 387–403.
- (20) Gomez, L.; Breitenbucher, J. G. PDE2A inhibition: potential for the treatment of cognitive disorders. *Bioorg. Med. Chem. Lett.* **2013**, *23*, 6522–6527.
- (21) Wu, Y.; Li, Z.; Huang, Y.-Y.; Wu, D.; Luo, H.-B. Novel phosphodiesterase inhibitors for cognitive improvement in Alzheimer's disease. *J. Med. Chem.* **2018**, *61*, 5467–5483.
- (22) Gomez, L.; Massari, M. E.; Vickers, T.; Freestone, G.; Vernier, W.; Ly, K.; Xu, R.; McCarrick, M.; Marrone, T.; Metz, M.; Yan, Y. G.; Yoder, Z. W.; Lemus, R.; Broadbent, N. J.; Barido, R.; Warren, N.; Schmelzer, K.; Neul, D.; Lee, D.; Andersen, C. B.; Sebring, K.; Aertgeerts, K.; Zhou, X.; Tabatabaei, A.; Peters, M.; Breitenbucher, J. G. Design and synthesis of novel and selective phosphodiesterase 2 (PDE2a) inhibitors for the treatment of memory disorders. *J. Med. Chem.* **2017**, *60*, 2037–2051.
- (23) Mikami, S.; Nakamura, S.; Ashizawa, T.; Nomura, I.; Kawasaki, M.; Sasaki, S.; Oki, H.; Kokubo, H.; Hoffman, I. D.; Zou, H.; Uchiyama, N.; Nakashima, K.; Kamiguchi, N.; Imada, H.; Suzuki, N.; Iwashita, H.; Taniguchi, T. Discovery of clinical candidate N-((1S)-1-(3-fluoro-4-(trifluoromethoxy)phenyl)-2-methoxyethyl)-7-methoxy-2-oxo-2,3-dihydropyrido[2,3-b]pyrazine-4(1H)-carboxamide (TAK-915): a highly potent, selective, and brain-penetrating phosphodiesterase 2A inhibitor for the treatment of cognitive disorders. *J. Med. Chem.* **2017**, *60*, 7677–7702.
- (24) Helal, C. J.; Arnold, E. P.; Boyden, T. L.; Chang, C.; Chappie, T. A.; Fennell, K. F.; Forman, M. D.; Hajos, M.; Harms, J. F.; Hoffman, W. E.; Humphrey, J. M.; Kang, Z.; Kleiman, R. J.; Kormos, B. L.; Lee, C.-W.; Lu, J.; Maklad, N.; McDowell, L.; Mente, S.; O'Connor, R. E.; Pandit, J.; Piotrowski, M.; Schmidt, A. W.; Schmidt, C. J.; Ueno, H.; Verhoest, P. R.; Yang, E. X. Application of structure-based design and parallel chemistry to identify a potent, selective, and brain penetrant Phosphodiesterase 2A inhibitor. *J. Med. Chem.* **2017**, *60*, 5673–5698.
- (25) Stachel, S. J.; Berger, R.; Nomland, A. B.; Ginnetti, A. T.; Paone, D. V.; Wang, D.; Puri, V.; Lange, H.; Drott, J.; Lu, J.; Marcus, J.; Dwyer, M. P.; Suon, S.; Uslander, J. M.; Smith, S. M. Structure-Guided design and procognitive assessment of a potent and selective phosphodiesterase 2A inhibitor. *ACS Med. Chem. Lett.* **2018**, *9*, 815–820.
- (26) Helal, C. J.; Arnold, E.; Boyden, T.; Chang, C.; Chappie, T. A.; Fisher, E.; Hajos, M.; Harms, J. F.; Hoffman, W. E.; Humphrey, J. M.; Pandit, J.; Kang, Z.; Kleiman, R. J.; Kormos, B. L.; Lee, C.-W.; Lu, J.; Maklad, N.; McDowell, L.; McGinnis, D.; O'Connor, R. E.; O'Donnell, C. J.; Ogden, A.; Piotrowski, M.; Schmidt, C. J.; Seymour, P. A.; Ueno, H.; Vansell, N.; Verhoest, P. R.; Yang, E. X. Identification of a potent, highly selective, and brain penetrant phosphodiesterase 2A inhibitor clinical candidate. *J. Med. Chem.* **2018**, *61*, 1001–1018.
- (27) Buijnsters, P.; De Angelis, M.; Langlois, X.; Rombouts, F. J. R.; Sanderson, W.; Tresadern, G.; Ritchie, A.; Trabanco, A. A.; Vanhoof, G.; Roosbroeck, Y. V.; Andrés, J.-I. Structure-based design of a potent, selective, and brain penetrating PDE2A inhibitor with demonstrated target engagement. *ACS Med. Chem. Lett.* **2014**, *5*, 1049–1053.
- (28) Rombouts, F. J. R.; Tresadern, G.; Buijnsters, P.; Langlois, X.; Tovar, F.; Steinbrecher, T. B.; Vanhoof, G.; Somers, M.; Andrés, J.-I.; Trabanco, A. A.-I.; Trabanco, A. A. Pyrido[4,3-e][1,2,4]triazolo[4,3-a]pyrazines as selective, brain penetrant phosphodiesterase 2 (PDE2A) inhibitors. *ACS Med. Chem. Lett.* **2015**, *6*, 282–286.
- (29) Jorgensen, W. L. Efficient drug lead discovery and optimization. *Acc. Chem. Res.* **2009**, *42*, 724–733.
- (30) Abel, R.; Wang, L.; Harder, E. D.; Berne, B. J.; Friesner, R. A. Advancing drug discovery through enhanced free energy calculations. *Acc. Chem. Res.* **2017**, *50*, 1625–1632.
- (31) Cournia, Z.; Allen, B.; Sherman, W. Relative binding free energy calculations in drug discovery: Recent advances and practical considerations. *J. Chem. Inf. Model.* **2017**, *57*, 2911–2937.
- (32) Ciordia, M.; Pérez-Benito, L.; Delgado, F.; Trabanco, A. A.; Tresadern, G. Application of free energy perturbation for the design of BACE1 inhibitors. *J. Chem. Inf. Model.* **2016**, *56*, 1856–1871.
- (33) Keränen, H.; Pérez-Benito, L.; Ciordia, M.; Delgado, F.; Steinbrecher, T. B.; Oehlich, D.; van Vlijmen, H. W. T.; Trabanco, A. A.; Tresadern, G. Acylguanidine beta secretase 1 inhibitors: A combined experimental and free energy perturbation study. *J. Chem. Theory Comput.* **2017**, *13*, 1439–1453.
- (34) Deflorian, F.; Pérez-Benito, L.; Lenselink, E. B.; Congreve, M.; Van Vlijmen, H.; Mason, J. S.; de Graaf, C.; Tresadern, G. Accurate prediction of GPCR ligand binding affinity with free energy perturbation. *J. Chem. Inf. Model.* **2020**, *60*, 4311–4325, DOI: 10.1021/acs.jcim.0c00449.
- (35) Pérez-Benito, L.; Keränen, H.; van Vlijmen, H. W. T.; Tresadern, G. Predicting binding free energies of PDE2A inhibitors. The difficulties of protein conformation. *Sci. Rep.* **2018**, *8*, 4883.
- (36) Pérez-Benito, L.; Casajuana-Martin, N.; Jiménez-Rosés, M.; van Vlijmen, H.; Tresadern, G. Predicting activity cliffs with free-energy perturbation. *J. Chem. Theory Comput.* **2019**, *15*, 1884–1895.
- (37) Gapsys, V.; Pérez-Benito, L.; Aldeghi, M.; Seeliger, D.; van Vlijmen, H.; Tresadern, G.; de Groot, B. L. Large scale relative protein ligand binding affinities using non-equilibrium alchemy. *Chem. Sci.* **2020**, *11*, 1140–1152.

- (38) Wan, S.; Tresadern, G.; Pérez-Benito, L.; Vlijmen, H.; Coveney, P. V. Accuracy and precision of alchemical relative free energy predictions with and without replica-exchange. *Adv. Theory Simul.* **2019**, *3*, 1900195.
- (39) Zhang, K. Y. J.; Card, G. L.; Suzuki, Y.; Artis, D. R.; Fong, D.; Gillette, S.; Hsieh, D.; Neiman, J.; West, B. L.; Zhang, C.; Milburn, M. V.; Kim, S.-H.; Schlessinger, J.; Bollag, G. Glutamine switch mechanism for nucleotide selectivity by phosphodiesterases. *Mol. Cell* **2004**, *15*, 279–286.
- (40) Jansen, C.; Kooistra, A. J.; Kanev, G. K.; Leurs, R.; de Esch, I. J. P.; de Graaf, C. PDEStrLAN: A Phosphodiesterase structure and ligand interaction annotated database as a tool for structure-based drug design. *J. Med. Chem.* **2016**, *59*, 7029–7065.
- (41) Wilson, L. S.; Brandon, N. J. Emerging biology of PDE10A. *Curr. Pharm. Des.* **2015**, *21*, 378–388.
- (42) Verhoest, P. R.; Chapin, D. S.; Corman, M.; Fonseca, K.; Harms, J. F.; Hou, X.; Marr, E. S.; Menniti, F. S.; Nelson, F.; O'Connor, R.; Pandit, J.; Proulx-LaFrance, C.; Schmidt, A. W.; Schmidt, C. J.; Suiciak, J. A.; Liras, S. Discovery of a novel class of phosphodiesterase 10A inhibitors and identification of clinical candidate 2-[4-(1-Methyl-4-pyridin-4-yl-1H-pyrazol-3-yl)-phenoxyethyl]-quinoline (PF-2545920) for the treatment of schizophrenia. *J. Med. Chem.* **2009**, *52*, 5188–5196.
- (43) Scapin, G.; Patel, S. B.; Chung, C.; Varnerin, J. P.; Edmondson, S. D.; Mastracchio, A.; Parmee, E. R.; Singh, S. B.; Becker, J. W.; Van der Ploeg, L. H. T.; Tota, M. R. Crystal structure of human phosphodiesterase 3B: Atomic basis for substrate and inhibitor specificity. *Biochemistry* **2004**, *43*, 6091–6100.
- (44) Li, Z.; Huang, Y.; Wu, Y.; Chen, J.; Wu, D.; Zhan, C.-G.; Luo, H.-B. Absolute binding free energy calculation and design of a subnanomolar inhibitor of phosphodiesterase-10. *J. Med. Chem.* **2019**, *62*, 2099–2111.
- (45) Moraca, F.; Negri, A.; de Oliveira, C.; Abel, R. Application of free energy perturbation (FEP+) to understanding ligand selectivity: A case study to assess selectivity between pairs of phosphodiesterases (PDE's). *J. Chem. Inf. Model.* **2019**, *59*, 2729–2740.
- (46) Abel, R.; Wang, L.; Mobley, D. L.; Friesner, R. A. A critical review of validation, blind testing, and real-world use of alchemical protein-ligand binding free energy calculations. *Curr. Top. Med. Chem.* **2017**, *17*, 2577–2585.
- (47) Mey, A. S.; Allen, B.; Macdonald, H. E. B.; Chodera, J. D.; Kuhn, M.; Michel, J.; Mobley, D. L.; Naden, L. N.; Prasad, S.; Rizzi, A.; Scheen, J.; Shirts, M. R.; Tresadern, G.; Xu, H.. Best practice for free energy calculations. 2020, arXiv:2008.03067. Published Online: August 21, 2020, <https://arxiv.org/abs/2008.03067> (accessed Sept 22, 2020).
- (48) Shirts, M. R.; Mobley, D. L.; Brown, S. P. Free-Energy Calculations in Structure-Based Drug Design. In *Drug Design. Structure- and Ligand-Based Approaches*; Merz, K. M., Jr., Ringe, D., Reynolds, C. H., Eds.; Cambridge University Press: New York, 2010; pp 61–86.
- (49) Abel, R.; Manas, E. S.; Friesner, R. A.; Farid, R. S.; Wang, L. Modeling the value of predictive affinity scoring in preclinical drug discovery. *Curr. Opin. Struct. Biol.* **2018**, *52*, 103–110.
- (50) (a) Van Roosbroeck, Y. E. M.; Van den Keybus, F. A. M.; Tresadern, G. J.; Buijnsters, P. J. J. A.; Velter, A. I.; Jacoby, E.; Macdonald, G. J.; Gijsen, H. J. M.; Ahnaou, A.; Drinkenburg, W. H. I. M. [1,2,4]Triazolo[1,5-a]pyrimidine Derivatives as PDE2 Inhibitors. WO 2018083098 A1, May 11, 2018. (b) Van Roosbroeck, Y. E. M.; Buijnsters, P. J. J. A.; Tresadern, G. J.; Jacoby, E.; Oehlich, D.; Gijsen, H. J. M. [1,2,4]Triazolo[1,5-a]pyrimidine Compounds as PDE2 Inhibitors. WO 2018083103 A1, May 11, 2018.
- (51) The absolute configuration was determined using vibrational VCD. See [Supporting Information](#).
- (52) Ghanakota, P.; Bos, P. H.; Konze, K.; Staker, J.; Marques, G.; Marshall, K.; Leswing, K.; Abel, R.; Bhat, S. Combining cloud-based free energy calculations, synthetically aware enumerations and goal-directed generative machine learning for rapid large scale chemical exploration and optimization. *J. Chem. Inf. Model.* **2020**, DOI: 10.1021/acs.jcim.0c00120.
- (53) Schindler, C.; Baumann, H.; Blum, A.; Böse, D.; Buchstaller, H.-P.; Burgdorf, L.; Cappel, D.; Chekler, E.; Czodrowski, P.; Dorsch, D.; Eguida, M. K. I.; Follows, B.; Fuchß, T.; Grädler, U.; Gunera, J.; Johnson, T.; Jorand Lebrun, C.; Karra, S.; Klein, M.; Knehans, T.; Kötzner, L.; Krier, M.; Leiendecker, M.; Leuthner, B.; Li, L.; Mochalkin, I.; Musil, D.; Neagu, C.; Rippmann, F.; Schiemann, K.; Schulz, R.; Steinbrecher, T. B.; Tanzer, E.-M.; Unzue Lopez, A.; Viacava Follis, A.; Wegener, A.; Kuhn, D. Large-Scale assessment of binding free energy calculations in active drug discovery projects. *J. Chem. Inf. Model.* **2020**, DOI: 10.1021/acs.jcim.0c00900.
- (54) Madhavi Sastry, G.; Adzhigirey, M.; Day, T.; Annabhimoju, R.; Sherman, W. Protein and ligand preparation: Parameters, protocols, and influence on virtual screening enrichments. *J. Comput.-Aided Mol. Des.* **2013**, *27*, 221–234.
- (55) Schrodinger LLC. 120 West 45th Street 17th Floor, Tower 45 New York, NY 10036-4041, USA at <http://www.schrodinger.com/Maestro/>, 2014. (accessed Sept 18, 2020).